# Engineering *Saccharomyces cerevisiae* for isobutanol production

By

Francesca V. Gambacorta

A dissertation submitted in partial fulfillment of the requirements for the degree of:

Doctor of Philosophy

(Chemical and Biological Engineering)

UNIVERSITY OF WISCONSIN-MADISON

2022

Date of Final Oral Examination: 13 September 2022

The dissertation is approved by the following members of the Final Oral Committee:

Brian F. Pfleger, Professor, Chemical and Biological Engineering

Eric V. Shusta, Professor, Chemical and Biological Engineering

Philip A. Romero, Assistant Professor, Chemical and Biological Engineering

Chris Todd Hittinger, Professor, Genetics

# Abstract

There is an increasing need for generating renewable and sustainable alternative transportation fuels to combat human-induced climate change. Here, we explore the use of *Saccharomyces cerevisiae* as a microbial host for generating the alternative transportation fuel, isobutanol. In order for this process to be economically viable, high titers, rates, and yields must be achieved in cultures grown on low-cost biomass feedstocks. This means that metabolic engineering strategies must be implemented to overpower *S. cerevisiae*'s dominant native flux to ethanol. This is a deceptively difficult challenge and the work presented here aims to understand how *S. cerevisiae*'s metabolism could be rewired for isobutanol production.

In order to optimize *S. cerevisiae*'s carbon-to-isobutanol flux, we implemented 2 different metabolic engineering approaches, pathway localization and redox cofactor-balancing, and investigated how they affected the performance and physiology of the engineered strains. Our results showed that pathway localization had a large effect on isobutanol production with the mitochondrial-localized pathway outperforming the cytosolic version. We then go on to show that the limitation in the cytosolic-localization could be overcome by increasing cellular iron in the cell thereby increasing the supply of a required cofactor, 2Fe-2S.

We next sought out to enhance the carbon-to-isobutanol flux by identification of a

highly active isobutanol pathway cassette. We constructed and screened a combinatorial pathway library that had variability introduced on 2 levels: coding sequences (homologs) and gene dosage (promoters). Then through a high-throughput growth-coupled screen, we identified and characterized a high-flux cassette. The resulting pathway's flux however, was not high enough to support the cellular maintenance energy requirement of the cell anaerobically in the absence of ethanol production. Therefore, additional engineering may be needed to further enhance pathway flux.

Lastly, we touched on the challenges associated with using biomass as a feedstock. We focused on generating a xylose-to-isobutanol platform strain and improving the tolerance to the inhibitor $\gamma$-valerolactone with use of a gene deletion library.

Overall, this work has contributed towards the metabolic engineering designs required to build an improved isobutnaol producing *S. cerevisiae* strain. However, future work is still required to completely eliminate *S. cerevisiae*'s reliance on ethanol production.

*To Jacob*

# Acknowledgments

As I reflect on my time at UW-Madison, I must acknowledge that I couldn't have gotten to where I am today without my friends, family, collaborators, mentors, and fellow researchers.

First, I'd like to thank my parents. While you don't understand what I am working on or why I've been in school for 5 more years after undergrad, you've respected the decision I made for myself. You guys have been my biggest supporters and I can't wait to live closer to you.

Jacob, you have given me your unconditional support over the years and especially these last 5 years. I'm so lucky to have you by my side. I say that you get an honorary PhD from all the code you've helped me with :).

I would like to thank all the Pfleger Lab members who have helped mold me into the person I am today. To Mike Jindra, Will Cordell, Dylan Courtney, and Taylor Cook, thank you for all the great times at the library and for all the game nights. I hope we'll continue to remain close friends. Will, thank you for all the tasty meals you've made me and for driving Jacob home from the hospital when he broke his hand. Dylan, thank you for always lending an ear and fueling my coffee addiction. Taylor, thank you for giving me your lab daddy roles. Mike, you're a beautiful person, we've been together every step of the way- thank you for always giving me that positive encouragement when I need

it. Also thank you for monopolizing the spotify playlist. Justin Baerwald, thank you for being my first undergrad and playing too many Broadway musical songs. Steph Brown, thank you for reminding me how much fun it can be to mentor a student and for making the last figures for my thesis. Qiang Yan, thank you for being such a great office-mate and friend. Josh Dietrich, thank you for picking up the slack on the yeast projects when I needed help. To the rest of the Pfleger lab, Will Bothfeld, Maya Venkataraman, Paul Perkovich, Joshua Abraham, Susan Hubbard, Yun Su, Audrey Ynigez-Gutierrez, Ted Chavkin, Shivangi Mishra, Nestor Hernandez, and Chris Mehrer, thank you for all your support and efforts to help keep the lab running. Hugh Purdy and Sanjan Gupta of the Reed Lab, thank you for the interesting discussions. Last but not least, Jackie Cooper, thank you for keeping the lab materials stocked.

I would like to thank all the members of the Hittinger, Sato, and Zhang labs for treating me like a member of your own lab. Chris Hittinger, Trey Sato, Mary Treamine, Russell Wrobell, Megan Young, and Lisa Liu, you guys taught me how to work with yeast and I'll be forever greatful. Dan Xie thank you for always putting a smile on my face when I come to pick up materials. Amanda Hulfachor, thank you for keeping the lab running. Trey Sato, thank you for all the discussions, lab materials, positive encouragement, and help editing my manuscripts. Chris Hittinger, thank you for all your guidance and bringing me on as a student when I first arrived in Madison.

I would like to thank all the GLBRC community members. The center has been such a great community and I've gotten to talk to and learn from so many of its members. Kevin Myers, thank you for all his bioinformatics help during COVID. Donna Bates, thank you for scheduling all the meetings and helping me edit my abstracts. Mick Mcgee, thank you for running all of my HPLC and GC samples. To all the members of Aim 9 especially

Dave Krause, Tyler Jacobson, and Ellen Wagnen thank you for helping me design and collect the data for my first paper.

I would like to thank all my collaborators outside of the GLBRC. Megan McClean, Stephanie Geller, Neydis Moreno, Taylor Scott, thank you for teaching me about optogenetics and giving me lab materials. Jeremy Cortez, thank you for all the Fe-S cluster conversations.

To all my other friends and acquaintances, thank you for making my time at UW memorable. Eric, thank you for being my friend since undergrad and having lunches with me. Paolo, Alec, Jonathan, and Koji thank you for all the study help and celebrations. Julio Rivera, thank you for all the fun nights at the library and for teaching me that dice game. Julia Martein and Ben Hall, thank you for the interesting conversations.

I would like to thank all the members of the Chemical and Biological Engineering Department for keeping the program running: Kate Fanis, Michael Morris, Susann Ely, Jill Mullen, and Russ Poyner.

I would like to thank my thesis committee members, Eric Shusta, Phil Romero, and Chris Hittinger for all their guidance, suggestions, and thoughtful edits.

Lastly, I would like to thank my advisor Brian Pfleger for having faith in abilities, allowing me to work collaboratively with many other GLBRC members, and guiding me through the scientific process.

To everyone listed on these pages and anyone I may have forgotten, thank you!

# Contents

# List of Figures

# List of Tables

# Chapter 1

# Introduction

## 1.1 Engineering microbes to produce chemicals

Currently, industrial chemical production predominantly consists of using chemical catalysts to produce products of interest from petroleum at a large-scale. While this has been highly successful, there is now interest in creating more sustainable processes by using biological catalysts and renewable feedstocks such as lignocellulosic biomass. This field of industrial chemical production is commonly referred to as industrial biotechnology. Industrial scale microbial fermentations have been successfully used to produce both high-volume/low-value and low-volume/high-value chemicals such as citric acid and antibiotics, respectively. Metabolic engineering, the science of rewiring cell metabolism, has enabled this field to flourish by improving the TRY production metrics: titer (concentration), rate (productivity), and yield (efficiency of substrate utilization) of a microbial production thus allowing it to become economically viable. A variety of metabolic engineering strategies exist for increasing production, but they all involve optimizing a metabolic pathway to produce the desired chemical. Additionally, systems biology, syn-

thetic biology, and protein discovery/characterization are a few tools that can be used to help metabolic engineers design, build, and optimize a high producing strain (Fig.1.1). In brief, synthetic biology offers the tools to manipulate DNA, RNA, and proteins to achieve a certain phenotype, systems biology is a tool to help better understand the biological system as a whole, and protein discovery/characterization is a way to identify or create enzymes with desired properties ($K_m$, $V_{max}$, and $K_{cat}$). In the following sessions, we will further describe the tools with a particular focus on the ones applied in this thesis.

### 1.1.1 Synthetic biology for metabolic engineering

Synthetic biology is one tool metabolic engineers use to redesign new abilities in organisms or rewire the existing metabolism for enhanced chemical production. The process can be split into 2 steps:

1. Establish the desired pathway in the host.
2. Increase flux through the desired pathway.

Both steps are often accomplished by manipulating DNA sequences (inserting, deleting, mutating) within the cell, but modifications can also be made at the RNA or protein level. These three parts (DNA, RNA, and protein) make up the central dogma of molecular biology which explains how information is shared and translated in a biological system (Fig.1.2). As engineers we are trying to establish and balance the level of proteins in a desired pathway such that flux through the pathway is maximized. This can be accomplished by using standardized and characterized genetic parts (promoters, genes, and terminators) and expression techniques (plasmids and chromosomal integrations).

For step 1, if a native host does not harbor the required protein/s for making the desired product, the necessary genes that encode heterologous enzymes can be expressed.

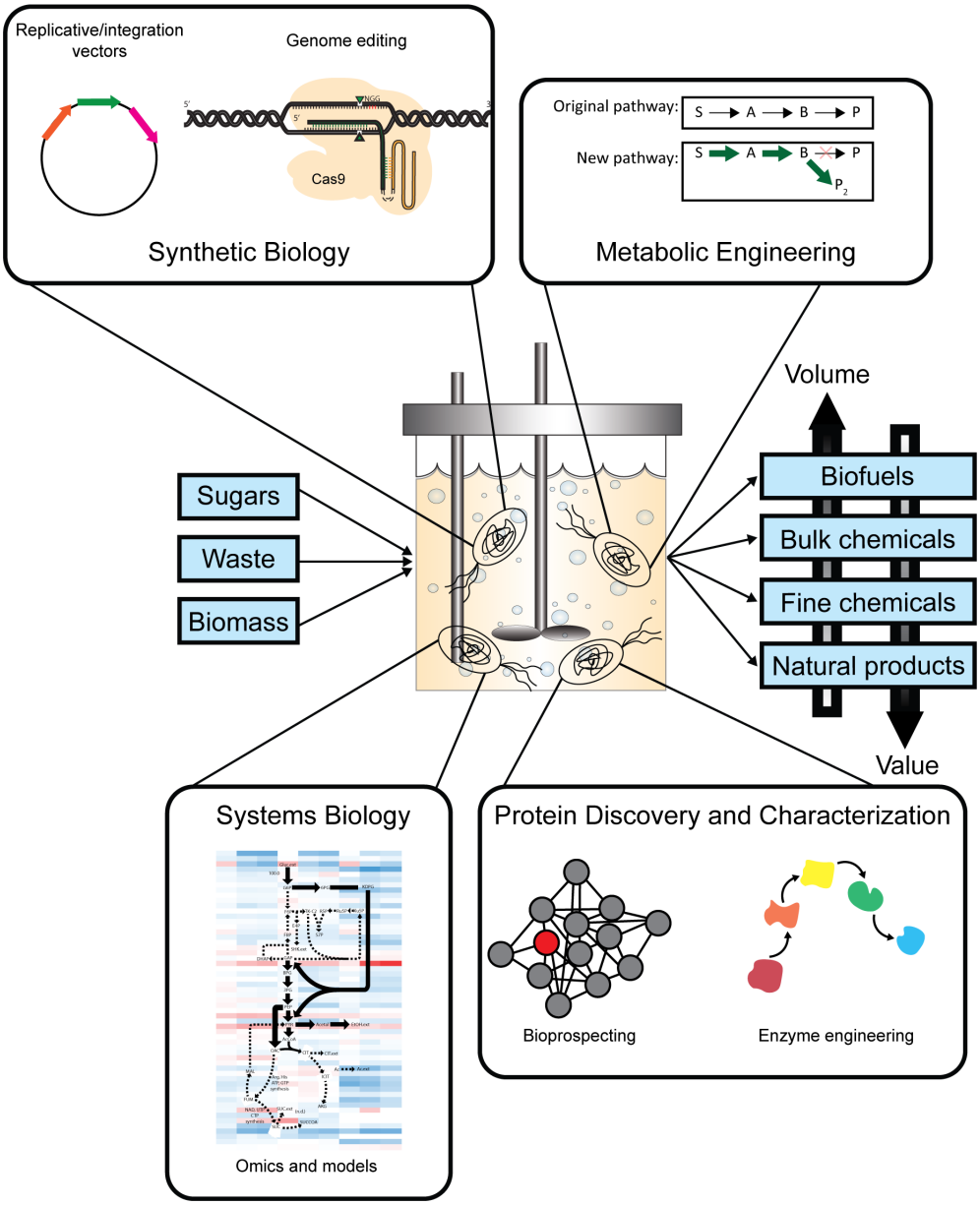


Figure 1.1: **Industrial biotechnology** involves the production of chemicals via microbial fermentations. The TRY production metrics: titer (concentration), rate (productivity), and yield (efficiency of substrate utilization) of a microbial production can be improved by implementing a variety of strategies (synthetic biology, systems biology, metabolic engineering, and protein discovery/characterization).

Once the pathway is established, flux through the pathway can be maximized by implementing metabolic engineering strategies. A common technique is called the push-pull-block strategy (Fig.1.3a). Push and pull both involve upregulating or overexpressing a gene that encodes an enzyme within the desired product's pathway. For the push strategy, the upstream portion of the pathway is generally targeted which saturates

downstream pathway intermediates such that the downstream pathway is upregulated to achieve homeostasis. Conversely, for the pull strategy, the downstream portion of the pathway is generally targeted which helps reduce backwards pathway flux and depletes upstream pathway intermediates such that the upstream pathway is upregulated to achieve homeostasis. Lastly, the block strategy involves deleting or downregulating genes that encode enzymes that compete with the desired product's carbon flux.

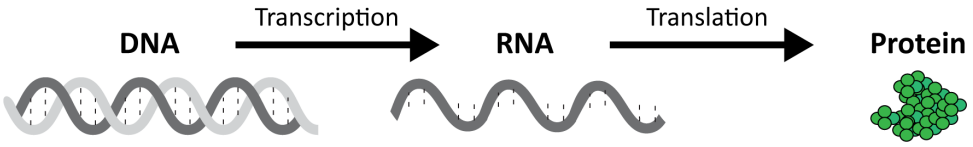


Figure 1.2: **The central dogma of molecular biology.** Metabolic engineers can establish and balance the level of proteins in a desired pathway by manipulations at 3 different levels: DNA, RNA, and protein.

Additionally, manipulating variables outside the desired pathway can increase flux to a desired product including: enzyme localization, redox power and cofactor synthesis (Fig.1.3b). Whether or not these factors are considered is dependent on the specific pathway and desired host. Pathway localization or where the pathway enzymes are localized (cytosol or organelle), is applicable if working in eukaryotic organisms such as yeast. Tuning additional factors such as redox power and/or cofactors is applicable if they are required by any enzyme within the desired pathway; if yes, guaranteeing a redox balanced pathway and having sufficient quantities of the cofactor is important.

### 1.1.2 Systems biology for metabolic engineering

Systems biology is another tool that metabolic engineers use to better understand our biological system as a whole and help us determine which part of the system we should modify to direct carbon towards our desired product. It relies on using mathematics and computational methods to analyze, model, and simulate complicated biological systems.

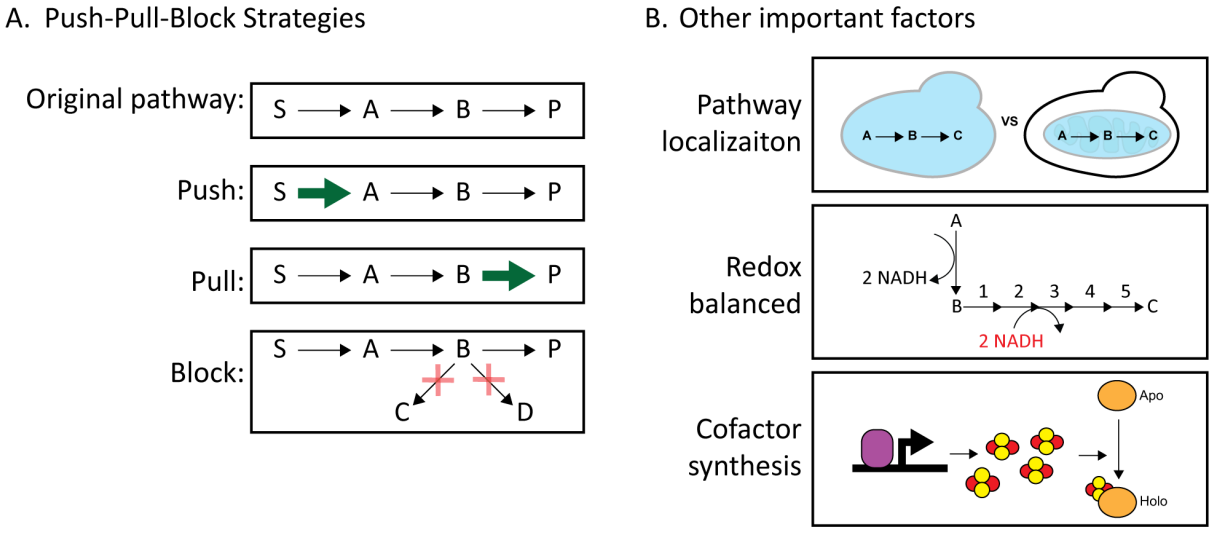


Figure 1.3: **Metabolic engineering strategies. a)** the push-pull-block strategy for increasing flux through a metabolic pathway. For the push strategy, the upstream portion of the pathway is generally targeted which saturates downstream pathway intermediates such that the downstream pathway is upregulated to achieve homeostasis. Conversely, for the pull strategy, the downstream portion of the pathway is generally targeted which helps reduce backwards pathway flux and depletes upstream pathway intermediates such that the upstream pathway is upregulated to achieve homeostasis. Lastly, the block strategy involves deleting or downregulating genes that encode enzymes that compete with the desired product's carbon flux **b)** Other variables that can be tuned to increase flux through a metbaolic pathway include enzyme localization, redox power and cofactor synthesis.

The process can be split into 2 steps.

1. Collect omics datasets.

2. Integrate omics data with models and interpret.

To understand cell metabolism at the systems-level, multiomics datasets including genomics (DNA), transcriptomics (RNA), proteomics (protein), and metabolomics (metabolite) can be collected [1]. These datasets offer a wealth of information, but extracting information from them is often nontrival. An easy an informative analysis effort for analyzing transcriptomics and proteomics datasets is hypergeometric testing. It uses statistical models to help summarize large datasets by determining if genes/proteins in your results are enriched for any particular attributes based off existing annotations [2].

Data can also be integrated with existing genome scale metabolic models (GEMs) [3]

or metabolism and expression models (MEs) [1] to provide a more comprehensive look into the metabolism of the production strain; by overlaying existing data onto models, one can uncover any discrepancies between experimental measurements and simulations and thus our understanding of the active metabolic pathways can be refined. Alternate methodologies like CAMEO [4], COBRA [5], and COSMOS [6], which are modeling packages can also be used to predict the effect of a metabolic alternation (gene knockout and/or overexpression) which can help determine the next metabolic engineering target. These models are extremely powerful, and can help minimize unnecessary trial-and-error type experiments. Model integration however often requires quantitative (absolute) data which is often not collected; for example, label-free proteomics is the most common proteomics method as it is simple and cost-effective, but it yields qualitative (relative) results. While there are methods to approximate quantitative data from label-free proteomics, like iBAq [7], the field is generally reluctant to use them due to their high error rate.

## 1.2 Motivation of this work

Greenhouse gas (GHG) emissions are the primary cause of human-induced climate change with the transportation sector being one of the largest contributors accounting for 29% of the total emitted GHGs [8]. Recent technologies with reduced GHG emissions have been of interest to try and combat the earth's rising temperatures. One such application is the generation of renewable alternative transportation fuels to replace the petroleum-based versions. The current biofuel industry in the United States primarily consists of corn-derived ethanol. However, food-based biomass feedstocks are not sustainable and they are insufficient to meet the current fuel demands so there has been extensive research into using lignocellulosic biomass (i.e. forest/agricultural wastes and residues, purpose-grown

grasses, and woody energy crops) as an alternative sustainable feed. Lignocellulosic biofuels have multiple advantages over corn-derived biofuels including having a 2-7 fold lower greenhouse gas (GHG) emission rate, having less land competition (don't compete with the food supply), and requiring 7-10 fold less pesticides [9]. Current next-generation biofuels research involves converting lignocellulosic biomass into higher molecular weight alcohols, such as isobutanol. Compared to ethanol, isobutanol has a higher energy density, a lower vapor pressure, a higher flash point, is less corrosive, and is less hydroscopic allowing it to be used as a true "drop-in replacement" with the current fuel pipping infrastructure and engines while being made in existing ethanol plants [10, 11]. Isobutanol is being made commercially by both Butamax and Gevo and has been successfully used as a 50/50 blend in US Army helicopters, affirming its use as a useful biofuel [12]. Additionally, it can be catalytically upgraded to diesel and jet fuels or used as a blend in gasoline up to 16% as approved by the EPA [13, 14]. While substantial progress has been made in commercially producing isobutanol via metabolic fermentations, the secrets remain elusive to academic researchers.

## 1.3 Objectives of thesis

The objective of this work was to understand how *S. cerevisiae*'s native metabolism can be rewiried for isobutanol production with the goal of converting lignocellulosic sugars into isobutanol for use as a specialty fuel. This requires the understanding of how yeast partition nutrients to growth, stress response, and desired products. Over the course of the thesis, we will see how metabolic engineering, systems biology, and protein engineering can be used to increase the production of the desired product, isobutanol.

### 1.3.1 Chapter 2

In Chapter 2, we do a deep dive of the literature to understand the challenges associated with creating a biomass-to-isobutanol producing yeast. Specifically, the first part dives into yeast's native ethanol-dominant metabolism, the second part dives into isobutanol metabolism, and the third part dives into using lignocellulosic biomass as a feedstock.

### 1.3.2 Chapter 3

In Chapter 3, we investigate how different metabolic engineering strategies affect the performance and physiology of isobutanol producing strains. Specifically, we combined transcriptomic, proteomic, and metabolomic analyses to generate a wealth of data on how enzyme pathway localization and redox cofactor-balancing affect isobutanol biosynthesis and physiology in genetically engineered *S. cerevisiae* strains. We show that localizing the isobutanol pathway enzymes to the cytosol resulted in lower titers due to a Fe-S cluster shortage from a limitation in cytosolic Fe–S cluster biogenesis machinery. We then demonstrate that this limitation could be overcome by increasing Fe uptake through the deletion of *FRA2*.

### 1.3.3 Chapter 4

In Chapter 4, we build upon our findings in Chapter 3 and investigated how different isobutanol enzyme orthologs and their gene dosage could affect isobutanol production. We constructed a combinatorial isobutanol pathway library that had variability introduced on 2 levels: coding sequences (homologs) and gene dosage (promoters). We then identified and characterized a high-flux isobutanol cassette by developing a high-throughput growth-coupled screen. We then aimed to balance the high-flux cassette's cofactor specificity with

glycolysis via protein engineering, but the resulting pathway's flux was too low to achieve anaerobic growth.

### 1.3.4 Chapter 5

In Chapter 5, we tackle the challenges associated with growing *S. cerevisiae* on lignocellulosic biomass. First, we focus on how *S. cerevisiae*'s tolerance to inhibitors, $\gamma$-valerolactone and levulinic acid, can be improved by 2 different strategies, chemical genomics and biodetoxification, respectively. We then focus on engineering a hydrolysate tolerant *S. cerevisiae* platform strain for increased isobutanol production by incorporating the findings from Chapter 3 and 4.

### 1.3.5 Chapter 6

Finally, in Chapter 6, we present the future directions of the work described here. First, we take a look at the additional follow-up experiments required to develop the hydrolysate-to-isobutanol producing *S. cerevisiae* strain with a focus on $\gamma$-valerolactone tolerance and xylose consumption. Then, we present the techniques that need to be further explored and implemented to push the carbon-to-isobutanol flux (multi-copy genomic integration and adaptive laboratory evolution).

# Chapter 2

# Literature review

**Authors and Contributors:**

- **Francesca V. Gambacorta** researched, wrote, and edited the manuscript.
- **Josh J. Dietrich** Aided in writing, editing, and reviewing section 2.1 concerning the Crabtree positive yeast, *S. cerevisiae*.
- **Dr. Qiang Yan** provided guidance, edited, and reviewed section 2.1 concerning the Crabtree positive yeast, *S. cerevisiae*.
- **Dr. Brian F. Pfleger** Provided guidance, edited, and reviewed the manuscript.

A section of this chapter (Section 2.1) was originally written as part of a review article in Current Opinion in Chemical Biology [15].

## 2.1 Challenges with engineering the Crabtree positive yeast *Saccharomyces cerevisiae*

The yeast *Saccharomyces cerevisiae* has long been an important species to humans, from its use in brewing and baking to its role as a model organism for studying eukaryotic biology. Over the past few decades, *S. cerevisiae* has also gained prominence as a platform for synthesizing chemical products due to several attractive attributes: a well-developed genetic toolkit [16][17]; fast growth (doubling time  90 min [18]); and tolerance to a variety of industrial stressors [19]. To date, *S. cerevisiae* has been engineered to produce molecules used in a wide variety of applications including: biofuels, pharmaceuticals, food additives, beauty agents, bulk-chemicals and specialty-chemicals [20, 12]. In order for these products to be produced economically, high titers, rates, and yields must be achieved in cultures grown on low-cost feedstocks. This means that metabolic engineering strategies must overpower the dominant native flux to ethanol. In other organisms, such as *Escherichia coli*, this can be simply accomplished by deleting the genes involved in ethanol biosynthesis [21]. Unfortunately, ethanol production is integrated with many central aspects of *S. cerevisiae* biology including regulation, substrate uptake, and energy generation. As such, substantial efforts have been undertaken in the metabolic engineering community to break *S. cerevisiae's* reliance on and preference for ethanol production.

The significance of ethanol production is clearly seen in the Crabtree-Warburg effect, a central feature of *S. cerevisiae* metabolism. Under glucose rich conditions, Crabtree-positive yeast ferment sugars into ethanol even under aerobic conditions. The Crabtree effect, thoroughly reviewed elsewhere [22, 23, 24], is triggered by overflow metabolism at the pyruvate node (short-term effect) and by glucose-driven repression of respiratory

enzymes (long-term effect). The evolutionary driving force behind the Crabtree effect is still debated [24, 25], but the leading theory opines that it is an economical approach to maximize growth (biomass generation), while minimizing resource allocation to protein synthesis [26]. The theory is supported by the fact that the catalytic capacity of fermentation is higher than respiration (more ATP is produced per protein mass) [26]. Simulations have also captured the Crabtree effect and overflow metabolism by using an enzyme-constraint based approach to optimize biomass generation in a genome-scale metabolic model [26, 27]. While advantageous in the natural world, these effects are not helpful to industrial chemical producing yeasts. Ethanol produced either via fermentation or the Crabtree effect reduces flux to desired chemical products and therefore needs to be by-passed to engineer industrially viable biocatalysts.

Efforts to eliminate ethanol production have proven challenging since ethanol synthesis plays an essential role in redox balance (i.e. reoxidizing NADH produced in glycolysis) and other aspects of *S. cerevisiae* biology. Non-ethanol producing strains have been created by deleting either the complete set of three pyruvate decarboxylases (*PDC1*, *PDC5*, and *PDC6*) [28] or the set of six alcohol dehydrogenases (*ADH1*, *ADH2*, *ADH3*, *ADH4*, *ADH5*, and *SFA1*)[29], which catalyze the final two catalytic steps in ethanol production respectively (Fig.2.1). Strains lacking these enzymes produce no ethanol but also experience severe physiological defects [30]. Complete deletion of Pdc activity prevents the production of acetaldehyde which in addition to being the substrate for ethanol production is also the primary precursor of cytosolic acetyl-CoA. Without supplementation of ethanol, acetate, or heterologous pathways discussed below, cells cannot produce sufficient acetyl-CoA flux to support fatty acid biosynthesis and other biosynthetic requirements. When supplemented, strains still grow slowly in part because cells are unable to rapidly

replenish the $NAD^+$ supply required for glucose catabolism. In the presence of high glucose concentrations, this redox imbalance is exacerbated by native regulation of key catabolic components. In summary, rerouting carbon flux away from ethanol requires an alternate, balanced, high-flux NADH-oxidizing pathway, an alternative cytosolic acetyl-CoA generation pathway, and fine-tuning of internal metabolic regulation.

### 2.1.1 Cytosolic acetyl-CoA generation in *S. cerevisiae* in the absence of ethanol synthesis

$Pdc^-$ strains are auxotrophic for C2-compounds due to their inability to produce cytosolic acetyl-CoA with the native pyruvate dehydrogenase (Pdh) bypass consisting of pyruvate decarboxylase (Pdc), acetaldehyde dehydrogenase (Ald), and acetyl-CoA synthetase (Acs) (Fig.2.1). Acetyl-CoA supply is further complicated by the fact that in eukaryotes it cannot transverse the membranes of subcellular compartments such that mitochondria-made acetyl-CoA cannot be directly exported to the cytosol. Some reports propose that evolved $Pdc^-$ strains circumvent this barrier through use of a CoA-transferase, Ach1p, that converts acetyl-CoA into acetate which can cross into the cytosol and subsequently be reactivated as acetyl-CoA at the cost of ATP [31]. Another report suggests that the native shuttle system is not sufficient [32]. Alternatively, the C2-auxotrophy can be circumvented by providing a heterologous synthesis pathway or by supplementation with a C2-compound (ethanol or acetate). Alternative acetyl-CoA producing pathways include: pyruvate-formate lyase (Pfl), acetylating acetaldehyde dehydrogenase (A-Ald), cytosolic-pyruvate dehydrogenase ($Pdh_{cyto}$), pyruvate oxidase (Po)/phosphotransacetylase (Pta), phosphoketolase (Pk)/phosphotransacetylase (Pta), threonine aldolase (Gly), carnitine shuttle (Cat), and citrate-oxaloacetate shuttle (Cit/Acl) (Fig.2.1) [33, 34]. The genetics

and biochemistry of these pathways is thoroughly reviewed in reference [34]. While many alternative pathways exist, heterologous expression by itself is not sufficient to restore growth in a Pdc$^-$ strain to wild-type levels. As discussed below, additional modifications are necessary, but overcoming acetyl-CoA auxotrophy is a critical first step.

### 2.1.2 Balancing NAD$^+$ regeneration with glycolysis in the absence of ethanol synthesis

It is widely known that ethanol is produced during yeast fermentation in order to regenerate the NAD$^+$ needed to enable glycolysis. Analogously, when oxygen is available, non-ethanol producing yeast grown in glucose-limited conditions regenerate NAD$^+$ through oxidative phosphorylation, which can support a low glycolytic flux. However, at high glucose concentrations, genes involved in oxidative phosphorylation are downregulated while genes involved in glucose transport and glycolysis are upregulated [35]. This phenomenon is controlled by the three glucose sensing systems (Rgt2p/Snf3p, Snf1p/Mig1p, and cAMP/PKA; see Figure 3 of reference [36] for a detailed depiction) and is associated with the Crabtree effect [23, 36]. Elevated rates of glucose import ultimately lead to an increased glycolytic flux above the catalytic capacity of the respiratory chain, resulting in insufficient NAD$^+$ regeneration and a bottleneck in the catabolism of glucose [22]. The bottleneck is caused in part by the indirect repression of the mitochondrial pyruvate dehydrogenase (Pdh) by Mig1p [37]. Thus, under excess glucose conditions, non-ethanol producing strains do not grow due to the NADH/NAD$^+$ redox imbalance caused by a metabolic bottleneck at the pyruvate node. Strategies to overcome the imbalance include relieving glucose repression caused by the Crabtree-effect, restricting glucose uptake, downregulating glycolytic flux, providing alternative redox sinks, and throttling

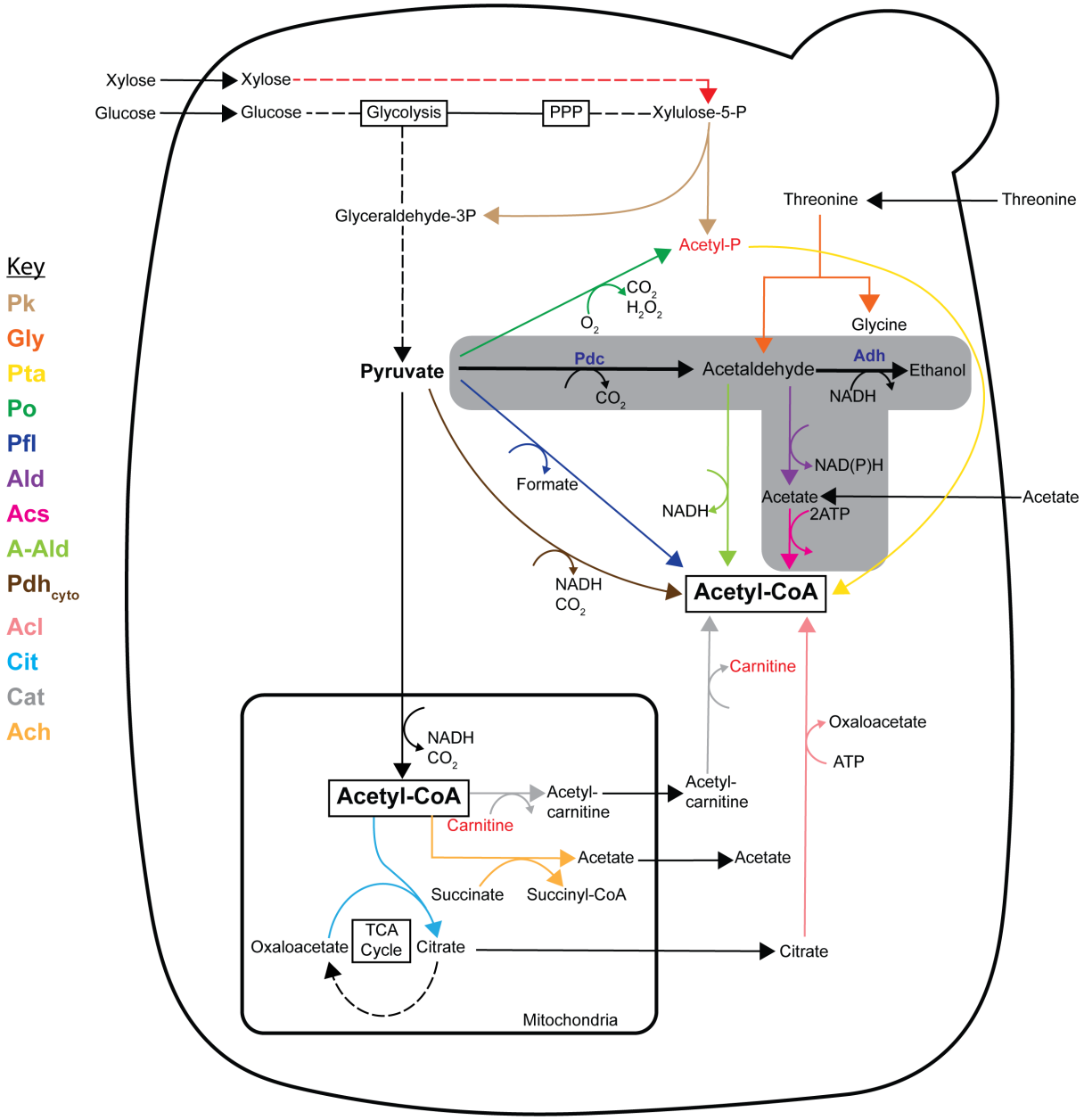


Figure 2.1: **Metabolic map of native and heterologous acetyl-CoA biosynthetic pathways in *S. cerevisiae*.** Naturally, cytosolic acetyl-CoA is derived from the pyruvate dehydrogenase (Pdh) bypass consisting of pyruvate decarboxylase (Pdc), acetaldehyde dehydrogenase (Ald, purple), and acetyl-CoA synthetase (Acs, pink); ethanol is also derived from an intermediate in this bypass (grayed box). Other native metabolic pathways include threonine aldolase (Gly, dark orange) and the mitochondrial shuttle system consisting of a CoA-transferase (Ach1, light orange). Heterologous tested pathways for the synthesis of cytosolic acetyl-CoA include the following: phosphoketolase (Pk, tan), phosphotransacetylase (Pta, yellow), pyruvate oxidase (Po, dark green), pyruvate-formate lyase (Pfl, dark blue), acetylating aldehyde dehydrogenase (A-Ald, light green), pyruvate dehydrogenase ($Pdh_{cyto}$, brown), citrate lyase (Acl, light pink), citrate synthase (Cit, light blue), and carnitine acetyl-CoA transferase (Cat, gray). Non-native metabolites (acetyl-P and carnitine) and pathway (xylose catabolism) are indicated in red.

the delivery of glucose to cells with fed-batch bioreactors [38].

#### 2.1.2.1 Adaptive Laboratory Evolution to enhance growth of Pdc$^-$ strains on glucose

Adaptive laboratory evolution (ALE) has been widely used to enhance growth of Pdc$^-$ strains on glucose since the early 2000s. Recent efforts have tried to understand the role and optimize the function of ALE-created mutations in regulating glucose catabolism, ethanol production, and the Crabtree effect. Through multiple studies, researchers identified mutations or deletions in *MTH1*, a transcriptional repressor in the Rgt2p/Snf3p glucose-sensing cascade involved in hexose transporter (Hxt) expression [30, 32, 39, 40]. These mutations reduce expression of the Hxts, thereby limiting glucose uptake and preventing the respiratory chain from being overloaded. Cells carrying a *mth1* mutation can grow on glucose because glucose-repression is alleviated, however, growth comes at a reduced rate (less than 30% of Pdc$^+$ strains), which is insufficient for industrial purposes. In an attempt to overcome the growth rate limitation, researchers performed extra rounds of ALE starting with strains carrying the *mth1* mutation and isolated a strain with a higher growth rate when grown on 2% glucose. The resulting strain had a mutation in *YAK1* and a growth rate that increased 2.5-fold over the base strain, albeit at rates still below the Pdc$^+$ parent [41]. *YAK1* encodes a serine/threonine protein kinase involved in regulating cell growth in the presence of glucose. In a separate study, downregulating *PYK1*, a.k.a. *CDC19*, which encodes the major pyruvate kinase, was also shown to relieve glucose repression in the context of another Pdc$^-$ strain [42]. Pyk1p is considered a control node in glycolysis and its activity is tightly regulated by fructose-1,6-biphosphate (FBP) concentrations. Engineering the allosteric sites on Pyk1p could be an alterna-

tive strategy to the regulatory approaches discovered in the evolutionary studies. While ALE has provided the initial insights into the importance of the regulatory network in allowing Pdc$^-$ strains to grow on glucose, the problem is not yet solved. Evolved mutants often have undesirable characteristics, such as lower than wild-type growth, that must be overcome before these strains can become useful platforms for bioproduction.

#### 2.1.2.2 Rational re-wiring of native sugar metabolism regulation

Increasing the catalytic capacity of the respiratory chain by rational engineering is also a valid yet underdeveloped strategy for enabling Pdc$^-$ strains to grow on glucose. The signaling and regulation involved in the Crabtree effect have been heavily studied, and recent work has shown that the Snf1p/Mig1p glucose repression pathway [43] as well as the ratio of glucose-6-phosphate (G6P) to FBP [44] is directly linked to the Crabtree phenotype. The Snf1p signaling pathway negatively regulates genes associated with the uptake and catabolism of non-glucose sugars and expression of gluconeogenesis, respiratory, and Hxt genes by direct interaction with many transcription factors such as Mig1p, Rgt1p, Msn2p, and Cat8p [23, 37]. Deletion of *SNF1*, *HXK2*, or *MIG1* increases respiratory capacity and reduces overflow metabolism, suggesting that these regulators are promising targets for shifting production from ethanol to other compounds [43, 45]. This strategy is supported by increased transcript levels of Mig1p-mediated repressed genes in Pdc$^-$ strains that have undergone ALE [40]. Tps1p is also an important glycolytic regulator that has been recently linked to Snf1p signaling and may provide another engineering target [46]. The intentional rewiring of regulation is a promising strategy for increasing the growth rates of Pdc$^-$ strains by increasing the respiratory capacity rather than limiting sugar metabolism. Furthermore, it could allow for intentional tuning of metabolism while min-

imizing undesirable effects. Alternatively, non-Crabtree yeasts such as *Kluyveromyces. lactis*, which natively contain the desired regulatory structure, could be engineered to produce desired products.

#### 2.1.2.3 NADH-oxidation coupled to pyruvate-derived metabolites

While strategies that reduce glucose import lead to improved growth, the glucose utilization rate is an important parameter in industrial bioprocessing that should be as large as possible. Alternatively, the NADH/$NAD^+$ redox balance in $Pdc^-$ strains can be maintained by producing products that require the same amount of reducing equivalents as ethanol. Pyruvate is a common metabolic node from which these products are derived (Fig.2.2). Products such as 2,3-butanediol [39, 41, 47, 48, 49, 50] and lactate [51, 52, 53, 54, 55] can directly replace ethanol fermentation and each product has been produced in substantial quantities in $Pdc^-$ strains. Malate production is also redox-balanced with glycolysis, but requires ATP [56]. Other desirable products such as isobutanol and free fatty acids require NADPH reducing equivalents, necessitating a means for converting glycolytic NADH into NADPH [42, 57]. This can be overcome by introducing a transhydrogenase reaction ($NADPH + NAD^+ \Longleftrightarrow NADP^+ + NADH$) into *S. cerevisiae* [42, 58, 59]. Heterologous expression of an *E. coli* transhydrogenase in *S. cerevisiae* has been shown to increase growth and pyruvate production [60]. Similarly, relocalization of *S. cerevisiae* malic enzyme to the cytosol creates a transhydrogenase cycle that has been shown to improve isobutanol production [61]. Alternatively, diverting carbon from glycolysis into the pentose phosphate pathway makes more NADPH available and can increase both free fatty acid [42] and isobutanol [62] production. Engineering NADPH-dependent enzymes to instead utilize NADH is another approach and has been

demonstrated in isobutanol production, though with limited effect on production in *S. cerevisiae* [57, 63].

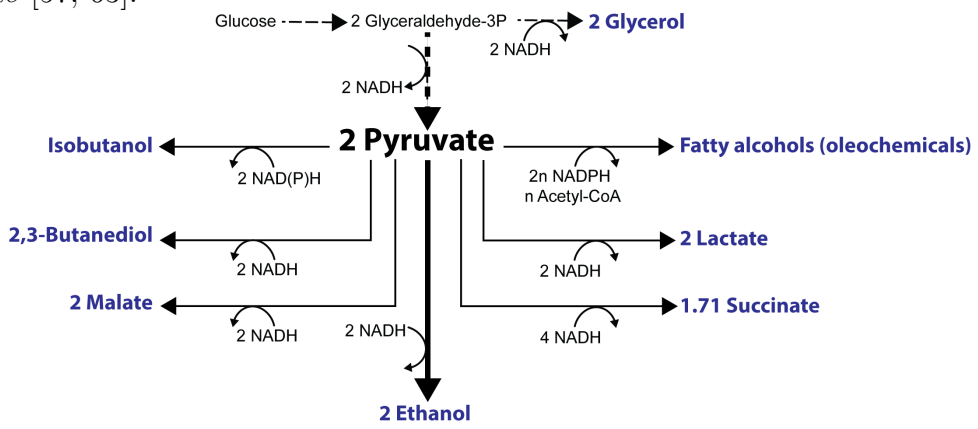


Figure 2.2: **Schematic depicting pyruvate-derived products.** Glycerol, malate, lactate, and succinate [64] production require NADH reducing equivalents, while isobutanol and fatty alcohols/other oleochemicals require NADPH reducing equivalents.

#### 2.1.2.4 Regenerating $NAD^+$ for anabolism

Although replacing ethanol with other products can balance glycolytic NADH generation, *S. cerevisiae* anabolism also produces NADH, which is normally balanced by glycerol production [65]. Glycerol production in *S. cerevisiae* can divert up to 8.5% of carbon, making its removal via GPD1 and GPD2 deletion a common metabolic engineering strategy, even when ethanol is the desired product [66]. However, glycerol is important in *S. cerevisiae* osmotic tolerance so completely blocking its synthesis is often undesirable [67]. Glycerol formation can be reduced by providing other routes to oxidize NADH, such as through succinate production, which requires two reducing equivalents per pyruvate. Succinate has been produced in $Pdc^-$ *S. cerevisiae* in significant amounts, but only under aerobic conditions [68, 69]. Other NADH oxidizing routes include heterologous expression of a water-forming NADH oxidase [47, 50] or an alternative oxidase [22]. These enzymes require aerobic conditions to function, and thus, it is common to see them used under semi-aerobic conditions with a fermentation product. Carbon fixation is also a

common sink of excess reducing power in photoautotrophs. When Calvin-cycle enzymes RuBisCo and phosphoribulokinase were heterologously expressed in *S. cerevisiae*, it coupled NADH oxidation with $CO_2$ reduction and significantly decreased glycerol production [70]. Acetate, which is present in high amounts in lignocellulosic hydrolysates, can also be fermented into ethanol to oxidize residual NADH via Ald and Adh and reduce glycerol formation (Fig.2.1) [71][56]. In many cases, it may be possible to couple NADH recycling with production of a desired product. In others, feedstocks may need to be optimized such that redox balance, ATP generation, and product synthesis are optimized.

### 2.1.3 Metabolic rewiring to reduce ethanol production without its complete elimination

#### 2.1.3.1 Redirecting flux using metabolic circuits

Controlling when and where carbon flux is directed in a fermentation process can be achieved with dynamic control strategies, including inducible metabolic valves [72, 73, 74]. In practice, the fermentation occurs in alternating decoupled phases (growth and production). During the growth phase, biomass generation is promoted via $NAD^+$ regeneration through ethanol fermentation as flux is directed through glycolysis. During the production phase, ethanol flux is restricted and resources are directed toward a product of interest. This switch is achieved by turning on transcription of pathway genes using either a chemical inducer or light via an optogenetics switch. The balance between growth and product synthesis has been successfully demonstrated with isobutanol production [75, 76]. Expansion of this idea will depend on finding ways to minimize the amount of time cells spend in the biomass generation phase such that maximum titers, rates, and yields of products can be achieved.

#### 2.1.3.2 Nonpreferreed carbon sources

Many of the challenges to removing ethanol production depend on glucose being present. Using alternative carbon sources, such as xylose or glycerol that do not induce the Crabtree effect, is another way to decrease ethanol production [77, 78, 79]. *S. cerevisiae* cannot naturally assimilate xylose, but xylose catabolism has been extensively studied and introduced into yeast by many groups [80, 81]. In one case, isobutanol-producing strains generated 2-fold less ethanol and 6-fold more isobutanol when grown on xylose instead of glucose [78]. Improved performance is not restricted to xylose. In another case, a strain produced 1.5-fold more 1,2-propanediol than ethanol when grown on glycerol [82]. Recently, there has also been interest in the generation of xylose-utilizing $Pdc^-$ strains for generating pyruvate-derived products, but the strains suffer from low productivities due to slow growth [83, 84, 85]. While catabolism of xylose and glycerol has proved beneficial in decreasing ethanol production in defined media on a lab scale, the ultimate application will be growth of $Pdc^-$ strains on lignocellulosic hydrolyzates containing mixtures of sugars, organic acids, and inhibitors.

### 2.1.4 Recent engineering strategies to increase production of non-ethanol products

The metabolic engineering community has leveraged many of the strategies described earlier to improve the production of non-ethanol products. In Table.2.1, we summarize recent studies by tabulating the approaches used and commonly reported performance metrics for several key products.

Table 2.1: Summary of strategies for non-ethanol chemical production in *S. cerevisiae*

| References | PDC⁻ phenotype | Relieve Crabtree effect | Alternate acetyl-CoA routes | $NAD^+$ regeneration | Control of ethanol production | Alternate carbon source | Product(s) | Yield (g/g carbon source) | Titer (g/L) |
|---|---|---|---|---|---|---|---|---|---|
| [86] | ✓ | ✓ | ✓ | | | | *Acetate* | 0.14[a] | <0.5 |
| | | | | | | | *Pyruvate* | 0.007[a] | <0.5 |
| [39] | ✓ | ✓ | | ✓ | | | **2,3-Butanediol** | 0.28 | 96.2 |
| | | | | | | | *Glycerol* | 0.09[a] | >30[c] |
| | | | | | | | *Acetoin* | 0.01[a] | ∼5 [c] |
| [47] | ✓ | | | ✓ | | | **2,3-Butanediol** | 0.407 | 72.91 |
| | | | | | | | *Acetoin* | 0.01[a] | 1.38 |
| [48] | ✓ | | | ✓ | | | **2,3-Butanediol** | 0.359 | 32.31[c] |
| | | | | | | | *Glycerol* | 0.069 | 6.21[c] |
| | | | | | | | *Acetoin* | 0.052 | 4.68[c] |
| [49] | ✓ | | ✓ | ✓ | | | **2,3-Butanediol** | 0.404 | 154.3 |
| | | | | | | | *Glycerol* | 0.088 | 33.5[c] |
| | | | | | | | *Acetate* | 0.006[a] | 2.3 |
| [50] | ✓ | ✓ | ✓ | ✓ | | | **2,3-Butanediol** | 0.462 | 108.6 |
| | | | | | | | *Acetoin* | 0.02[a] | 4.6 |
| | | | | | | | *Acetate* | 0.0004[a] | 0.1 |
| [41] | ✓ | ✓ | | ✓ | | | **2,3-Butanediol** | 0.27 | 81 |
| | | | | | | | *Glycerol* | 0.239[a] | 71.8 |
| | | | | | | | *Succinate* | 0.013[a] | 4 |
| [87] | ✓ | | | ✓ | | | **n-Butanol** | 0.012 | 0.13 |
| | | | | | | | *Ethanol* | 0.1 | ∼1[c] |
| | | | | | | | *Glycerol* | 0.17 | ∼2[c] |
| [57] | ✓ | ✓ | | ✓ | | | **Isobutanol** | 0.0074[a] | [b] |
| | | | | | | | *Ethanol* | 0.033[a] | [b] |
| | | | | | | | *Glycerol* | 0.26[a] | [b] |
| | | | | | | | *Pyruvate* | 0.02[a] | [b] |
| | | | | | | | *2,3-butanediol* | 0.325[a] | [b] |
| | | | | | | | *Dihydroxyisovalerate* | 0.05[a] | [b] |
| | | | | | | | *Isobutyrate* | 0.03[a] | [b] |
| [76] | | | | ✓ | ✓ | | **Isobutanol** | 0.0535 | 8.49 |
| | | | | | | | **2-Methyl-1-butanol** | 0.01417 | 2.38 |
| | | | | | | | *Ethanol* | 0.187 | 39.8 |
| | | | | | | | *Glycerol* | [b] | [b] |
| [42] | ✓ | ✓ | ✓ | ✓ | | | **Free fatty acids** | 0.1 | 25 |
| | | | | | | | *Glycerol* | [b] | [b] |

| References | PDC⁻ phenotype | Relieve Crabtree effect | Alternate acetyl-CoA routes | $NAD^+$ regeneration | Control of ethanol production | Alternate carbon source | Product(s) | Yield (g/g carbon source) | Titer (g/L) |
|---|---|---|---|---|---|---|---|---|---|
| | | | | | | | **Malic acid** | 0.31[a] | 59 |
| | | | | | | | *Succinate* | 0.04[a] | 8 |
| [56] | ✓ | ✓ | | ✓ | | | *Glycerol* | 0.13[a] | 25 |
| | | | | | | | *Pyruvate* | 0.02[a] | 3 |
| | | | | | | | *Fumarate* | 0.01[a] | 2 |
| | | | | | | | **Succinic acid** | 0.044[a] | 2.2 |
| [69] | ✓ | ✓ | | ✓ | | | *Pyruvate* | 0.364[a] | 18.2 |
| | | | | | | | *Malate* | 0.022[a] | 1.1 |
| | | | | | | | *Glycerol* | 0.076[a] | 3.8 |
| | | | | | | | **Gluconate** | [b] | 2.31 |
| [75] | | | | ✓ | ✓ | | *Ethanol* | [b] | 1.01 |
| | | | | | | | *Glycerol* | [b] | [b] |
| | | | | | | | **Lactic acid** | 0.6 | 80 |
| [55] | ✓ | | | ✓ | | | *Ethanol* | 0.01 | 1.6 |
| | | | | | | | *Glycerol* | 0.02 | 2.6 |
| [54] | | | | ✓ | | | **Lactic acid** | 0.8 | 112 |
| | | | | | | | *Ethanol* | 0.02[a] | 2.6 |
| | | | | | | | **Lactic acid** | 0.43[a] | 7.8 |
| [84] | ✓ | | | ✓ | | ✓ | *Acetate* | 0.16[a] | 3[c] |
| | | | | | | | *Xylitol* | 0.01[a] | 0.17[c] |
| | | | | | | | **Lactic acid** | 0.67 | 60 |
| | | | | | | | *Ethanol* | 0.01[a] | <1 |
| [85] | | | | ✓ | | ✓ | *Xylitol* | 0.01[a] | <1 |
| | | | | | | | *Glycerol* | 0.01[a] | <1 |
| | | | | | | | *Acetate* | 0.01[a] | <1 |
| | | | | | | | **2,3-Butanediol** | 0.46[a] | 96.8 |
| [83] | ✓ | | ✓ | ✓ | | ✓ | *Glycerol* | 0.11[a] | 23.3 |
| | | | | | | | *Ethanol* | 0.08[a] | 16.3 |
| | | | | | | | *Xylitol* | 0.03[a] | 5.9 |
| | | | | | | | **2,3-Butanediol** | 0.26[a] | 43.6 |
| [88] | ✓ | | | ✓ | | ✓ | *Glycerol* | 0.26[a] | 45 |
| | | | | | | | *Xylitol* | 0.03[a] | 4.7 |
| | | | | | | | **Isobutanol** | 0.026[a] | 2.6 |
| [78] | | | | ✓ | | ✓ | *Ethanol* | 0.275[a] | ∼27.5[c] |
| | | | | | | | *Glycerol* | 0.10[a] | ∼10[c] |
| | | | | | | | **Isobutanol** | 0.0196 | 3.1 |
| | | | | | | | **2-Methyl-1-butanol** | 0.0053 | 0.79 |
| [77] | | | | ✓ | | ✓ | *Ethanol* | 0.32[a] | <50[c] |
| | | | | | | | *Glycerol* | [b] | [b] |

| References | PDC⁻ phenotype | Relieve Crabtree effect | Alternate acetyl-CoA routes | $NAD^+$ regeneration | Control of ethanol production | Alternate carbon source | Product(s) | Yield (g/g carbon source) | Titer (g/L) |
|---|---|---|---|---|---|---|---|---|---|
| [82] | | | ✓ | | ✓ | | **1,2-Propanediol** | 0.129 | 4.3 |
| | | | | | | | *Ethanol* | ∼0[a] | ∼0[c] |

(**Bold** = product of interest)
(*Italics = by-product*)
Absence of ethanol or glycerol in a row indicates it was not detected or that the yield or titer was <0.01
[a] = Yield not directly reported. Yield is either read from a graph, converted from a molar yield, calculated as g/g consumed carbon source, or calculated by dividing production rate by carbon source uptake rate
[b] = Not reported.
[c] = Titer not directly reported. Titer is either read from a graph, converted from molar concentration, or calculated as g/L fed carbon source, which is quantified by multiplying the reported yield (g/g carbon source) by the carbon source concentration (g/L).

## 2.2 Isobutanol production from branched chain amino acid biosynthesis and the Ehrlich pathway

Naturally, *S. cerevisiae* has the capacity to produce a variety of fusel alcohols from amino acid degradation via the Ehrlich pathway enzymes. In brief, there are three enzymatic steps in the Ehrlich pathway to convert an amino acid into a fusel alcohol: transamination, decarboxylation, and reduction; branched-chain amino acid catabolism is described in Fig.2.3 where isobutanol is derived from valine, 3-methyl-1-butanol from leucine, and 2-methyl-1-butanol from isoleucine. *S. cerevisiae* can also use the Ehrlich pathway to produce fusel alcohols from aromatic amino acids (phenylalanine, tyrosine, and tryptophan) and the sulfur-containing amino acid, methionine; the pathways are thoroughly reviewed here [89].

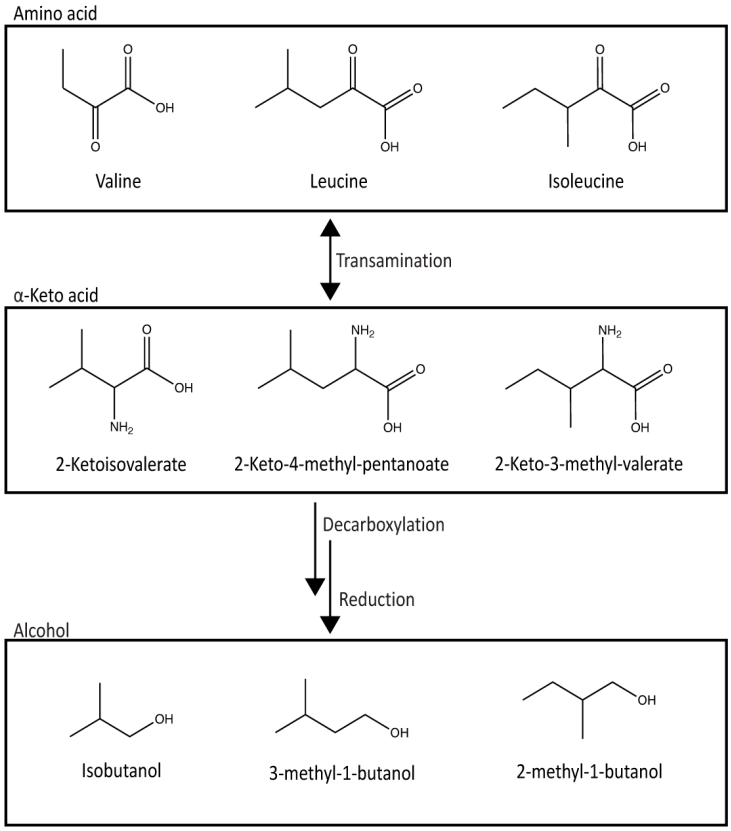


Figure 2.3: **Ehrlich pathway**. Catabolism of branched-chain amino acids into fusel alcohols.

*S. cerevisiae* synthesizes isobutanol, from pyruvate via enzymes involved in valine biosynthesis and the Ehrlich pathway. Specifically, the first half of the pathway converts pyruvate to $\alpha$-ketoisovalerate (KIV) by mitochondrial-localized ILVp enzymes: acetolactate synthase (ALS, encoded by *ILV2*), a NADPH-dependent ketol-acid reductoisomerase (KARI, encoded by *ILV5*), and a 2Fe-2S cluster-requiring dihydroxyacid dehydratase (DHAD, encoded by *ILV3*). The second part of the pathway, the Ehrlich pathway, converts KIV to isobutanol by promiscuous cytosolic enzymes: ketoacid decarboxylase (KDC, encoded by pyruvate decarboxylases, *PDC1*, *PDC5* or *PDC6*, or phenylpyruvate decarboxylase, *ARO10*) and a NADH-dependent alcohol dehydrogenase (ADH, encoded by *ADH1-5*) (Fig.2.4).

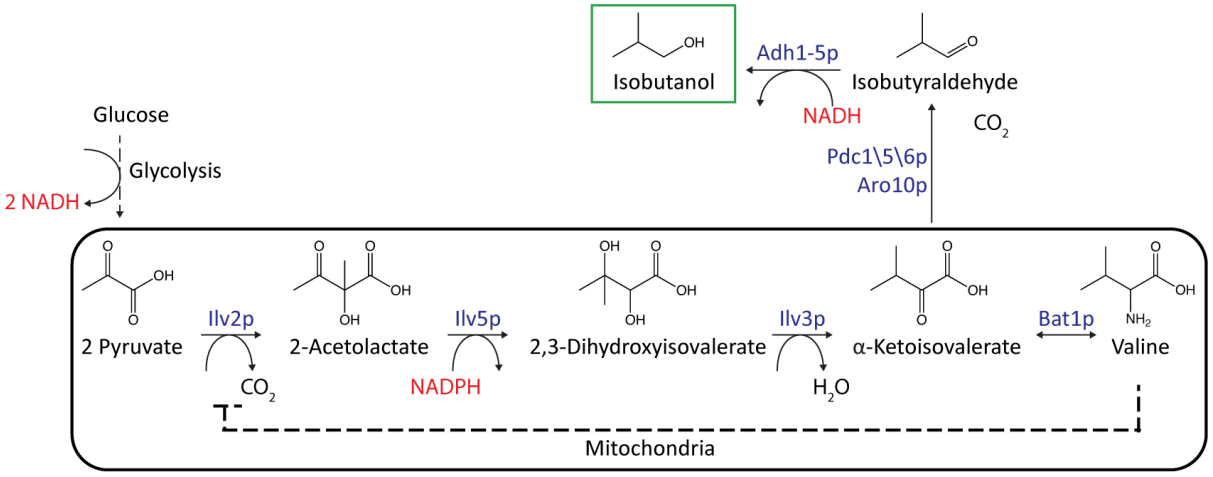


Figure 2.4: **Isobutanol biosynthesis pathway in *S. cerevisiae*.** Shows the endogenous isobutanol synthesis pathway from pyruvate. The first half of the pathway converts pyruvate to $\alpha$-ketoisovalerate (KIV) by the mitochondrial-localized valine biosynthesis enzymes Ilv2p, Ilv5p, and Ilv3p. The second part of the pathway, the Ehrlich pathway, converts KIV to isobutanol by promiscuous cytosolic-localized decarboxylase enzymes Pdc1/5/6p or Aro10p and Adh1-5p.

### 2.2.1 Engineering *S. cerevisiae* for microbial production of isobutanol from glucose

*S. cerevisiae*'s native isobutanol production is low ($<$ 1% of the theoretical maximum yield) as most of the glucose is directed towards ethanol production as part of the Crabtree effect (see section 2.1). High-yielding isobutanol producing strains have been reported in industry (Gevo has achieved at least 83% of the theoretical maximum yield [10]) but the research approaches used remain elusive to academic researchers. Academica has implemented a variety of metabolic engineering strategies in efforts to increase production however, to date, only 15% of the theoretical maximum yield has been achieved [90]. The main limitation academic researchers encounter is accumulation of pathway intermediates and by-product formation. The following sections will describe the metabolic engineering strategies implemented (also reviewed [91]) and then the most successful approaches used in academic literature will be tabulated.

#### 2.2.1.1 Pathway overexpression

There have been three common routes taken in academic literature to overexpress the isobutanol pathway enzymes: one, manipulate the endogenous (native) isobutanol pathway in *S. cerevisiae*; establish a heterologous (non-native) isobutanol pathway; three, a combination of the two. Using the native pathway enzymes is beneficial if expressing heterologous enzymes proves difficult, however, heterologous enzymes or homologs from different organisms may have a higher activity than endogenous enzymes. There have been several studies conducted to identify highly active variants for each step in the 5-step isobutanol pathway (see section 5.3.1 for details) [41, 92, 93, 94, 95]. The most utilized heterologous variants in literature are for the 2$^{nd}$ and 5$^{th}$ step in the pathway: ketol-acid reductoisomerase, $ilvC^{P2D1\text{-}A1}$, from *Escherichia coli* [92] and alcohol dehydrogenase, $adhA^{29C8}$, from *Lactococcus lactis* [95].

#### 2.2.1.2 Pathway compartmentalization

The native isobutanol pathway enzymes in *S. cerevisiae* are spatially segregated to multiple compartments, both the mitochondria and the cytosol. Many have opted to overcome this spatial segregation by localizing the five-step pathway into the cytosol; this can be achieved by using heterologous cytosolic-localized enzymes (typically from bacteria) or by removing the mitochondrial localization sequence (MLS) from the genes in *S. cerevisiae*'s native valine biosynthesis pathway (*ILV2*, *ILV5*, and *ILV3*) [96, 97]. It has been proposed that a cytosolic localization would be preferable in the context of industrially relevant conditions such as high glucose concentrations or anaerobic growth. This is in part because the mitochondria are known to enter a minimal energy-requirement mode under those conditions [98, 99]. Additionally, a cytosolic localization would eliminate any bottleneck

associated with the need to transport intermediates in/out of the mitochondria. Others have opted to overcome this spatial segregation by localizing the five-step pathway into the mitochondria; this can be achieved by using heterologous mitochondrial-localized enzymes (typically from fungi), adding a MLS to heterologous cytosolic-localized enzmyes, or by adding a MLS to the *S. cerevisiae*'s native Ehrlich pathway enzymes (*PDC1/5/6* or *ARO10* and *ADH1-5*). It has been proposed that a mitochondrial localization would increase the availability of enzyme and pathway intermediates and reduce the loss of intermediates to competing pathways [96]. Both pathway localizations have achieved similar isobutanol titers and yields (Table.2.2).

Table 2.2: Highlight report of engineered *S. cerevisiae* strains for isobutanol production

| Pathway localization | $NAD^+$ regeneration | Overexpress IBA genes | Block competing pathway | Metabolic control of ethanol production | **Isobutanol titer** (mg/L) | **Isobutanol yield** (mg/g carbon source) | **Refs** | **Year** |
|---|---|---|---|---|---|---|---|---|
| Mito | | ✓ | | | 635 +/- 23 | 6.4 +/- 0.2 | [96] | 2013 |
| Cyto | | ✓ | ✓ | | 630.27 +/- 14.18 | 14.86 +/- 0.55 | [97] | 2012 |
| Cyto and mito | ✓ | ✓ | ✓ | | 1620 +/- 110 | 16.0 +/- 1.0 | [61] | 2013 |
| Mito | | ✓ | ✓ | | 1245 +/- 33 | 12.45 | [100] | 2017 |
| Cyto and mito | ✓ | ✓ | ✓ | | 224 +/- 5 | 12.04 +/- 0.23 | [59] | 2015 |
| Cyto and mito | | ✓ | ✓ | | 330.9 | 16.55 | [101] | 2016 |
| Cyto | | ✓ | ✓ | | 2090 | 59.55 | [90] | 2019 |
| Cyto | | ✓ | ✓ | | 263.2 | 13.16 | [102] | 2019 |
| Mito | | ✓ | ✓ | ✓ | 8494.6 +/- 305.3 | 53.5 +/- 8.4 | [76] | 2018 |
| Cyto | ✓ | ✓ | ✓ | | 148 +/- 24 | 7.4 +/-1.2 | [57] | 2016 |
| Mito | | ✓ | | | 2600 | 26 | [78] | 2019 |
| Mito | | ✓ | | | 3100 ± 180 | 38.8 ± 2.4 | [77] | 2019 |
| Mito | | ✓ | | ✓ | 167.2 | 3.4 | [75] | 2016 |
| Cyto and mito | | ✓ | ✓ | | 283 ± 13 | 11.46 | [62] | 2017 |
| Cyto and mito | | ✓ | | | 85.2 | 2.13 | [103] | 2011 |

#### 2.2.1.3 Pathway redox-balancing

The native isobutanol pathway is redox cofactor-imbalanced with glycolysis; glycolysis produces two NADH per molecule of glucose, while isobutanol production consumes one NADPH by *ILV5* and one NADH by *ADH* resulting in an NADPH shortage and NADH excess. Overcoming this redox cofactor-imbalance is necessary to increase isobutanol production. One strategy to overcome the imbalance involves using a heterologous NADH-dependent KARI, such as the *E. coli* KARI variant, $ilvC^{P2D1\text{-}A1}$, that was previously engineered with improved specificity towards NADH [63, 92]. Another is to necessitate a means for converting glycolytic NADH into NADPH [42, 57] (See section 2.1.2.3 for details); in brief, introduction of a transhydrogenase reaction ($NADPH + NAD^+ \Longleftrightarrow NADP^+ + NADH$) via heterologous expression or relocalization of native *S. cerevisiae* enzmyes has been shown to improve isobutanol production [42, 58, 59, 60, 61].

#### 2.2.1.4 Eliminating by-product formation

The isobutanol pathway has a number of competing pathways including: acetyl-CoA, oxaloacetate, ethanol, lactate, and malate production from the pyruvate node; 2,3-butanediol and 2,3-dihydroxy-2-methyl butanoate production from the 2-acetolactate node; valine, leucine, and pantothenate production from the $\alpha$-ketoisovalerate node; and isobutyric acid production from the isobutyraldehyde node (Fig.2.5). Of these competing pathways, ethanol remains the main byproduct however there has been some success in deleting other non-essential competing pathways to boost production. Wess et. al. achieved the highest isobutanol yield reported in literature, 59.55 mg isobutanol / g glucose [90]; this was achieved in a strain with a cytosolic-localized isobutanol pathway and by blocking a number of non-essential isobutanol competing pathways, JWY23 ($\triangle ilv2$;

$\triangle bdh1$; $\triangle bdh2$; $\triangle leu4$; $\triangle leu9$; $\triangle ecm31$; $\triangle ilv1$; $\triangle adh1$; $\triangle gpd1$; $\triangle gpd2$; $\triangle ald6$). While high isobutanol yields were achieved in JWY23, 3-fold more ethanol (~6 g/L) than isobutanol (~2 g/L) was produced indicating more engineering is required to establish isobutanol as the main fermentative product in yeast. Milne et. al. and Kondo et. al. have made attempts to eliminate ethanol production by the generation of a PDC$^-$ strain, however, growth is severely inhibited as flux through the isobutanol pathway is too low to replenish the NAD$^+$ equivalents needed for glycolysis and cell growth [57, 104]. Additional engineering is required to enhance flux through the pathway before ethanol production can be completely eliminated.

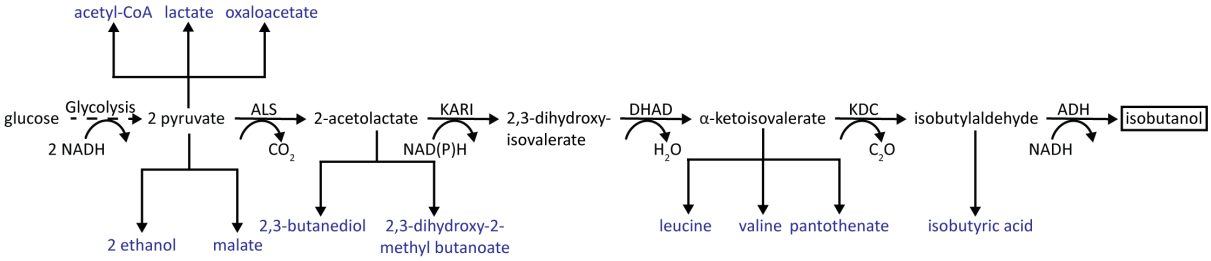


Figure 2.5: **Isobutanol competing pathways in *S. cerevisiae*.** Adapted from [90].

## 2.3 Challenges associated with engineering *S. cerevisiae* for microbial production of isobutanol from biomass

In order for isobutanol production to be economically viable, high titers, rates, and yields must be achieved with cultures grown on low-cost feedstocks such as lignocellulosic biomass (i.e. forest/agricultural wastes and residues, purpose-grown grasses, and woody energy crops). In general, biomass consists of 30-50% cellulose (a polymer of glucose), 15-35% hemicellulose (a heteropolymer of glucose and pentoses), and 10-30% lignin (a

complex polymer of crosslinked aromatic units) [105]. A thermo-chemical pretreatment and hydrolysis (chemical or enzymatic) step are required to liberate the monosaccharides, pentose and hexose sugars, from the polysaccharide hemicellulose and cellulose, respectively. One challenge with using the lignocellulosic hydrolysate is that *S. cerevisiae* does not naturally consume xylose, which can account for 30-50% of the total fermentable sugars [81]. The second challenge with using the lignocellulosic hydrolysate is the fact that the process to extract the fermentable sugars (pretreatment and hydrolysis) is harsh so inhibitory compounds such as furan derivatives (i.e. 5-hydroxymethylfurfural (HMF) and furfural), aliphatic acids (i.e. formic acid, acetic acid, levulinic acid (LA)), and phenolics compounds are generated and can be detrimental to fermenting microbes. These inhibitors are considered secondary products as they are produced from the degradation of the cellulose, hemicellulose, and lignin [105, 106]; HMF is produced from the degradation of cellulose/hemicellulose with further degradation yielding formic acid and LA; furfural is produced from the degradation of hemicellulose and further break down results in formic acid [106] (Fig.2.6). Additional inhibitory compounds could also be present in hydrolysate if chemical hydrolysis is used such as $\gamma$-valerolactone (GVL); residual GVL affects membranes and membrane-bound processes [107] and is toxic to fermenting microbes. The Great Lakes Bioenergy Research Center (GLBRC) is interested in GVL processed switchgrass hydrolysates, and the three most abundant inhibitory compounds ($\sim$10% of the total carbon recovered) are GVL, LA, and HMF [108, 107].

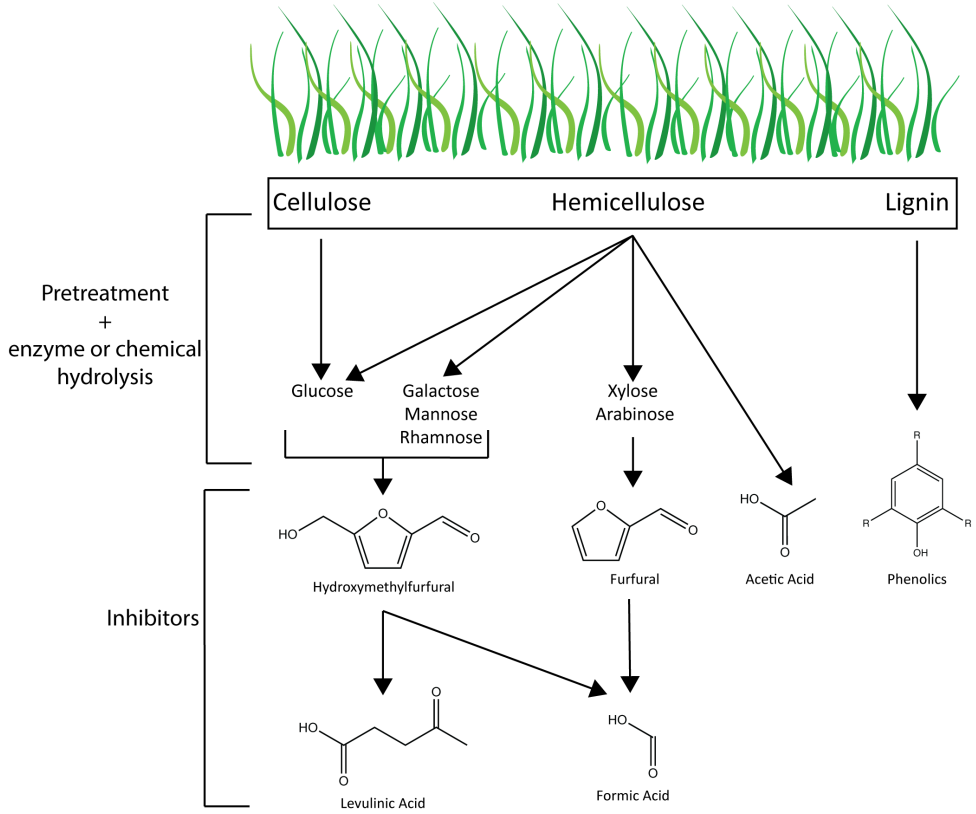


Figure 2.6: **Lignocellulosic biomass breakdown.** Formation of primary and secondary products (inhibitors). Adapted from [105].

### 2.3.1 Engineering *S. cerevisiae* for microbial production of isobutanol from xylose

To increase the yield and economically viability of fermentations using lignocellulosic feedstocks, xylose consuming strains have been produced through genetic engineering and adaptive laboratory evolution (ALE). Xylose is assimilated into the pentose phosphate pathway (PPP) by the intermediate, xylulose-5-phosphate (X5P), which can be derived by two distinct pathways (Fig.2.7). The xylose isomerase-xylulokinase (XI-XK) pathway, which is typically found in bacteria, and the xylose reductase–xylitol dehydrogenase-xylulokinase pathway (XR-XDH-XK), which is typically found in fungi [109, 110]. The XI-XK pathway has received more interest since it requires no redox cofactors: XR is NADPH-dependent and XDH is NADH-producing [111]. The different pathways are

thoroughly reviewed elsewhere [112, 111, 113].

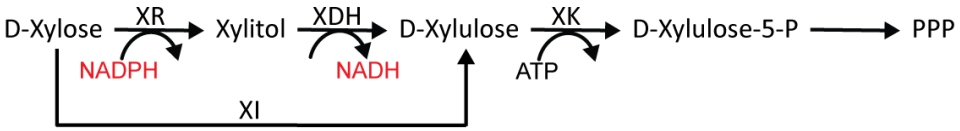


Figure 2.7: **Heterologous xylose assimilation pathway.** Xylose is assimilated into the pentose phosphate pathway (PPP) by the intermediate, xylulose-5-phosphate, which can be derived by two distinct pathways. The xylose isomerase-xylulokinase (XI-XK) pathway, which is typically found in bacteria, and the xylose reductase–xylitol dehydrogenase-xylulokinase pathway (XR-XDH-XK), which is typically found in fungi [109, 110].

There have been multiple reports of generating a xylose-to-isobutanol producing strain [77, 114, 115, 78, 116]. Success has been achieved by expressing a xylose assimilation pathway (either XI-XK or XR-XDH-XK) along with a isobutanol pathway cassette (mitochondrial or cytosolic localized). The highest reported titer, 3.1 g/L isobutanol, was achieved by Zhang et. al by expressing a XI-XK xylose assimilation pathway, a mitochondrial-localized isobutanol pathway, and by deleting key enzymes in competing pathways ($\triangle$*bat1*, $\triangle$*ald6*, and $\triangle$*pho13*). Some suggest that xylose consumption enhances mitochondrial activity and thus a mitochondrial-localized isobutanol pathway would outperform a cytosolic-localization under aerobic conditions. This is in part due to the fact that *S. cerevisiae* does not recognize xylose as a fermentative carbon source and does not induce the Crabtree effect (See section 2.1.3.2) [77]. Others believe that a mitochondrial-localized pathway would cause limitations at the industrial scale, since mitochondria are strongly reduced in *S. cerevisiae* under anaerobic cultivations or cultivation with high sugar concentrations [116].

### 2.3.2 Lignocellulosic inhibitors effects and detoxification strategies

The impact of furans, weak acids, and phenolic compounds on cell growth has been studied and their mechanism of action are known. Weak acids decrease cellular pH, inhibit DNA synthesis/repair, inhibit glycolytic enzymes, and decrease cellular ATP. Furans damage membranes/proteins/nucleic acids, inhibit enzymes, limit sulfur assimilation, and decrease cellular NADPH/NADH pools. Phenolics damage membranes, generate reactive oxygen species (ROS), damage proteins, and cause DNA mutagenesis [106]. Microbes cope by activating efflux pumps, damage control mechanisms, and detoxification; for example, *S. cerevisiae* has an innate ability to detoxify furans by reducing them to their less inhibitory alcohol forms at the cost of reducing power: NADH for furfural and NADPH for HMF [106, 117].

Additional coping mechanisms can also be engineered in the cell to improve the tolerance to inhibitors and allow for higher productivity and yields during fermentations [118]. A multitude of strategies have been implemented to identify genes that are important for hydrolysate tolerance including: $^{13}$C metabolic flux analysis, transcriptional profiling, transcriptomics analyses, directed evolution, and chemical genomics [107, 119, 120, 118, 121, 122]. Rational engineering has also been successfully used to increase tolerance to inhibitory compounds by overexpressing selected inhibitor resistance genes in different combinations [123]. With these strategies, a vast amount of data surrounding inhibitor tolerance has been generated, but there is no consensus due to the varity of inhibitors and their concentrations in different hydrolysates. Additionally, synergetic effects between inhibitors could be unpredictable and lethal [118]. The following paragraph will focus on the recent advances to improve tolerance to the two inhibitors

investigated in this thesis, levulinic acid and $\gamma$-valerolactone (GVL).

There are few reports of engineering *S. cerevisiae* for improved levulinic acid tolerance. In one study, rational engineering to improve cell growth ($\triangle$*pho13* and overexpress *TAL1*) led to an improvement in weak acid tolerance (acetic, formic, and levulinic acid) [124]. In another study, the general catabolite repressor, Mig1p, was targeted to remove repression of a number of target genes involved in stress tolerance [125]. For GVL, a chemical genomics study was conducted with a gene deletion library and two gene deletions that led to increased tolerance were identified, $\triangle$*pad1* and $\triangle$*fdc1* [107].

# Chapter 3

# Pathway compartmentalization as a metabolic engineering strategy for improved isobutanol production

**Authors and Contributors:**

- **Francesca V. Gambacorta** conceptualization, strain engineering, design of experiments, investigation, data analysis, data visualization, formal analysis, writing-methods, editing and reviewing manuscript.
- **Ellen R. Wagner** conceptualization, investigation, data analysis, data visualization, formal analysis, writing-methods, editing and reviewing manuscript.
- **Dr. Tyler B. Jacobson** conceptualization, investigation, data analysis, writing-methods, editing and reviewing manuscript.
- **Dr. Mary Tremaine** strain engineering and investigation.
- **Mick A. McGee** data analysis and writing-method.
- **Justin J. Baerwald** investigation, editing and reviewing manuscript.
- **Dr. Russell L. Wrobel** conceptualization and strain engineering.
- **Dr. John F. Wolters** investigation and writing-methods.
- **Dr. Mike Place** data analysis.
- **Dr. Joshua J. Dietrich** investigation.

- **Dr. Dan Xi** investigation.
- **Jose Serate** investigation.
- **Shabda Gajbhiye** investigation.
- **Lisa Liu** strain engineering.
- **Maikayeng Vang-Smith** strain engineering.
- **Dr. Joshua J. Coon** funding acquisition.
- **Dr. Yaoping Zhang** funding acquisition and conceptualization.
- **Dr. Audrey P. Gasch** funding acquisition, conceptualization, editing and reviewing manuscript.
- **Dr. Daniel Amador-Noguez** funding acquisition and conceptualization.
- **Dr. Chris Todd Hittinger** funding acquisition, conceptualization, design of experiments, editing and reviewing manuscript.
- **Dr. Trey K. Sato** funding acquisition, conceptualization, strain engineering, design of experiments, investigation, writing-methods, editing and reviewing manuscript.
- **Dr. Brian F. Pfleger** funding acquisition, conceptualization, design of experiments, editing and reviewing manuscript.

This chapter was originally written as an article in Synthetic and Systems Biotechnology [126].

## 3.1 Abstract

Metabolic engineering strategies have been successfully implemented to improve the production of isobutanol, a next-generation biofuel, in *Saccharomyces cerevisiae*. Here, we explore how two of these strategies, pathway re-localization and redox cofactor-balancing, affect the performance and physiology of isobutanol producing strains. We equipped yeast with isobutanol cassettes which had either a mitochondrial or cytosolic localized isobutanol pathway and used either a redox-imbalanced (NADPH-dependent) or redox-balanced (NADH-dependent) ketol-acid reductoisomerase enzyme. We then conducted transcriptomic, proteomic and metabolomic analyses to elucidate molecular differences between the engineered strains. Pathway localization had a large effect on isobutanol production with the strain expressing the mitochondrial-localized enzymes producing 3.8-fold more isobutanol than strains expressing the cytosolic enzymes. Cofactor-balancing did not improve isobutanol titers and instead the strain with the redox-imbalanced pathway produced 1.5-fold more isobutanol than the balanced version, albeit at low overall pathway flux. Functional genomic analyses suggested that the poor performances of the cytosolic pathway strains were in part due to a shortage in cytosolic Fe-S clusters, which are required cofactors for the dihydroxyacid dehydratase enzyme. We then demonstrated that this cofactor limitation may be partially recovered by disrupting iron homeostasis with a *fra2* mutation, thereby increasing cellular iron levels. The resulting isobutanol titer of the *fra2* null strain harboring a cytosolic-localized isobutanol pathway outperformed the strain with the mitochondrial-localized pathway by 1.3-fold, demonstrating that both localizations can support flux to isobutanol.

## 3.2 Introduction

Isobutanol is a branched four-carbon alcohol targeted by many as a biofuel for light-duty engines and as a precursor to jet and diesel fuels via catalytic upgrading [127]. Relative to ethanol, isobutanol has a higher energy density, a lower vapor pressure, and a higher flash point, making it a better option for spark-ignition engines. Isobutanol is also less corrosive and less hygroscopic, making it a better biofuel for current piping infrastructure [11]. Isobutanol biosynthesis is redox balanced with glycolysis and can therefore be made via fermentation. *Saccharomyces cerevisiae*, the workhorse for industrial fermentations, is therefore a suitable host for its production. While yeast have a natural ability to synthesize isobutanol, there are many barriers to making isobutanol the primary fermentation product at high rates [15].

*S. cerevisiae* synthesizes isobutanol from pyruvate via enzymes involved in valine biosynthesis and the Ehrlich pathway. The first half of the pathway converts pyruvate to $\alpha$-ketoisovalerate (KIV) by mitochondria-localized *ILV* enzymes: acetolactate synthase (ALS, encoded by *ILV2*), a NADPH-dependent ketol-acid reductoisomerase (KARI, encoded by *ILV5*), and a 2Fe-2S cluster-requiring dihydroxyacid dehydratase (DHAD, encoded by *ILV3*). The second part of the pathway, the Ehrlich pathway, converts KIV to isobutanol by promiscuous cytosolic enzymes: $\alpha$-ketoacid decarboxylase (KDC, encoded by pyruvate decarboxylases, *PDC1*, *PDC5*, or *PDC6*, or phenylpyruvate decarboxylase, *ARO10*) and a NADH-dependent alcohol dehydrogenase (ADH, encoded by *ADH*1-5) (Fig.3.1a). *S. cerevisiae*'s native isobutanol production is low ($< 1\%$ of the theoretical maximum yield), so substantial work is needed to make isobutanol the primary fermentation product [90, 96, 97].

The spatial segregation of the native pathway enzymes, split between the mitochon-

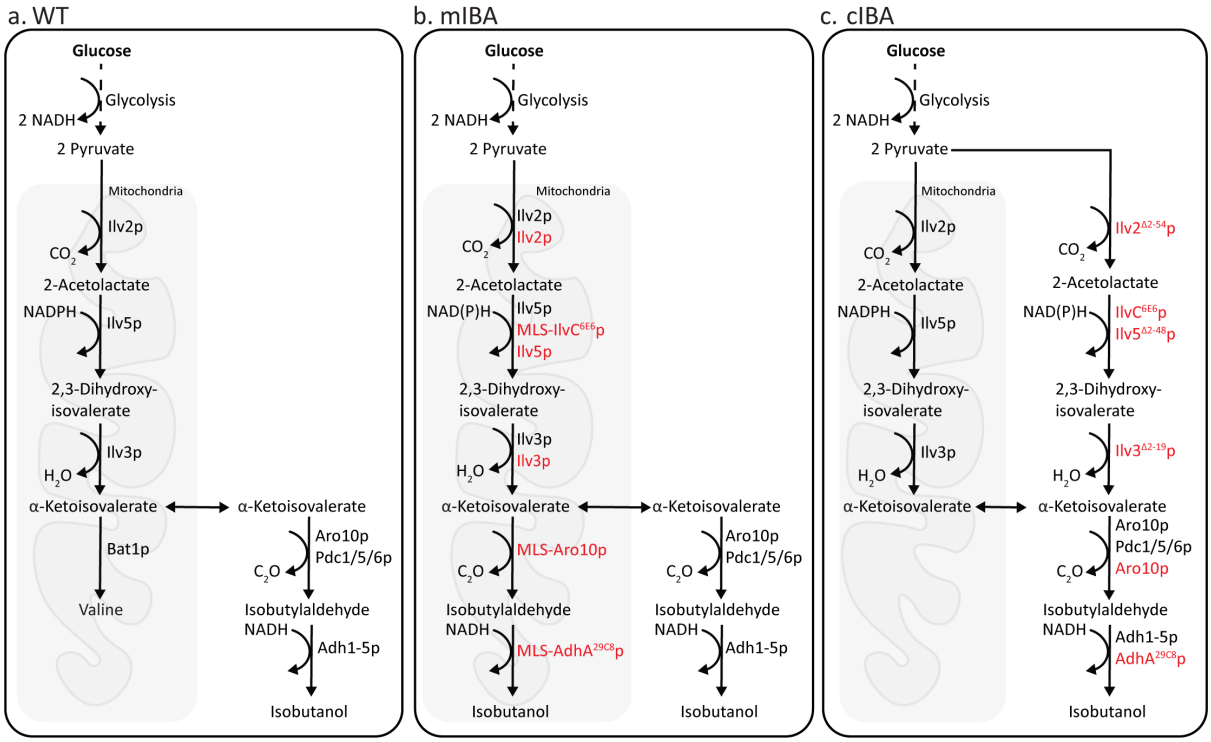


Figure 3.1: **Native and engineered *S. cerevisiae* isobutanol pathways. a)** Shows the endogenous isobutanol synthesis pathway from pyruvate. The first half of the pathway converts pyruvate to $\alpha$-ketoisovalerate (KIV) by the mitochondrial-localized valine biosynthesis enzymes Ilv2p, Ilv5p, and Ilv3p. The second part of the pathway, the Ehrlich pathway, converts KIV to isobutanol by promiscuous cytosolic-localized decarboxylase enzymes Pdc1/5/6p or Aro10p and Adh1-5p. **b)** Mitochondrial-localized isobutanol pathway (mIBA) consists of codon-optimized variants of *S. cerevisiae* Ilv2p, *S. cerevisiae* Ilv3p, mitochondrial targeted *S. cerevisiae* Aro10p, mitochondrial targeted *L. lactis* AdhA$^{29C8}$p, and either *S. cerevisiae* Ilv5p or mitochondrial targeted *E. coli* IlvC$^{6E6}$p for the redox cofactor imbalanced and balanced pathways respectively (red enzymes). **c)** Cytosolic-localized isobutanol pathway (cIBA) consists of codon-optimized variants of *S. cerevisiae* Ilv2$^{\triangle 2\text{-}54}$p, *S. cerevisiae* Ilv3$^{\triangle 2\text{-}19}$p, *S. cerevisiae* Aro10p, *L. lactis* AdhA$^{29C8}$p, and either *S. cerevisiae* Ilv5$^{\triangle 2\text{-}48}$p or *E. coli* IlvC$^{6E6}$p for the redox cofactor imbalanced and balanced pathways respectively (red enzymes). For both the mIBA and cIBA pathways, the endogenous/native enzymes (Ilv2p, Ilv5p, Ilv3p, Aro10p, Pdc1/5/6p, Adh1-5p, and Bat1p) in black remain in each strain.

dria and the cytosol, may be a limiting factor for synthesizing isobutanol at high levels. The segregation can be overcome by localizing the five-step pathway into a single compartment: mitochondrial localization is achieved by adding a mitochondrial localization sequence (MLS) to the genes in the Ehrlich pathway (*PDC1/5/6* or *ARO10* and *ADH1-5*), and cytosolic localization is achieved by removing the MLS sequence from the genes in the valine biosynthesis pathway (*ILV2*, *ILV5*, and *ILV3*) [96, 97]. However, the role

that localization plays in isobutanol production is obscured by conflicting reports in the literature as both pathway localizations have achieved similar isobutanol titers and yields (Table.2.2). It has been shown that a strain with mitochondrial-localization benefits from having a higher local concentration of enzyme and pathway intermediates [96]. On the other hand, it has been proposed that cytosolic localization would be preferable in the context of industrially relevant conditions such as high glucose concentrations or anaerobic growth. This is in part because the mitochondria are known to enter a minimal energy-requirement mode under those conditions [98, 99].

A second limitation in the isobutanol pathway is the redox cofactor-imbalance that exists between glycolysis and isobutanol fermentation; glycolysis produces two NADH per molecule of glucose, while isobutanol fermentation consumes one NADPH by *ILV5* and one NADH by *ADH*. This results in an NADPH shortage and NADH excess. One strategy to resolve this imbalance is to use a heterologous NADH-dependent KARI, such as the *E. coli* KARI variant, $ilvC^{6E6}$, that was previously engineered with improved specificity towards NADH [57, 63]. Another strategy is to increase the supply of NADPH by introducing a transhydrogenase-like shunt (NADH + $NADP^+ \rightarrow NAD^+$ + NADPH) into *S. cerevisiae* [61]. Both strategies have been successful in improving isobutanol titers, demonstrating the importance of having a redox cofactor-balanced pathway (Table.2.2).

In this work, we aimed to provide insight into how pathway localization and redox cofactor-balancing affect the performance and physiology of isobutanol producing strains. We conducted a functional genomics analysis to elucidate differences between *S. cerevisiae* strains equipped with DNA cassettes that localized isobutanol biosynthesis to specific compartments, i.e. mitochondria vs. cytosol, and included either a NADPH-dependent (cofactor-imbalanced) or NADH-dependent (cofactor-balanced) KARI enzyme. Here,

we report that pathway localization had a greater effect on isobutanol production than redox-balancing; the strain harboring the mitochondrial-localized isobutanol pathway outperformed the cytosolic version by 3.8-fold. The main limitation in the cytosolic-localization is the supply of the 2Fe-2S cluster cofactor for the DHAD enzyme; however, we found that this limitation may be partially overcome by increasing the availability of iron in the cell by perturbing iron homeostasis. Our findings contribute towards improving the metabolic engineering designs for building further improved isobutanol producing strains.

## 3.3 Materials and methods

### 3.3.1 Yeast media

Complex lab media for culturing, YP, consisted of 10 g/L yeast extract, 20 g/L peptone, and 20 g/L dextrose (YPD). 200 µg/mL Geneticin (US Biological, Swampscott, MA), 200 µg/mL Hygromycin B (US Biological, Swampscott, MA), 100 µg/mL Nourseothricin (Jena Bioscience, Jena, Germany), or 200 µg/mL Zeocin (Thermo Fisher Scientific, Waltham, MA) were added for maintenance of expression constructs where needed. Defined minimal medium contained 6.7 g/L yeast nitrogen base (YNB) without amino acids with ammonium sulfate, 19.5 g/L MES, 100 g/L dextrose, 4 mL/L 250X tween/ergosterol stock (62.5mL Tween80 + 625mg Ergosterol in 187 mL 95% EtOH) and pH adjusted to 5.5. Defined synthetic complete media contained 6.7 g/L yeast nitrogen base (YNB) without amino acids with ammonium sulfate, 1 g/L drop-out mix without yeast nitrogen base, and 20g/L dextrose.

### 3.3.2 Cloning and yeast strain engineering

*S. cerevisiae* strains used in this study are described in Table.3.1. The parental WT strain [128] was generated by transforming [129] a polymerase chain reaction (PCR) product containing the *URA3* open reading frame (ORF), 225 bp of the 5' UTR and 173 bp of the 3' UTR from the GLBRCY22-3 strain ([19], G3) into the CEN.PK113-5D strain and plating on SC minus uracil plates. Transformants were confirmed for growth on auxotrophic medium without uracil and Sanger-sequenced. To generate strains expressing the isobutanol pathway genes, DNA containing codon-optimized versions of *ILV2*, *ILV3*, *ILV5* and *ARO10* from *S. cerevisiae*, and $adhA^{29C8}$ from *Lactobacillus lacti* [95] were synthesized (Life Technologies) and cloned between various yeast promoters and terminators (together called the "isobutanol pathway cassette"). Specifically, expression was driven by the following promoter and terminator pairs: $P_{ADH1}$-*ILV2*-$T_{CYC1}$; $P_{PGK1}$-*ILV3*-$T_{TEF2}$; $P_{TEF2}$-$adhA^{29C8}$-$T_{TDH3}$; $P_{TDH3}$-*ARO10*-$T_{TEF1}$; $P_{TEF1}$-*ILV5*-$T_{TUB1}$. The $P_{ADH1}$ consisted of 408 bp upstream of the *ScADH1* protein-coding sequence, $T_{CYC1}$ consisted of 251 bp downstream of *ScCYC1* protein-coding sequence, $P_{PGK1}$ consisted of 998 bp upstream of the *ScPGK1* protein-coding sequence, $T_{TEF2}$ consisted of 293 bp downstream of the *ScTEF2* protein-coding sequence, $P_{TEF2}$ consisted of 402 bp upstream of the *ScTEF2* protein-coding sequence, $T_{TDH3}$ consisted of 514 bp downstream of the *ScTDH3* protein-coding sequence, $P_{TDH3}$ consisted of 672 bp upstream of the *ScTDH3* protein-coding sequence, $T_{TEF1}$ consisted of 350 bp downstream of the *ScTEF1* protein-coding sequence, $P_{TEF1}$ consisted of 577 bp upstream of the *ScTEF1* protein-coding sequence, $T_{TUB1}$ consisted of 380 bp downstream of the *ScTUB1* protein-coding sequence. The transcriptional units (promoter-gene-terminator pairs) for the five genes were then cloned in the above order into the *SacI-KpnI* polylinker sites of a modified pRS426 plasmid containing *HygMX4* as

the selection marker in place of *URA3* [130]. Homology arms to the *HO* locus (*HO-L* and *HO-R*) were inserted 5' and 3' of the isobutanol pathway cassette to facilitate genome insertion by homologous recombination [131]. The *HO-R* homology arm also included the *LoxP-KanMX-LoxP* selection marker, which was inserted 3' of *ScTUB1* protein-coding sequence [132]. For expressing *ARO10* and $adhA^{29C8}$ in the mitochondria, coding sequence for the *COX4* MLS was synthesized in-frame at the 5' ends of codon-optimized *ARO10* and $adhA^{29C8}$. The full length isobutanol pathway cassette containing mitochondrial-localized enzymes and flanking *HO* arms (GenBank: MZ541859) was excised from the plasmid by digestion with *SacI*-HF and *KpnI*-HF, purified and transformed into the WT strain. After selection on YPD+Geneticin plates, PCR and Sanger sequencing were used to confirm the insertion of the isobutanol pathway cassette into the *HO* locus. The *LoxP-KanMX-LoxP* selection marker was then excised by Cre recombinase to generate the final $\text{mIBA}^{ILV5}$ strain [132]. The inserted isobutanol pathway cassette was amplified by PCR with multiple primer sets from $\text{mIBA}^{ILV5}$ genomic DNA (gDNA) and confirmed for complete insertion by Sanger-sequencing (Fig.3.7a). To generate the $\text{cIBA}^{IlvC6E6}$ strain, CRISPR/Cas9 was used to delete the MLSs at the N-terminus of the engineered isobutanol pathway enzymes in $\text{mIBA}^{ILV5}$ (Fig.3.7b). In brief, an sgRNA sequence targeting the MLS of each synthetic isobutanol pathway enzyme were identified by CRISpy-pop [133] and cloned into the pXIPHOS plasmid as described previously [134]. sgRNA targeting sequences are as follows: *ILV2*, CTTAATAGCGAAGTTCTTCA; *ILV3*, AGTAGTAGAGAATTGTCTAG; *ILV5*, GCAGATCAATCTAGCAGCTT; *MLS-*$adhA^{29C8}$ and *MLS-ARO10*, AAATCTGATGGACTGTCTCA. Each mitochondrial-localized gene in the synthetic isobutanol pathway was sequentially replaced by transforming the pXIPHOS plasmid containing a single sgRNA to one gene along with the appropriate PCR

repair template of the gene lacking the MLS in the following order: *ILV5* → *ilvC*$^{6E6}$, *MLS-ARO10* and *MLS-adhA*$^{29C8}$ simultaneously → *ARO10* and *adhA*$^{29C8}$, *ILV3* → *ILV3*$^{\triangle 2\text{-}19}$, *ILV2* → *ILV2*$^{\triangle 2\text{-}54}$. To generate repair templates with the cytosol-localized isobutanol pathway enzymes, individual genes were first cloned into the TOPO vector and then the appropriate MLS was removed (*ILV2*$^{\triangle 2\text{-}54}$, *ILV3*$^{\triangle 2\text{-}19}$, and *ILV5*$^{\triangle 2\text{-}48}$, *ARO10*$^{\triangle 2\text{-}MLS}$,and *adhA*$^{29C8,\triangle 2\text{-}MLS}$ [97]) by restriction digestion/PCR-aided Gibson assembly and confirmed with Sanger-sequencing. These vectors were then used as the PCR repair template which contained part of the promoter and part of the gene lacking the MLS. The repair template for replacing *ILV5* with *ilvC*$^{6E6}$ was generated by amplifying the *E. coli ilvC*$^{6E6}$ CDS from pIBA1 [135] and cloning it in place of the ILV5$^{\triangle 2\text{-}48}$ CDS in the TOPO vector; this vector was Sanger-sequenced and used for the PCR repair template in the same manner as described earlier. To generate the cIBA$^{ILV5}$ strain, the cIBA$^{IlvC6E6}$ strain was transformed with the pXIPHOS plasmid containing an sgRNA to *ilvC*$^{6E6}$ (AGTTTTAATTACAACCGGTA) and a PCR repair template containing *ILV5*$^{\triangle 2\text{-}48}$, (Fig.3.7c). To generate the mIBA$^{IlvC6E6}$ strain, the mIBA$^{ILV5}$ strain was transformed with the pXIPHOS plasmid containing an sgRNA to codon-optimized *ILV5* (GCAGATCAATCTAGCAGCTT) and a PCR repair template containing *MLS-ilvC*$^{6E6}$ (Fig.3.7d). For the cIBA$^{ILV5}$, cIBA$^{IlvC6E6}$, and mIBA$^{IlvC6E6}$ strains, DNA sequence changes where CRISPR/Cas9 editing occurred were confirmed by Sanger-sequencing. Deletions of codon-optimized *ILV3*, native *ILV3* and/or native *FRA2* from the cIBA$^{ILV5}$, mIBA$^{ILV5}$, and cIBA$^{IlvC6E6}$ strains were performed by integration of PCR products generated from *LoxP-KanMX-LoxP* (pUG6) or *LoxP-HphMX-LoxP* (pUG75) plasmid templates and primers containing 40-60 bp of homology flanking the targeted genes [136]. PCR products were purified and transformed into the appropriate strains and selected for growth on the appropriate antibiotic. Gene

deletions were confirmed by PCR of gDNA and Sanger-sequencing.

### 3.3.3 Fermentation growth conditions and sample collection

For aerobic growth, starter cultures were grown in a shaking incubator at 30°C. For anaerobic growth, media was allowed to degas in a 30°C Coy anaerobic chamber (10% $H_2$, 10% $CO_2$, and 80% $N_2$) for >12 h prior to use and cultures were grown with stir bars on a magnetic stir plate to prevent flocculation. Fermentations for multi-omic sampling were performed in biological triplicate. Yeast cells were grown aerobically in YPD until stationary phase ∼12 h. The cultures were then shifted to minimal medium and anaerobic conditions by diluting the culture to $OD_{600}$ 0.3 in minimal medium and allowed to reach exponential phase ∼8.5 h. Working cultures, which were used for sampling, were then inoculated from the shifted culture to $OD_{600}$ 0.2 in minimal medium and allowed to grow anaerobically for 48 h. Cell growth was monitored by taking $OD_{600}$ measurements with the Beckman DU720 spectrophotometer. Samples for end-product analysis were taken by collecting 2 mL of culture supernatant. Samples for protein isolation were obtained by collecting and flash freezing ∼$1x10^{11}$/$1x10^{12}$ cells. Similarly, samples for RNA isolation were obtained by collecting and flash freezing the equivalent of 25 mL of cells at an $OD_{600}$ of 1. Samples for intracellular metabolite quantification were collected inside the anaerobic chamber by vacuum filtrations of culture through 0.45 $\mu$m hydrophilic nylon filters. Filters with the retained cells were immediately placed cell-side down in 1.5 mL of extraction solvent (40 vol% acetonitrile, 40 vol% methanol, 20 vol% water) kept on dry ice to quench metabolism and extract metabolites.

### 3.3.4 End product analysis

#### 3.3.4.1 Determination of isobutanol concentration by automated headspace GC/MS

The equipment used included the following: an Agilent 7890A GC system (Agilent Technologies, Inc. Palo Alto, CA); a LPAL3 autosampler and sample preparation system equipped with a heated agitator/stirrer and heated headspace sampling syringe (Agilent Technologies, Inc. Palo Alto, CA); and a Pegasus 4D ToF-MS (Leco Corp., Saint Joseph, Michigan). Typical analysis range is 0.065 mM – 8.4 mM isobutanol and uses an aliquot volume of 500 mL and 2-Methylpropyl-d9 alcohol (as internal standard). Instrument run control and conditions are set by the Chromatof (®Leco Corp.) software (version 4.72.0.0) provided with the Pegasus 4D GcxGC ToF MS system. Samples were incubated at 70°C for 5 minutes in the heated agitator set to 350 rpm. 0.5 mL of the headspace is then sampled by the autosampler with a 2.5 mL gastight syringe heated to 75°C and injected into the GC system. The sample was withdrawn at 100 mL/sec and injected into the GC at 1000 mL/sec. The syringe was purged with nitrogen gas for 0.5 min prior to the next injection. The analytical capillary GC column was a Stabilwax-DA® (Restek, Inc. Bellefonte, PA) length 30 m, 0.25 mm ID, 0.25 mm film thickness. Helium was used as a carrier gas with a pressure corrected constant flow rate of 1 mL/min. The GC inlet was fitted with a 4 mm deactivated glass liner and held at 250 °C throughout the run. The inlet split ratio was set to 50:1. The GC oven was initially set to 50°C and held for 1 minute then increased to 200° C at 40°C/min and held at 200°C for 5 min. The filaments of the mass spectrometer were turned on 42.5 seconds after injection and 10 spectra/sec were recorded from m/z 10 to m/z 250. The MS source temp was 200°C, electron energy set to 70 eV, and the detector voltage was adjusted to approximately 50V above the

minimum voltage determined by the instrument tune check procedure. The peak area of isobutanol was measured using the extracted ion chromatogram of m/z 43 and the peak area of 2-Methylpropyl-d9 alcohol was measured from the extracted ion chromatogram of m/z 46. An unpaired t-test was performed to determine statistical significance.

#### 3.3.4.2 Analysis of fermentation supernatants by HPLC-RID

End-product analytes (glucose, ethanol, glycerol, lactate, and acetate) were measured with an analytical system consisting of an Agilent 1260 Infinity HPLC system (Agilent Technologies, Inc., Palo Alto, CA) with a quaternary pump, chilled (4°C autosampler, vacuum degasser, refractive index detector, and a Aminex HPX-87H column with a Cation-H guard column (BioRad, Inc. Hercules, CA; 300x7.8mm, catalog number 125-0140). Operating parameters were as follows: 0.02 N H2SO4 mobile phase, 0.500 mL/min flow rate, 50°C column temperature, 50°C detector temperature, 28 minutes run time, and a 50 $\mu$L injection volume. Instrument control, data collection and analysis/calculation are done using Chem Station V. B04.03 software (Agilent Technologies, Inc., Palo Alto, CA). An unpaired t-test was performed to determine statistical significance.

### 3.3.5 Intra- and extra-cellular metabolomics preparation, quantification, and analysis

After collecting all samples at a given time point, the filter disks in extraction solvent were removed from the anaerobic chamber and the cells were washed off the filter into the solvent. The entire suspension was transferred into a centrifuge tube and centrifuged for 5 min at 16,000 xg at 4°C to remove cellular debris. The supernatant was collected in another centrifuge tube and immediately prepped for quantification.

The extraction solvent containing intracellular metabolites was dried under $N_2$ and the metabolites were resuspended in Solvent A (97:3 H2O:methanol with 10 mM tributylamine adjusted to pH 8.2 by addition of 10 mM acetic acid). Samples were analyzed by LC-MS as described previously [137, 138]. Data analysis was performed using MAVEN software [139, 140] and compounds were identified by retention time (matched to pure standards). "Peak Area Top" values were extracted and normalized by $OD_{600}$ equivalent of sample injected into the LC-MS. Extracellular metabolite samples for LC-MS analysis were diluted to appropriate concentration, then analyzed using the above method. An unpaired t-test was performed to determine statistical significance.

### 3.3.6 Transcriptomic sample preparation, library construction, sequencing, and analysis

Total RNA was extracted with hot phenol lysis [141], DNA was digested with Turbo-DNase (Life Technologies, Carlsbad, CA) for 30 min at 37°C, and RNA was precipitated with 2.5 M LiCl for 30 min at 20°C. In brief, RNA-Seq libraries were generated using the Illumina TruSeq® Stranded mRNA HT kit, AMPure XP bead for PCR purification (Beckman Coulter, Indianapolis, IN), and SuperScriptII reverse transcriptase (Invitrogen, Carlsbad, CA) as described in the Illumina kit. Single-end 50-bp reads were generated using an Illumina NovaSeq 6000 at the University of Wisconsin-Madison Biotechnology Center. Reads were processed with Trimmomatic version 0.3 [142] and mapped to the S288C genome (with foreign mutant sequences added) using Bowtie 2 version 2.2.2 with default settings [143]. Read counts were calculated using HTseq version 0.6.0 [143]. edgeR version 3.6.8 [144] was used to perform differential gene analysis, taking a Benjamini and Hochberg false discovery rate (FDR) of $< 0.05$ as significant [145]. Raw sequencing counts

were normalized using Trimmed Means of M-values (TMM). Samples were clustered using Cluster 3.0 [146] and visualized in Java TreeView [147], and functional GO term enrichment was performed using SetRank [148] with an FDR set to $< 0.05$ for significance.

### 3.3.7 Label-free quantitative proteomics preparation, quantification, and analysis

Yeast pellets were resuspended in 150 $\mu$L of 6 M guanidine, 100 mM Tris (pH 8) and boiled for 5 minutes at 100°C. Methanol was then added to 90% to precipitate proteins, and the samples were centrifuged for 5 min at 9,000 G. The supernatant was discarded, and the protein pellet was resuspended in lysis buffer (8 M urea, 100 mM Tris pH 8, 20 mM TCEP, 80 mM Chloroacetamide). LysC was added to an estimated 50:1 protein to enzyme ratio and incubated for 4 hrs at room temperature. The samples were diluted with 100 mM Tris to a urea concentration of 1.5 M. Trypsin was added to an estimated 50:1 protein to enzyme ratio and incubated overnight at room temperature. Samples were desalted with Strata C18 solid phase extraction cartridges and dried in a vacuum centrifuge. Peptide concentration was then determined from a NanoDrop One spectrophotometer before resuspending in 0.2% formic acid and injecting onto the mass spectrometer.

Samples were analyzed using an LC-MS/MS instrument comprising an Orbitrap Eclipse Tribrid mass spectrometer and UltiMate 3000 RSLCnano liquid chromatography system (Thermo Fisher Scientific). Mobile phase A consisted of 0.2% formic acid in water and mobile phase B consisted of 0.2% formic acid in 80% acetonitrile. Peptides were loaded in 0% B and separated at a flow rate of 310 nL/min over a 120 min gradient of increasing % B. Peptides were injected onto a 1.7 $\mu$m C18 column (75 $\mu$m i.d.) packed in-house to a length of 30 cm [149] and heated to 50°C. Survey scans of peptide precursors

were collected every second from 300-1350 Th with an AGC target of 1,000,000 and a resolution of 240,000 in the orbitrap. Precursors were isolated from a 0.5 Th window in the quadrupole and HCD MS/MS scans at 35% collision energy were collected in the ion trap with an AGC target of 35,000 from 150-1350 Th.

The resulting LC-MS/MS proteomics data were processed using MaxQuant [150] software version 1.5.2.8 and searched against a *Saccharomyces cerevisiae* database (with foreign mutant proteins added) downloaded from Uniprot. The digestion enzyme was set to Trypsin/P with up to two missed cleavages, and oxidation of methionine and protein N-terminal acetylation were set as variable modifications. Cysteine carbamidomethylation was set as a fixed modification. Label-free quantification was enabled with a minimum ratio count of 1, and the match between runs feature was utilized to decrease missing data values within the dataset. Peptides were filtered to a 1% FDR and combined to protein groups based on the rules of parsimony. Differential protein analysis was done taking a Benjamini and Hochberg false discovery rate (FDR) of $< 0.05$ as significant [145][42]. Functional enrichment was assessed using the FunSpec database [2].

### 3.3.8 Petite frequency

To assess the propensity of different strains to form petite colonies due to loss of respiratory competence each strain was revived on YPD media and streaked for single colonies on YPG (2% glycerol) media to ensure all starting cells could respire. Single colonies were used to inoculate 3 independent 5 mL YPD cultures, which were grown rolling overnight at 30°C. Each culture was plated for single colonies on YPDG (0.1% dextrose, 3% glycerol) media to differentiate petite and respiring colonies and colonies were counted after 3 days of growth at 30°C.

## 3.4 Results and discussion

### 3.4.1 Engineered isobutanol producing strains

In order to evaluate the effects of pathway localization and redox cofactor-balancing on isobutanol production, we constructed four engineered strains: a mitochondrial-localized isobutanol pathway with a NADPH-dependent Ilv5p KARI, mIBA$^{ILV5}$; a mitochondrial-localized isobutanol pathway with a NADH-dependent IlvC$^{6E6}$p KARI, mIBA$^{IlvC6E6}$; a cytosolic-localized isobutanol pathway with a NADPH-dependent Ilv5p KARI, cIBA$^{ILV5}$; and a cytosolic-localized isobutanol pathway with a NADH-dependent IlvC$^{6E6}$p KARI, cIBA$^{IlvC6E6}$ (Fig.3.1b-c, Table.3.1, Fig.3.7). DNA cassettes for expressing each pathway were assembled from genes previously tested [96], including those encoding an alcohol dehydrogenase (*adhA*$^{29C8}$, from *Lactococcus lactis* [25]), an acetolactate synthase (*ILV2*, from *S. cerevisiae*), a dihydroxyacid dehydratase (*ILV3*, from *S. cerevisiae*), a $\alpha$-ketoacid decarboxylase (*ARO10*, from *S. cerevisiae*), and a ketol-acid reductoisomerase (*ILV5*, from *S. cerevisiae* or *ilvC*$^{6E6}$, from *E. coli* [135]). Each open reading frame was codon-optimized, synthesized commercially, and cloned in frame with promoters (P) and terminators (T) resulting in the following pairs: $P_{ADH1}$-*ILV2*-$T_{CYC1}$; $P_{PGK1}$-*ILV3*-$T_{TEF2}$; $P_{TEF2}$-*adhA*$^{29C8}$-$T_{TDH3}$; $P_{TDH3}$-*ARO10*-$T_{TEF1}$; $P_{TEF1}$-*ILV5*-$T_{TUB1}$.

Mitochondrial localization was achieved by adding DNA encoding the previously characterized Cox4p N-terminal MLS [96] to the N-terminus of genes which natively localized to the cytosol (MLS-*ARO10*, MLS-*adhA*$^{29C8}$, and MLS-*ilvC*$^{6E6}$). Conversely, cytosol targeting was achieved by removing sequences encoding previously identified MLS from genes which natively localized to the mitochondria (*ILV2*$^{\triangle 2\text{-}54}$, *ILV3*$^{\triangle 2\text{-}19}$, *ILV5*$^{\triangle 2\text{-}48}$) [97]. DNA cassettes containing each of the five genes were assembled and integrated into the

*S. cerevisiae* genome at the *HO* locus via homologous recombination. When constructing the mIBA$^{IlvC6E6}$ strain we uncovered an unexpected petite phenotype. The frequency at which the petite colonies arose in the mIBA$^{IlvC6E6}$ strain was 166-fold that of the wild-type (WT) strain (Table.3.2). All other engineered strains had a low petite frequency consistent with natural *S. cerevisiae* isolates [151, 152]. The mIBA$^{IlvC6E6}$ strain was not included in further studies due to this irreversible fitness defect.

### 3.4.2 Engineered strains produce varied amounts of isobutanol

A fermentation experiment was performed to evaluate and compare the physiological and molecular phenotypes of the engineered strains and WT. Each strain was cultivated anaerobically at 30°C in minimal medium containing 100 g/L glucose. We collected samples every 2 hrs to monitor growth, glucose consumption, isobutanol production, and ethanol production. Samples for functional genomics analyses (transcriptomic, proteomic and metabolomic) were collected at 4, 10, and 26 hrs post inoculation to represent the different phases of cell growth: early-exponential phase, mid-exponential phase, and early-stationary phase (Fig.3.2). The three engineered strains grew slower than the WT strain (Fig.3.2); doubling times during the exponential phase of the mIBA$^{ILV5}$, cIBA$^{ILV5}$ and cIBA$^{IlvC6E6}$ strains were 1.1, 1.3, and 1.3-fold larger than the WT strain, respectively. All strains completely consumed the glucose provided and reached similar final $OD_{600}$ (5.3-5.6) values by the end of the 48 hr fermentation. All strains produced ethanol titers of 45-47 g/L by hr 44 of the fermentation corresponding to yields over 90% of the theoretical maximum (Fig.3.2). These metrics indicate that ethanol remains the dominant fermentation product and that pathway localization and cofactor-balance alone were not the limiting factor in isobutanol fermentation.

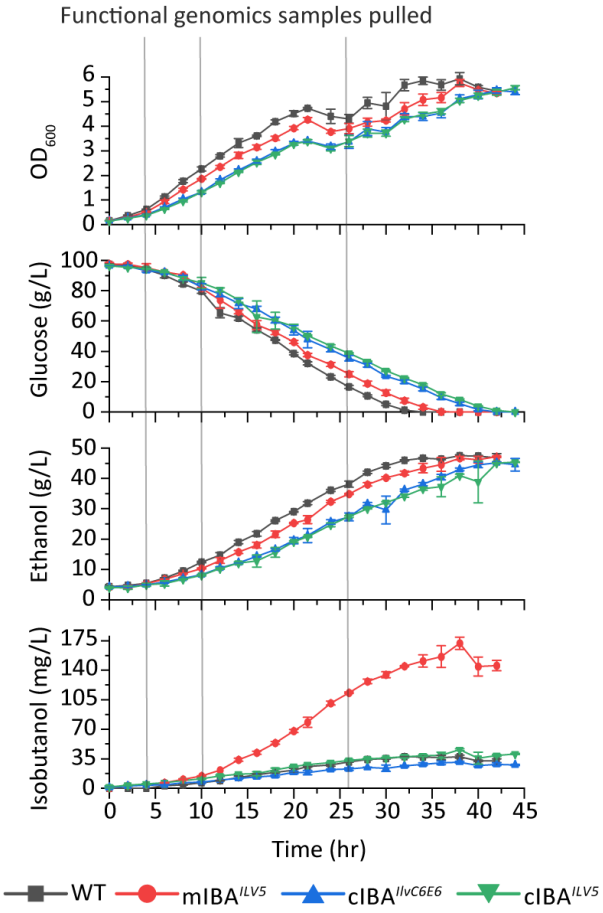


Figure 3.2: **Mitochondrial-localized isobutanol pathway is sufficient for increasing isobutanol titers.** Fermentation was performed on the isobutanol producing *S. cerevisiae* strains under anaerobic conditions in minimal medium for 48 h. Cell growth ($OD_{600}$), glucose, ethanol and isobutanol production were measured. Error bars represent the standard deviation of three biological replicates. Samples for functional genomics analysis (proteomics, transcriptomics, and metabolomics) were pulled at 4, 10, and 26 h indicated by vertical gray lines.

Isobutanol production varied significantly among the engineered strains. The cIBA$^{ILV5}$ and cIBA$^{IlvC6E6}$ strains produced isobutanol at levels less than or equal to WT; at 38 hr, the isobutanol titers were 37, 46, and 31 mg/L in the WT, cIBA$^{ILV5}$, and cIBA$^{IlvC6E6}$ strains, respectively. The cIBA$^{ILV5}$ strain produced 1.5-fold ($P < 5E\text{-}5$) more isobutanol than the cIBA$^{IlvC6E6}$ strain indicating that redox cofactor-balancing is not a limiting factor for driving flux to isobutanol synthesis in these strains and $NAD^+$ is preferentially regenerated through ethanol fermentation. The highest isobutanol titer was achieved by the mIBA$^{ILV5}$ strain, which produced 170 mg/L at 38 hrs, corresponding to a yield of 1.8

mg isobutanol/g glucose. This metric is similar to other isobutanol overproducing strains grown under anaerobic conditions [103]. In summary, the mIBA$^{ILV5}$ strain outperforms the other engineered strains and had a 3.8-fold (P < 5E-6) higher isobutanol titers than the cIBA$^{ILV5}$ strain.

### 3.4.3 Strains with cytosolic-localized isobutanol pathway have an altered transcriptome and proteome

We next assessed the molecular phenotypes of the engineered strains and WT using the functional genomics samples collected during the above-mentioned fermentation experiment. We identified and collected data for 59 intracellular metabolites using LC-MS, 34 extracellular metabolites (28 LC-MS and 6 HPLC/GC), 4339 proteins by LC-MS/MS proteomics, and 6434 genes by RNA-seq (File S1-S4, Data availability).

The transcriptome and proteome data collected from our top isobutanol producer, mIBA$^{ILV5}$, was more similar to WT than the cIBA$^{IlvC6E6}$ and cIBA$^{ILV5}$ strains which both displayed a larger number of differentially expressed RNA and proteins (Fig.3.3a, Table.3.3). The cIBA$^{IlvC6E6}$ and cIBA$^{ILV5}$ strains shared 175 of the same differentially expressed genes, which were enriched for oxidation-reduction processes, mitochondrial respiration, and TATA-containing genes (Fig.3.3b). Hierarchical clustering of the data was also performed, and the strains clustered together in a distinct clade within each timepoint (Fig.3.3c). Taken together, we concluded that the cIBA$^{IlvC6E6}$ and cIBA$^{ILV5}$ strains have functionally similar transcriptomes and that a cytosolic-localized isobutanol pathway induces gene expression changes in specific biological processes.

The metabolite dataset showed that all engineered strains had significantly altered levels of aromatic amino acid biogenesis intermediates (Fig.3.8 and Fig.3.9). We suspect

a.

| Strains | Differentially expressed genes at an reduced level | Differentially expressed genes at an elevated level |
|---|---|---|
| mIBA$^{ILV5}$ | 0 | 0 |
| cIBA$^{IlvC6E6}$ | 105 | 110 |
| cIBA$^{ILV5}$ | 224 | 234 |

b.

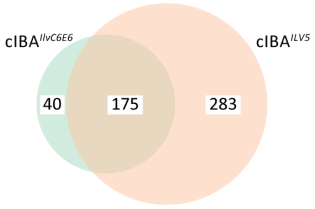


*No significant DE genes between mIBA$^{ILV5}$ and WT

| **Enriched ovelapping genes in cIBA$^{ILV5}$ and cIBA$^{IlvC6E6}$** |
|---|
| TATA-containg genes |
| Mating |
| Oxidation-reduction process |
| Hydrogen ion transmembrane transport |
| Mitochondrial electron transport, ubiquinol to cytochrome C |

c.

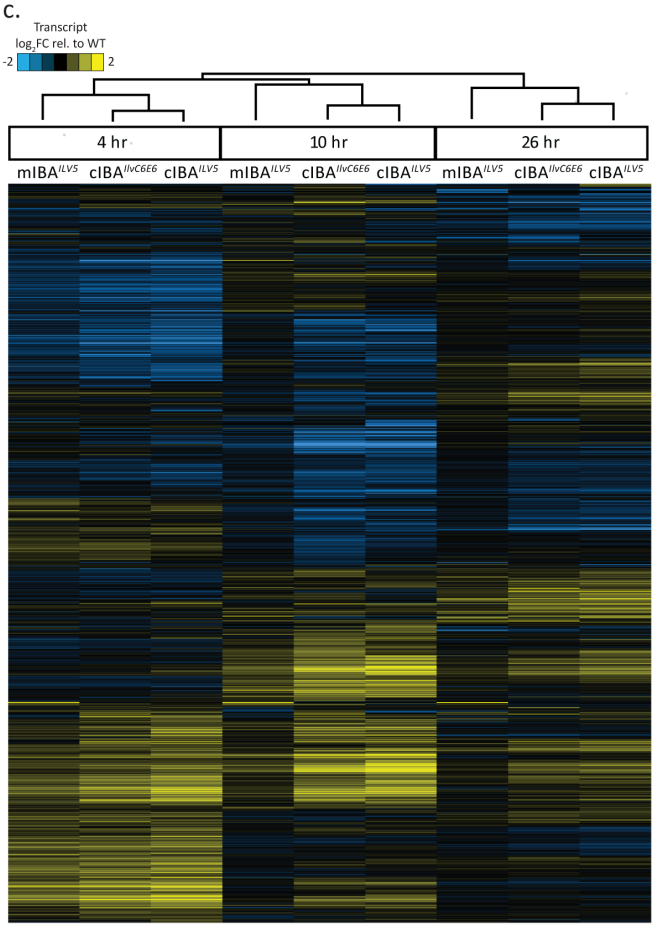


Figure 3.3: **Transcriptomics overview of the engineered isobutanol strains. a)** Number of differentially expressed genes at an elevated or reduced level in the engineered strains relative to WT **b)** Venn Diagram showing the number of overlapping differentially expressed genes in the cIBA$^{IlvC6E6}$ and cIBA$^{ILV5}$ strains and the GO terms enrichment results (Bonferroni adjusted P $<$ 1E-05). **c)** Heatmap shows the average relative $Log_2$ fold change of genes (rows) for each strain/time point (columns) relative to WT. The three sampling times were early-exponential phase (4 h), mid-exponential phase (10 h), and early-stationary phase (26 h) for strains mIBA$^{ILV5}$, cIBA$^{ILV5}$, and cIBA$^{IlvC6E6}$ grown in minimal medium anaerobically. Yellow denotes induced expression, blue denotes repressed expression, and black denotes unchanged values according to the key. Hierarchical clustering was performed with Cluster 3.0 and visualized in Java TreeView. The transcriptome of the cIBA$^{ILV5}$ and cIBA$^{IlvC6E6}$ strains were more similar than the mIBA$^{ILV5}$ strain.

this was due to overexpression of the synthetic KDC enzyme, Aro10p, in our engineered strains enhancing aromatic amino acid degradation flux (Fig.3.9). The depletion of phenylalanine (Phe) and tyrosine (Tyr) did not cause any unexpected changes in cell growth as supplementation with 0.1% (w/v) Phe and Tyr yielded no improvement in growth rate (Fig.3.10). Metabolites in the IBA pathway were also dramatically altered but more so

in the cIBA$^{IlvC6E6}$ and cIBA$^{ILV5}$ strains when compared to WT (Fig.3.8). The remainder of the manuscript will discuss conclusions we drew after integrating specific aspects of the functional genomics data.

### 3.4.4 Cytosolic-localized isobutanol pathway has a bottleneck at Ilv3p

We first examined data related to enzymes in the isobutanol pathway. To judge if each of our synthetic enzyme variants was expressed, the mRNA counts and protein abundance data were investigated. Normalized counts (RPKM) for all synthetic codon-optimized isobutanol genes (*ILV2*, *ILV2*$^{\triangle 2\text{-}54}$, *ILV5*, *ILV5*$^{\triangle 2\text{-}48}$, *ilvC*$^{6E6}$, *ILV3*, *ILV3*$^{\triangle 2\text{-}19}$, *MLS-adhA*$^{29C8}$, *adhA*$^{29C8}$, *MLS-ARO10*, and *ARO10*) were successfully detected in the transcriptomes of the engineered strains (Table.3.4). In general, the amount of RNA detected for each transcript correlated with the predicted promoter strengths of each gene ($P_{TDH3}$-*ARO10* > $P_{PGK1}$-*ILV3* > $P_{TEF1}$-*ILV5*/*ilvC*$^{6E6}$ > $P_{TEF2}$-*adhA*$^{29C8}$ > $P_{ADH1}$-*ILV2*) (Table.3.4) [153, 154]. The transcript levels of the native *ILV2*, *ILV5*, *ILV3*, and *ARO10* genes were also investigated, and as expected, the mRNA abundances of the native genes were not statistically significantly altered in any of the engineered strains compared to the WT strain (File S1). The protein levels of the isobutanol enzymes (Ilv2p, Ilv3p, Ilv5p, and Aro10p) were elevated across all the engineered strains when compared to WT (Fig.3.4). This elevated protein abundance in our engineered strains can be a result of our synthetic variants being successfully translated and contributing to the protein pool. Overall, neither the mRNA counts nor the protein abundance data yielded an explanation for the differences in isobutanol production we observed between the engineered strains. We contribute the higher isobutanol production in the mIBA$^{ILV5}$ strain to be the result

of added activity from the mitochondrial pathway localization.

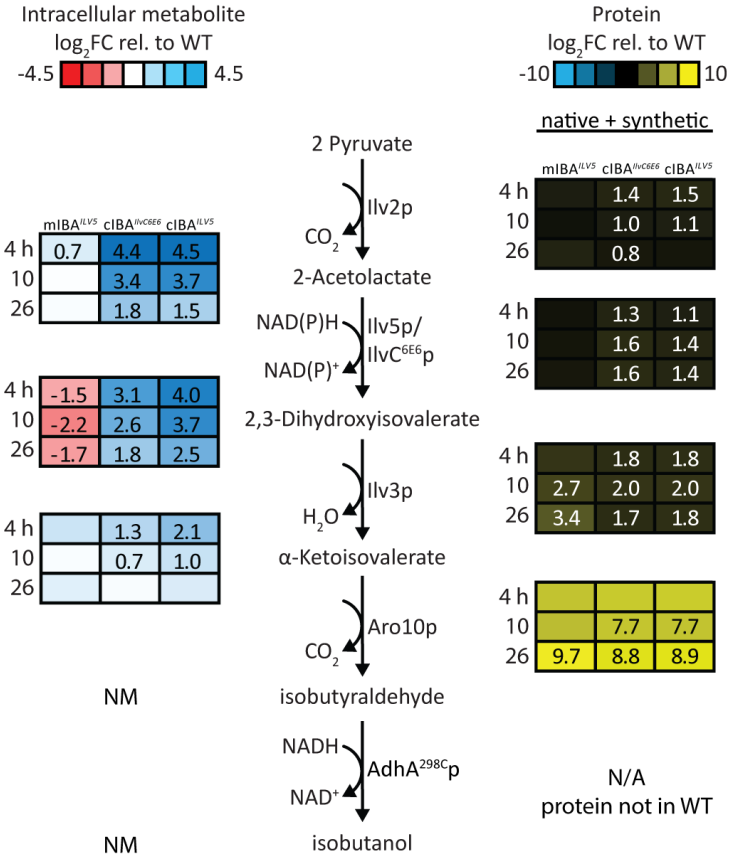


Figure 3.4: **Intracellular metabolite and protein levels of the isobutanol pathway.** Heat map values correspond to average $Log_2$ fold change relative to WT at the 3 sampling times (4, 10, and 26 h). For the intracellular metabolite data, red denotes lower metabolite levels, blue denotes higher metabolite levels, and white denotes unchanged values; for the protein data, blue denotes lower protein levels, yellow denotes higher protein levels, and black denotes unchanged values. Protein values represent the sum of the native and synthetic proteins. Statistical significance (P/FDR $<$ 0.05) is indicated by the presence of a number in the heatmap cell. NM stands for not measured, and N/A stands for not applicable as the protein is not endogenous to WT.

Next, we looked at the intracellular levels of the isobutanol pathway intermediates in our engineered strains and saw that 2-acetolactate (AL), 2,3-dihydroxyisovalerate (DHIV), and $\alpha$-ketoisovalerate (KIV) were significantly altered compared to the WT strain. At hr 4, the cIBA$^{ILV5}$ strain had a 23-fold (P $<$ 5.0E-4), 16-fold (P $<$ 5.0E-5), and 4.1-fold (P $<$ 0.005) increase in intracellular AL, DHIV, and KIV, respectively when compared to WT. Similarly, at hr 4, the cIBA$^{IlvC6E6}$ strain had a 22-fold (P $<$ 5e-6), 8.6-fold (P $<$ 0.0005), and 2.5-fold (P $<$5E-4) increase in intracellular AL, DHIV, and

KIV, respectively when compared to WT (Fig.3.5). This trend of elevated intracellular AL, DHIV, and KIV in the cIBA$^{IlvC6E6}$ and cIBA$^{ILV5}$ strains was also seen at the other timepoints, hr 10 and 26, but to a lesser extent. The significant accumulation of AL and DHIV in these strains suggests that *ILV3* is a rate-limiting step. This finding was also in agreement with a previous study where additional copies of *ILV3* were added to boost production of KIV from DHIV [102]. In contrast to the cIBA$^{IlvC6E6}$ and cIBA$^{ILV5}$ strains, intracellular levels of DHIV in the mIBA$^{ILV5}$ strain were at lower levels compared to the WT strain; specifically, the level of DHIV was 2.8-fold ($P < 5E\text{-}4$), 4.5-fold ($P < 0.005$), and 3.2-fold ($P < 0.005$) lower when compared to WT at hr 4, 10, and 26 respectively, which indicates mitochondrial-localized Ilv3p is not a bottleneck.

We hypothesized that the mitochondrial-localized Ilv3p is not a rate-limiting step in the mIBA$^{ILV5}$ strain because the required cofactor for the enzyme, a 2Fe-2S cluster, is more accessible in the mitochondria where its biogenesis begins. This is not the case for the cIBA$^{IlvC6E6}$ and cIBA$^{ILV5}$ strains since the synthesis and delivery of the required 2Fe-2S cluster into the cytosolic-localized Ilv3p requires Fe-S cluster biogenesis machinery that spans multiple compartments (both the mitochondria and cytosol). Specifically, the mitochondrial iron sulfur cluster (ISC) machinery is responsible for generating the sulfur-containing intermediate (X-S), which is then exported to the cytosol via the ABC transporter Atm1p [155]. In the cytosol, the X-S intermediate is matured into a cluster and loaded onto the cytosolic-localized apoprotein by the cytosolic iron sulfur cluster assembly (CIA) machinery (Fig.3.5a). We hypothesized that the Ilv3p step is rate-limiting in the cIBA$^{IlvC6E6}$ and cIBA$^{ILV5}$ strains due to this added complexity of the cross-compartmental assembly of the required cofactor. To confirm that our cytosolic-localized Ilv3p was functional, we deleted the endogenous mitochondrial-localized *ILV3*

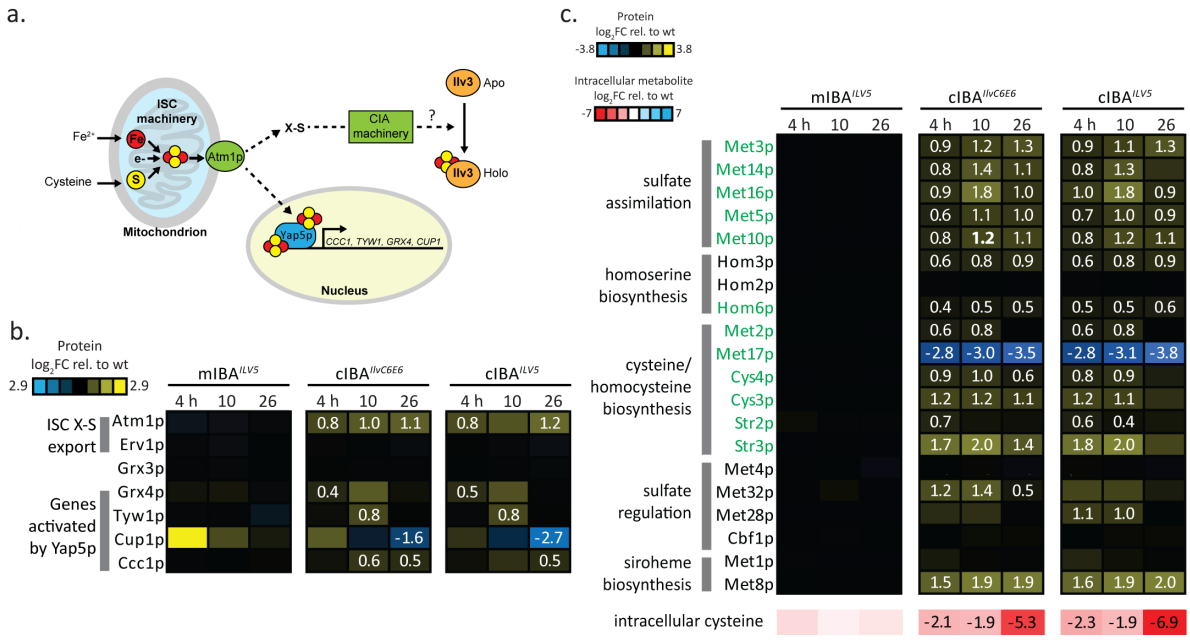


Figure 3.5: **Proteomic response of sulfur-related pathways in the engineered strains a)** Model for cytosolic 2Fe–2S cluster biogenesis, delivery, and sensing. Fe–S cluster biogenesis begins with the mitochondrial iron sulfur cluster (ISC) machinery where a sulfur containing compound (X–S) is made and exported to the cytosol via the ABC transporter, Atm1p. Through a yet unknown mechanism, the X–S intermediate is matured into a 2Fe–2S cluster and loaded into the cytosolically localized DHAD/Ilv3p apoprotein to form the holo form; we hypothesize that this process is facilitated by the cytosolic iron sulfur cluster assembly (CIA) machinery. High cytosolic iron conditions are sensed by the transcription factor Yap5p via binding two 2Fe–2S clusters; once clusters are bound, Yap5p undergoes a conformational change and activates transcription of genes in the nucleus including *CCC1*, *TWY1*, *GRX4*, and *CUP1*. **b)** Heat map shows the protein levels of such genes in model a. **c)** Heat map shows the protein levels of genes in sulfur-related pathways and the intracellular level of cysteine. Genes that are transcriptionally activated by Met4p under cysteine-depleted conditions are indicated in green. For all heatmaps, values correspond to average $Log_2$ fold change relative to WT at the 3 timepoints (4, 10, and 26 h). For the protein data, blue denotes lower protein levels, yellow denotes higher protein levels, and black denotes unchanged values. For the intracellular metabolite data, red denotes lower metabolite levels, blue denotes higher metabolite levels, and white denotes unchanged values. Statistical significance (P/FDR $< 0.05$) is indicated by the presence of a number in the heatmap cell.

in the cIBA$^{IlvC6E6}$ strain and performed a growth complementation assay to see if our synthetic cytosolic-localized Ilv3p could restore growth on synthetic complete medium lacking valine; indeed, the strain harboring only the cytosolic-localized Ilv3p grew on synthetic complete medium minus valine plates indicating it was functional in its non-native subcellular compartment (Fig.3.11). In summary, the lower performance of the

strain with the cytosolic-localized pathway was due to a rate-limiting step in the pathway at Ilv3p.

### 3.4.5 Proteomic analysis revealed a cytosolic-localized isobutanol pathway results in altered sulfur metabolism

To further explore our hypothesis that the Fe-S cluster requiring enzyme was the rate-limiting step in the cIBA$^{IlvC6E6}$ and cIBA$^{ILV5}$ strains, we took a closer look at genes involved in Fe-S cluster synthesis. The protein levels of enzymes in the ISC and CIA machinery between the engineered strains and WT were relatively unchanged, with the exception of Atm1p, the mitochondrial X-S intermediate transporter (Table.3.5). Atm1p was upregulated approximately 2.0-fold in the cIBA$^{IlvC6E6}$ and cIBA$^{ILV5}$ strains at all time points when compared to WT (Fig.3.5b). Atm1p overexpression is predicted to increase the number of available clusters in the cytosol by increasing the abundance of the X-S intermediate used by the CIA machinery for generating cytosolic Fe-S clusters [155]. In the cytosol, excess Fe-S clusters are sensed by the iron responsive transcription factor, Yap5p. Yap5p can stably bind to 2Fe-2S clusters, inducing a conformational change that activates the transcription of genes to help regulate iron storage including *CCC1*, *TWY1*, *GRX4*, and *CUP1* (Fig.3.5a). Indeed, protein levels of Ccc1p, Tyw1p, and Grx4p were elevated in the cIBA$^{IlvC6E6}$ and cIBA$^{ILV5}$ strains for at least one of the time points with Tyw1p having the highest fold change of 1.7 at hr 10 when compared to WT (Fig.3.5b). This increase in Yap5p responsive genes indicated there was an increased number of 2Fe-2S clusters in the cytosol of the cIBA$^{IlvC6E6}$ and cIBA$^{ILV5}$ strains compared to WT, which was expected with the increased level of Atm1p.

We next asked if the different isobutanol pathways could affect other aspects of the

strain's proteome. Pathway enrichment analysis using Funspec [2] was performed on the statistically significant protein hits from the cIBA$^{IlvC6E6}$ and cIBA$^{ILV5}$ strains to identify any enriched patterns. Proteins at a higher abundance compared to WT were enriched (P < 5E-5) for sulfur-related pathways (methionine biosynthesis [GO:0009086], cysteine biosynthesis [GO:0019344], and sulfate assimilation [GO:0000103]) (File S5). The protein abundance of enzymes in sulfate assimilation, sulfate regulation, homoserine biosynthesis, cysteine biosynthesis, and siroheme biosynthesis pathways were elevated in the cIBA$^{IlvC6E6}$ and cIBA$^{ILV5}$ strains compared to WT (Fig.3.5c). This response was largely due to the depletion of intracellular cysteine since *MET* gene expression is induced by Met4p under cysteine-limited conditions [156]; in fact, the intracellular cysteine levels were depleted in all engineered strains but more significantly in the cIBA$^{IlvC6E6}$ and cIBA$^{ILV5}$ strains (Fig.3.5c). Cysteine is used as the sulfur donor for synthesizing Fe-S clusters, and we hypothesized the altered sulfur metabolism was related to the 2Fe-2S cluster requirement of the rate-limiting enzyme, Ilv3p. The elevated levels of Atm1p in conjunction with the elevated sulfur metabolism suggests that the strains with the cytosolic pathway are trying to overcome a limitation in the quantity of cytosolic Fe-S clusters. We hypothesize that the insufficient availability of cytosolic Fe-S clusters causes the Ilv3p to be the bottleneck in the cIBA$^{IlvC6E6}$ and cIBA$^{ILV5}$ strains.

### 3.4.6 Increasing iron availability boosts production with a cytosolic-localized pathway

We next sought to determine if the cIBA$^{IlvC6E6}$ and cIBA$^{ILV5}$ strains' performance would benefit from increased Fe-S cluster biogenesis in the cell. This strategy was successful in increasing the activity of a different cytosolic-localized Fe-S cluster requiring enzyme,

xylonate dehydratase, in *S. cerevisiae* [157, 158]. This can be accomplished by increasing the availability of iron in the cell through deregulation of the iron regulon genes. To test our hypothesis, we disrupted iron homeostasis by deleting the transcriptional repressor Fra2p (also referred as its standard name Bol2p) of the iron regulon transcriptional activator, Aft1/2p, in the cIBA$^{ILV5}$ and mIBA$^{ILV5}$ strains (Fig.3.6a) [155, 159]. We then performed a time-course experiment where extracellular isobutanol production was monitored periodically and intracellular isobutanol metabolites were measured during mid-exponential phase (10 hr) and early-stationary phase (26 hr) (Fig.3.6b-c). We observed that the deletion of *FRA2* significantly altered the isobutanol titer in the cIBA$^{ILV5}$ background strain, but not in the mIBA$^{ILV5}$ strain; the cIBA$^{ILV5}$*fra2*△ strain produced 190 mg/L isobutanol at 48 hr which is 2.4-fold more than the cIBA$^{ILV5}$ strain ($P < 5E\text{-}5$) (Fig.3.6b). Furthermore, the titer achieved by the cIBA$^{ILV5}$*fra2*△ strain surpassed the isobutanol titer in our previous best producer, mIBA$^{ILV5}$, by 1.3-fold ($P < 5E\text{-}5$) indicating a high titer with a cytosolic isobutanol pathway localization can be achieved. We hypothesize the *fra2* deletion had no effect on isobutanol titer in the mIBA$^{ILV5}$ strain because the cofactor availability for the mitochondrial-localized Ilv3p was not limited.

We next tested if the deletion of *FRA2* specifically benefited Ilv3p by looking at the intracellular metabolite levels of the enzyme's reactant, DHIV, and product, KIV (Fig.3.6c). Indeed, the cIBA$^{ILV5}$*fra2*△ strain had lower levels of DHIV compared to the cIBA$^{ILV5}$ strain indicating the Ilv3p bottleneck was partially relieved; the normalized peak area (peak area /$OD_{600}$) of DHIV was 1.7-fold ($P < 0.05$) and 2.9-fold ($P < 0.005$) lower in cIBA$^{ILV5}$*fra2*△ compared to cIBA$^{ILV5}$ at hr 10 and 26, respectively. The KIV level was also measured, but we did not observe an increased level of KIV in the cIBA$^{ILV5}$*fra2*△ strain compared to the cIBA$^{ILV5}$ strain as one might expect from relieving the bottleneck

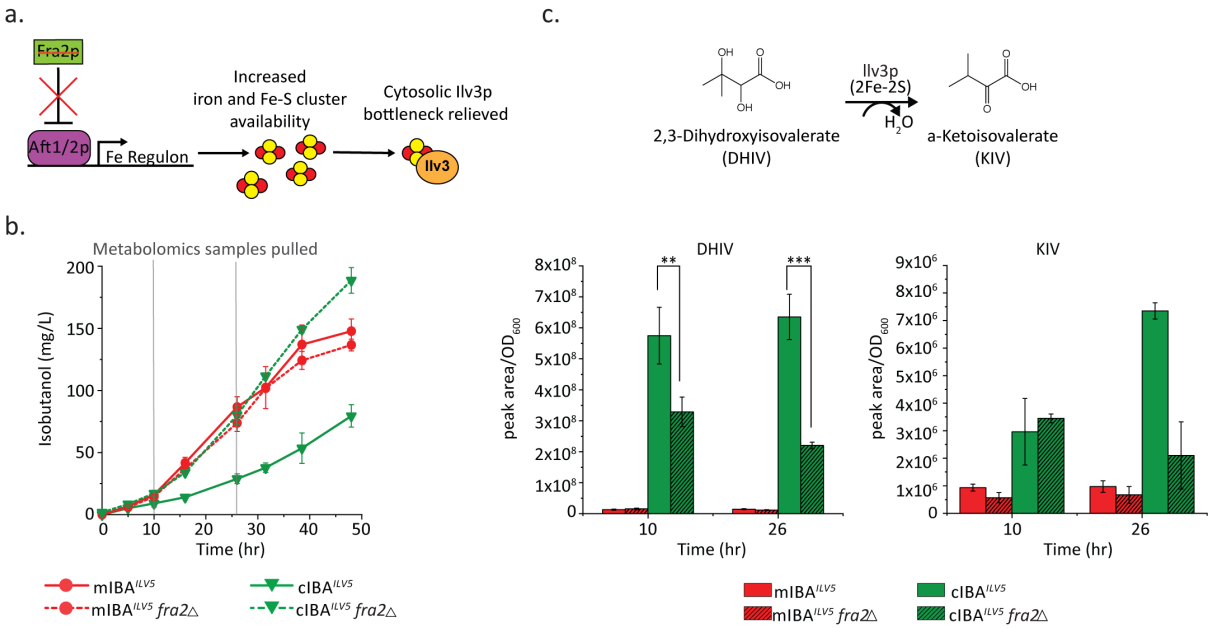


Figure 3.6: **Increasing iron availability improves isobutanol production with cytosolic-localized pathway a)** Schematic demonstrating how Ilv3p activity may be enhanced by altering iron homeostasis. The transcriptional activator, Aft1/2p, is negatively regulated by Fra2p. **b)** Isobutanol titer of engineered isobutanol producing strains with and without *FRA2* deletion. **c)** Normalized peak area (peak area/$OD_{600}$) of Ilv3p's metabolites (reactant DHIV and product KIV) observed by LC-MS. Samples for metabolomics were pulled at 10 and 26 h post inoculation. Fermentation was performed under anaerobic conditions in minimal medium. Error bars represent the standard deviation of three biological replicates. Asterisks denote statistically significant differences by pairwise t-test (*, $P < 0.05$; **, $P < 0.005$; ***, $P < 0.0005$).

at Ilv3p. Instead, the KIV level between the engineered strains was not significantly altered, except at hr 26 where the cIBA$^{ILV5}$ strain had a 3.5-fold increase in KIV compared to the cIBA$^{ILV5}$*fra2*△ strain ($P < 0.05$). We suspect an accumulation of KIV was not seen because KIV is readily consumed in the subsequent step. Taken together, the *fra2* mutation in the cIBA$^{ILV5}$ strain resulted in an increase in isobutanol titer, potentially by partially overcoming the 2Fe-2S cluster cofactor limitation for cytosolic Ilv3p.

## 3.5 Conclusions

Here, we combined transcriptomic, proteomic, and metabolomic analyses to generate a wealth of data on how enzyme pathway localization and redox cofactor-balancing affect isobutanol biosynthesis and physiology in genetically engineered *S. cerevisiae*. Localizing isobutanol pathway enzymes to the mitochondria resulted in higher titers, while cytosolic localization resulted in much lower titers. Metabolomic analysis uncovered a potential limitation in cytosolic Fe-S cluster biogenesis. This limitation could be overcome by increasing Fe uptake through deletion of *FRA2*. This strategy of increasing the availability of iron in the cell was also successful in increasing the activity of another Fe-S cluster requiring enzyme xylonate dehydratase; however, this strategy may not be effective for all Fe-S cluster requiring enzymes as this strategy had no effect on 6-phosphogluconate dehydratase activity [157, 160]. While we did not observe a beneficial effect in having a redox cofactor-balanced isobutanol pathway, we hypothesize that the cofactor imbalance will have to be resolved for the capacity of the isobutanol pathway to be enhanced. Furthermore, any problems caused by an imbalance will be exacerbated when ethanol flux is displaced to enhance the rate of isobutanol synthesis. Future functional genomics studies with engineered strains disabled for ethanol production should uncover new genetic targets for achieving greater isobutanol titers and yields.

## 3.6 Data availability

The mass spectrometry proteomics data have been deposited to the MassIVE database with the identifier MSV000088169. The transcriptomics data discussed in this publication has been deposited in NCBI's Gene Expression Omnibus [161] and is accessible

through GEO Series accession number GSE186126 (https://www.ncbi.nlm.nih.gov/ geo/-query/acc.cgi?acc=GSE186126). Intracellular metabolomics data is available on GitHub (https://github.com/AmadorNoguezLab/compartmentalized-isobutanol-pathways-in-S.-cerevisiae). The full isobutanol pathway cassette sequence containing mitochondrial-localized enzymes and flanking HO arms is available on GenBank with the identifier MZ541859. The supplumental files (FileS1-S5) is available on GitHub (https://github.com/Pfleger-Lab/Theses/tree/main/Francesca%20Gambacorta/Chapter3).

# 3.7 Supplemental Information

## 3.7.1 Supplementary Figures

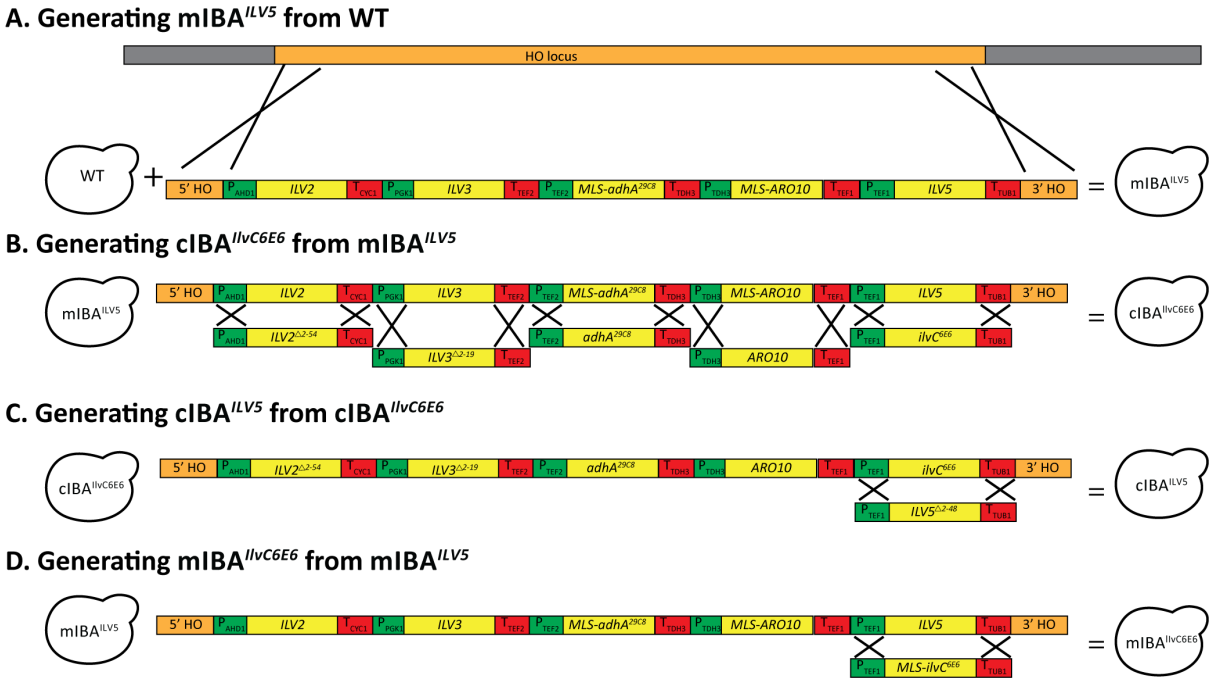


Figure 3.7: **Graphical description for the construction of the engineered isobutanol producing *S. cerevisiae* strains.** Synthetic isobutanol pathways were integrated via CRISPR/Cas9 editing at the *HO* locus. Naming convention is as follows: mitochondrial-localized isobutanol pathway (mIBA), cytosolic-localized isobutanol pathway (cIBA), NADPH-dependent KARI enzyme (Ilv5p), and NADH-dependent KARI enzyme (IlvC$^{6E6}$p) (Materials and methods 2.2). *HO* locus is indicated by an orange box, promoters are in green boxes, genes are in yellow boxes, and terminators are in red boxes.

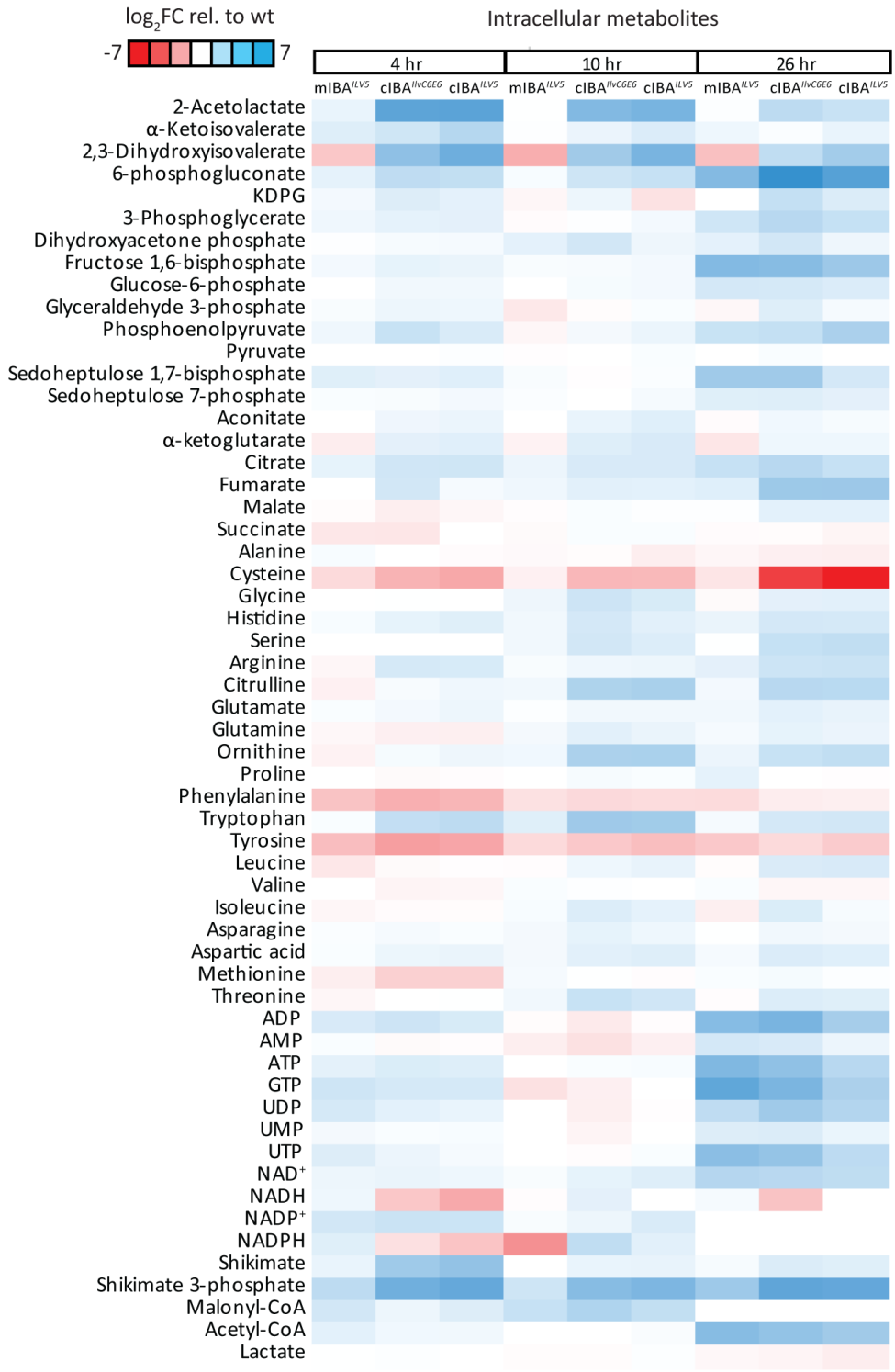


Figure 3.8: **Intracellular metabolite data for engineered strains.** Heatmap shows the average $\log_2$ fold change of intracellular metabolites (rows) for each strain/timepoint (columns) relative to WT. Values were normalized by $OD_{600}$. The three sampling times were early-exponential phase (4 hr), mid-exponential phase (10 hr), and early-stationary phase (26 hr) for strains mIBA$^{ILV5}$, cIBA$^{ILV5}$, and cIBA$^{IlvC6E6}$ grown in minimal medium anaerobically. Blue denotes higher metabolite levels and red denotes lower metabolite levels, while white denotes unchanged values.

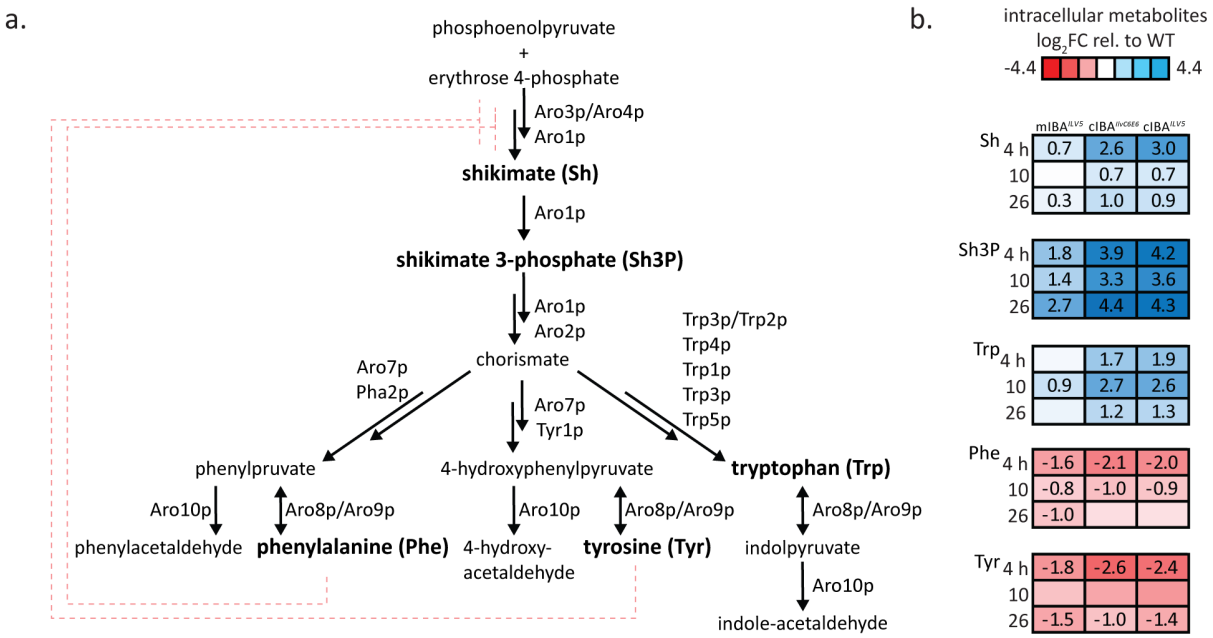


Figure 3.9: **Aromatic amino acid intermediates altered in engineered strains. a)** Pathway of aromatic amino acid biosynthesis and catabolism in *S. cerevisiae*. The red dashed lines indicate feedback inhibition of Aro3p by phenylalanine and Aro4p by tyrosine. Bolded metabolite names indicate intracellular metabolite levels were quantified. **b)** Heat map shows the intracellular metabolite levels of chorismate biosynthesis intermediates and aromatic amino acids: shikimate (Sh), shikimate 3-phosphate (Sh3P), tryptophan (Trp), phenylalanine (Phe), and tyrosine (Tyr). Values correspond to average $\log_2$ fold change relative to WT at the 3 timepoints (4, 10, and 26 hr). Red denotes lower metabolite levels, blue denotes higher metabolite levels, and white denotes unchanged values. Statistical significance ($P < 0.05$) is indicated by the presence of a number in the heatmap cell.

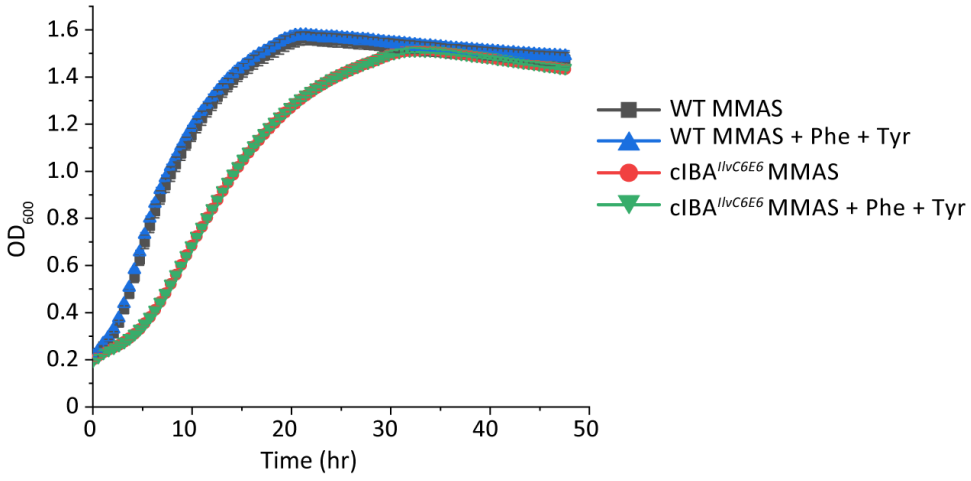


Figure 3.10: **Aromatic amino acid supplementation does not boost growth in engineered strain.** Growth curve of WT and the cIBA$^{IlvC6E6}$ strains on minimal medium with ammonium sulfate (MMAS) supplemented with and without 0.1% wt/v phenylalanine and tyrosine. Fermentation was performed under anaerobic conditions in a 24-well plate for 48 hrs. Error bars represent the standard deviation of three biological replicates.

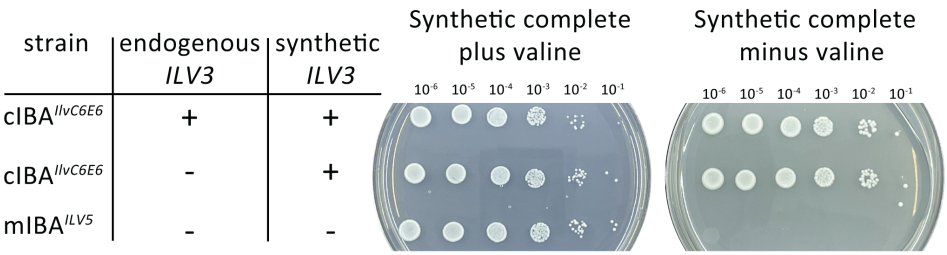


Figure 3.11: **Growth complementation assay for cytosolic-localized synthetic Ilv3p.** Growth phenotypes of engineered strain cIBA$^{IlvC6E6}$ with and without the endogenous *ILV3* plus mIBA$^{ILV5}$ lacking endogenous and synthetic *ILV3* (negative control or mIBA$^{ILV5}$*ilv3-null*). 10 $\mu$L cell suspensions with 10-fold serial dilutions were plated on a synthetic complete media plate (left) and synthetic complete minus valine medium plate (right). Pictures demonstrate that the engineered copy of Ilv3p in cIBA$^{IlvC6E6}$, which is localized to the cytosol, is functional as it restores the growth on medium lacking valine.

### 3.7.2 Supplementary Tables

Table 3.1: *S. cerevisiae* strains used in this work

| **Strain Name** | **Relevant Genotype** |
|---|---|
| CEN.PK113-5D | *MATa ura3-52 MAL2-8c* (REF DOI: 10.3303/CET1438078) or EUROSCARF collection (www.uni-frankfurt.de/fb15/mikro/euroscarf) |
| WT | CEN.PK113-5D, ura3::*URA3* |
| mIBA$^{ILV5}$ | WT with *ho*△::$P_{ADH1}$-*ILV2*-$T_{CYC1}$-$P_{PGK1}$-*ILV3*-$T_{TEF2}$-$P_{TEF2}$-*MLS-adhA*$^{29C8}$-$T_{TDH3}$-$P_{TDH3}$-*MLS-ARO10*-$T_{TEF1}$-$P_{TEF1}$-*ILV5*-$T_{TUB1}$ |
| mIBA$^{IlvC6E6}$ | WT with *ho*△::$P_{ADH1}$-*ILV2*-$T_{CYC1}$-$P_{PGK1}$-*ILV3*-$T_{TEF2}$-$P_{TEF2}$-*MLS-adhA*$^{29C8}$-$T_{TDH3}$-$P_{TDH3}$-*MLS-ARO10*-$T_{TEF1}$-$P_{TEF1}$-*MLS-ilvC*$^{6E6}$-$T_{TUB1}$ |
| cIBA$^{IlvC6E6}$ | WT with *ho*△::$P_{ADH1}$-*ILV2*-$T_{CYC1}$-$P_{PGK1}$-*ILV3*-$T_{TEF2}$-$P_{TEF2}$-*adhA*$^{29C8}$-$T_{TDH3}$-$P_{TDH3}$-*ARO10*-$T_{TEF1}$-$P_{TEF1}$-*ilvC*$^{6E6}$-$T_{TUB1}$ |
| cIBA$^{ILV5}$ | WT with *ho*△::$P_{ADH1}$-*ILV2*-$T_{CYC1}$-$P_{PGK1}$-*ILV3*-$T_{TEF2}$-$P_{TEF2}$-*adhA*$^{29C8}$-$T_{TDH3}$-$P_{TDH3}$-*ARO10*-$T_{TEF1}$-$P_{TEF1}$-*ILV5*-$T_{TUB1}$ |
| cIBA$^{ILV5}$ *fra2*△ | cIBA$^{ILV5}$ with *fra2*△::*LoxP-hphMX-LoxP* |
| mIBA$^{ILV5}$ *fra2*△ | mIBA$^{ILV5}$ with *fra2*△::*LoxP-hphMX-LoxP* |
| mIBA$^{ILV5}$ *ilv3-null* | WT with *ilv3*△::*LoxP*, *ho*△::$P_{ADH1}$-*ILV2*-$T_{CYC1}$-$P_{PGK1}$-*LoxP-kanMX-LoxP*-$T_{TEF2}$-$P_{TEF2}$-*MLS-adhA*$^{29C8}$-$T_{TDH3}$-$P_{TDH3}$-*MLS-ARO10*-$T_{TEF1}$-$P_{TEF1}$-*ILV5*-$T_{TUB1}$ |
| cIBA$^{IlvC6E6}$ *ilv3*△ | cIBA$^{IlvC6E6}$ with *ilv3*△::*LoxP* |

Table 3.2: Average petite frequencies of the engineered strains and WT. Data was collected from three biological replicates.

| **Strain Name** | **Petite frequency (%)** |
|---|---|
| WT | 0.22 ± 0.26 |
| mIBA$^{ILV5}$ | 1.09 ± 1.21 |
| mIBA$^{IlvC6E6}$ | 36.53 ± 2.47 |
| cIBA$^{IlvC6E6}$ | 0.38 ± 0.24 |
| cIBA$^{ILV5}$ | 0.36 ± 0.21 |

Table 3.3: Number of differentially expressed proteins in the engineered strains relative to WT at an reduced or elevated level for the 3 timepoints (4, 10, and 26 hr).

| **Hr** | **Strains** | **Reduced** | **Elevated** |
|---|---|---|---|
| 4 | mIBA$^{ILV5}$ | 0 | 0 |
| | cIBA$^{IlvC6E6}$ | 311 | 267 |
| | cIBA$^{ILV5}$ | 174 | 189 |
| 10 | mIBA$^{ILV5}$ | 2 | 4 |
| | cIBA$^{IlvC6E6}$ | 213 | 183 |
| | cIBA$^{ILV5}$ | 239 | 223 |
| 26 | mIBA$^{ILV5}$ | 1 | 2 |
| | cIBA$^{IlvC6E6}$ | 194 | 320 |
| | cIBA$^{ILV5}$ | 123 | 194 |

Table 3.4: RNA counts of the native and synthetic isobutanol genes at the 3 sample times (4, 10, and 26 hr). Counts were normalized using Trimmed Means of M-values (TMM).

| | | **WT** | **mIBA$^{ILV5}$** | **cIBA$^{IlvC6E6}$** | **cIBA$^{ILV5}$** |
|---|---|---|---|---|---|
| native 4 hr | *ILV2* | 1199.5±156.6 | 891.1±162.1 | 867.5±68.1 | 729.7±5.3 |
| | *ILV5* | 2578.7±600.5 | 2088.6±386.4 | 7863.4±991.7 | 6654.9±357.5 |
| | *ILV3* | 3054.4±478.4 | 2122±142.4 | 3539.7±585.4 | 3651.9±400 |
| | *ARO10* | 33.4±6.6 | 19.9±3.5 | 23.5±5.7 | 18.2±1.7 |
| synthetic 4 hr | m*ILV2* | 0±0 | 220.4±16.4 | 0±0 | 0±0 |
| | c*ILV2* | 0±0 | 0±0 | 103.2±0.9 | 94.3±28 |
| | m*ILV5* | 0±0 | 1373.5±131.7 | 0±0 | 0±0 |
| | c*ILV5* | 0±0 | 0±0 | 0±0 | 2.2±2.3 |
| | c*IlvC$^{6E6}$* | 0±0 | 0±0 | 7344.3±1375.6 | 0±0 |
| | m*ILV3* | 0±0 | 4286.7±376.9 | 0±0 | 0±0 |
| | c*ILV3* | 0±0 | 0±0 | 1759.2±290.4 | 1738.8±319.5 |
| | m*ARO10* | 0±0 | 3091.8±809.3 | 0±0 | 0±0 |
| | c*ARO10* | 0±0 | 0±0 | 1094.3±149.5 | 785.1±102.9 |
| | m*AdhA$^{29c8}$* | 0±0 | 1207.5±273.4 | 0±0 | 0±0 |
| | c*AdhA$^{29c8}$* | 0±0 | 0±0 | 1360.9±375.8 | 1275.6±222.3 |
| native 10 hr | *ILV2* | 168.5±1.5 | 249.4±24.3 | 240.3±6.6 | 336±14.3 |
| | *ILV5* | 612.1±104 | 718.8±10.9 | 2783±137.7 | 3736.5±588.6 |
| | *ILV3* | 217.1±19.9 | 319.8±44.1 | 1137.9±176.4 | 938±82.3 |
| | *ARO10* | 23.4±2.3 | 24.9±3.5 | 22.2±2.5 | 20.9±5.3 |
| synthetic 10 hr | m*ILV2* | 0±0 | 41.7±3.9 | 0±0 | 0±0 |
| | c*ILV2* | 0±0 | 0±0 | 35.7±6.4 | 33.8±0.2 |
| | m*ILV5* | 0±0 | 449.3±80.9 | 0±0 | 0±0 |
| | c*ILV5* | 0±0 | 0±0 | 0±0 | 0.5±0.3 |
| | c*IlvC$^{6E6}$* | 0±0 | 0.1±0.1 | 3815±658.4 | 0±0 |
| | m*ILV3* | 0±0 | 3167.3±383.1 | 4.1±1.4 | 1.5±0.8 |
| | c*ILV3* | 0±0 | 0±0 | 1832±314.1 | 1123.5±57.6 |
| | m*ARO10* | 0±0 | 1610.3±248.5 | 0±0 | 0±0 |
| | c*ARO10* | 0±0 | 0±0 | 644.5±61.7 | 535.7±52.1 |
| | m*AdhA$^{29c8}$* | 0±0 | 1581.2±225.5 | 0±0 | 0±0 |
| | c*AdhA$^{29c8}$* | 0±0 | 0±0 | 1278.5±224.8 | 1126.7±84.7 |
| native 26 hr | *ILV2* | 72.5±10.1 | 93.2±9.3 | 94.5±8.6 | 108.7±12.6 |
| | *ILV5* | 596.4±36.2 | 537.1±10.9 | 831.7±192.4 | 875±52.5 |
| | *ILV3* | 137.6±14.9 | 177.3±6.7 | 192.8±18.8 | 239.1±44.6 |
| | *ARO10* | 42±0.4 | 42.9±5.8 | 47.8±11.5 | 58.1±10.1 |
| synthetic 26 hr | m*ILV2* | 0±0 | 113.7±98.5 | 0±0 | 0±0 |
| | c*ILV2* | 0±0 | 0±0 | 100.7±73.8 | 50.7±9.8 |
| | m*ILV5* | 0±0 | 96±83.6 | 0.1±0.1 | 0±0 |
| | c*ILV5* | 0±0 | 0±0 | 0±0 | 340.2±481.1 |
| | c*IlvC$^{6E6}$* | 0.1±0.2 | 0±0 | 346.2±180.4 | 0±0 |
| | m*ILV3* | 0±0 | 382±331.9 | 0±0 | 0±0 |
| | c*ILV3* | 0±0 | 0±0 | 393.1±133.6 | 289.1±49.8 |
| | m*ARO10* | 0±0 | 120.5±105.2 | 0±0 | 0±0 |
| | c*ARO10* | 0±0 | 0±0 | 118.1±54.9 | 99.1±2.4 |
| | m*AdhA$^{29c8}$* | 0±0 | 320.4±277.6 | 0±0 | 0±0 |
| | c*AdhA$^{29c8}$* | 0±0 | 0±0 | 324.7±88.9 | 277±39.3 |

Table 3.5: Protein abundance data for proteins involved in synthesizing Fe-S clusters. Including proteins in the core ISC and CIA machinery, along with accessory proteins. Values are $\log_2$ fold change relative to WT at the 3 timepoints (4, 10, and 26 hr). Data is significant if FDR $< 0.05$.

| | | **4 hr** | | | | | |
|---|---|---|---|---|---|---|---|
| | | **$\log_2$ FC relative to WT** | | | **FDR** | | |
| | Protein | **mIBA *ILV5*** | **cIBA *IlvC6E6*** | **cIBA *ILV5*** | **mIBA *ILV5*** | **cIBA *IlvC6E6*** | **cIBA *ILV5*** |
| Iron sensing and regulation | Mrs3p | 0.27 | 1.22 | 0.81 | 0.73 | 0.07 | 0.14 |
| | Mrs4p | 0.00 | 0.09 | -0.17 | 1.00 | 0.65 | 0.38 |
| | Ccc1p | -0.06 | 0.16 | 0.13 | 0.58 | 0.10 | 0.24 |
| | Smf3p | -0.08 | -0.43 | -0.63 | 0.81 | 0.15 | 0.10 |
| Core ISC | Nfs1p | -0.10 | -0.08 | -0.01 | 0.55 | 0.44 | 0.89 |
| | Isd11p | 0.28 | 0.05 | -0.10 | 0.25 | 0.54 | 0.48 |
| | Arh1p | -0.14 | -0.07 | 0.01 | 0.61 | 0.22 | 0.95 |
| | Yah1p | -0.58 | -0.26 | -0.17 | 0.31 | 0.02 | 0.26 |
| | Yfh1p | -0.05 | -0.05 | -0.27 | 0.86 | 0.60 | 0.16 |
| | Isu1p | -0.08 | 0.02 | -0.23 | 0.81 | 0.94 | 0.36 |
| | Isu2p | 0.42 | -0.06 | -0.19 | 0.36 | 0.71 | 0.31 |
| | Ssq1p | -0.05 | 0.11 | 0.18 | 0.76 | 0.13 | 0.30 |
| | Jac1p | 0.27 | 0.37 | 0.45 | 0.63 | 0.35 | 0.28 |
| | Mge1p | 0.22 | -0.04 | -0.02 | 0.41 | 0.77 | 0.85 |
| | Grx5p | -0.16 | -0.03 | -0.12 | 0.54 | 0.89 | 0.67 |
| | Ssc1p | 0.42 | 0.07 | 0.09 | 0.17 | 0.26 | 0.34 |
| ISC targeting | Isa2p | 0.18 | 0.15 | 0.03 | 0.70 | 0.28 | 0.88 |
| | Iba57p | 0.40 | 0.05 | 0.10 | 0.22 | 0.78 | 0.38 |
| | Nfu1p | -0.10 | 0.28 | 0.31 | 0.59 | 0.09 | 0.07 |
| Core CIA | Cfd1p | -0.05 | 0.12 | 0.01 | 0.81 | 0.57 | 0.96 |
| | Nbp35p | 0.01 | 0.13 | 0.19 | 0.97 | 0.39 | 0.09 |
| | Nar1p | -0.20 | 0.15 | 0.04 | 0.67 | 0.23 | 0.68 |
| | Cia1p | -0.06 | 0.08 | 0.03 | 0.73 | 0.43 | 0.77 |
| | Dre2p | -0.08 | 0.21 | 0.09 | 0.71 | 0.07 | 0.24 |
| | Met18p | 0.02 | 0.07 | -0.01 | 0.95 | 0.27 | 0.95 |
| | Tah18p | -0.18 | -0.15 | -0.12 | 0.26 | 0.14 | 0.22 |
| Iron trafficking | Grx3p | -0.02 | 0.02 | 0.00 | 0.95 | 0.80 | 0.96 |
| | Grx4p | 0.16 | 0.44 | 0.52 | 0.23 | 0.02 | 0.02 |
| ISC X-S export | Atm1p | -0.40 | 0.80 | 0.84 | 0.21 | 0.01 | 0.04 |
| | Erv1p | -0.12 | 0.04 | 0.02 | 0.73 | 0.67 | 0.88 |

| | | 10 hr | | | | | |
|---|---|---|---|---|---|---|---|
| | | **$log_2$ FC relative to WT** | | | **FDR** | | |
| | Protein | **mIBA *ILV5*** | **cIBA *IlvC6E6*** | **cIBA *ILV5*** | **mIBA *ILV5*** | **cIBA *IlvC6E6*** | **cIBA *ILV5*** |
| Iron sensing and regulation | Mrs3p | -0.68 | 0.27 | -0.19 | 0.69 | 0.70 | 0.81 |
| | Mrs4p | 0.59 | -0.65 | -0.73 | 0.26 | 0.16 | 0.07 |
| | Ccc1p | 0.00 | 0.61 | 0.53 | 0.99 | 0.02 | 0.06 |
| | Smf3p | 0.23 | -0.67 | -0.78 | 0.31 | 0.03 | 0.05 |
| Core ISC | Nfs1p | 0.12 | -0.17 | -0.06 | 0.28 | 0.21 | 0.39 |
| | Isd11p | 0.17 | -0.08 | -0.21 | 0.83 | 0.87 | 0.66 |
| | Arh1p 0.09 | -0.11 | -0.13 | 0.33 | 0.12 | 0.09 | |
| | Yah1p | -0.37 | -0.20 | -0.34 | 0.20 | 0.36 | 0.17 |
| | Yfh1p | -0.29 | -0.07 | -0.48 | 0.45 | 0.65 | 0.23 |
| | Isu1p | 0.59 | 0.32 | 0.14 | 0.76 | 0.81 | 0.92 |
| | Isu2p | 1.69 | 0.96 | 1.15 | 0.08 | 0.04 | 0.16 |
| | Ssq1p | 0.02 | -0.07 | 0.00 | 0.91 | 0.48 | 0.97 |
| | Jac1p | 0.02 | 0.14 | 0.13 | 0.96 | 0.47 | 0.70 |
| | Mge1p | 0.05 | 0.01 | 0.05 | 0.57 | 0.92 | 0.43 |
| | Grx5p | -0.20 | 0.12 | 0.09 | 0.60 | 0.36 | 0.78 |
| | Ssc1p | 0.23 | -0.04 | -0.03 | 0.11 | 0.52 | 0.80 |
| ISC targeting | Isa2p | 0.08 | 0.00 | -0.05 | 0.69 | 1.00 | 0.46 |
| | Iba57p | 0.25 | -0.14 | -0.06 | 0.33 | 0.48 | 0.64 |
| | Nfu1p | -0.29 | 0.21 | 0.30 | 0.20 | 0.12 | 0.06 |
| Core CIA | Cfd1p | -0.11 | 0.15 | 0.06 | 0.65 | 0.37 | 0.75 |
| | Nbp35p | -0.07 | -0.20 | 0.14 | 0.73 | 0.22 | 0.30 |
| | Nar1p | -0.41 | 0.40 | 0.25 | 0.74 | 0.64 | 0.78 |
| | Cia1p | -0.01 | 0.22 | 0.19 | 0.93 | 0.14 | 0.18 |
| | Dre2p | 0.05 | 0.42 | 0.43 | 0.90 | 0.13 | 0.11 |
| | Met18p | 0.01 | -0.01 | 0.00 | 0.92 | 0.84 | 0.98 |
| | Tah18p | -0.01 | 0.11 | 0.13 | 0.97 | 0.31 | 0.23 |
| Iron trafficking | Grx3p | -0.11 | -0.05 | -0.02 | 0.47 | 0.55 | 0.73 |
| | Grx4p | 0.21 | 1.00 | 0.91 | 0.33 | 0.05 | 0.07 |
| ISC X-S export | Atm1p | -0.31 | 1.00 | 0.94 | 0.31 | 0.01 | 0.05 |
| | Erv1p | -0.23 | -0.08 | -0.11 | 0.37 | 0.69 | 0.43 |

| | | 26 hr | | | | | |
|---|---|---|---|---|---|---|---|
| | | $\log_2$ FC relative to WT | | | FDR | | |
| | Protein | **mIBA *ILV5*** | **cIBA *IlvC6E6*** | **cIBA *ILV5*** | **mIBA *ILV5*** | **cIBA *IlvC6E6*** | **cIBA *ILV5*** |
| Iron sensing and regulation | Mrs3p | 0.11 | 0.03 | 0.26 | 0.91 | 0.96 | 0.62 |
| | Mrs4p | 0.67 | 0.29 | 0.52 | 0.21 | 0.24 | 0.11 |
| | Ccc1p | 0.05 | 0.50 | 0.52 | 0.62 | 0.02 | 0.03 |
| | Smf3p | 0.60 | 0.74 | 0.65 | 0.18 | 0.04 | 0.05 |
| Core ISC | Nfs1p | -0.03 | -0.19 | -0.30 | 0.78 | 0.17 | 0.08 |
| | Isd11p | 0.07 | -0.24 | -0.96 | 0.84 | 0.25 | 0.33 |
| | Arh1p | 0.06 | 0.06 | -0.02 | 0.58 | 0.58 | 0.91 |
| | Yah1p | 0.20 | 0.04 | 0.00 | 0.48 | 0.65 | 0.99 |
| | Yfh1p | -0.33 | -0.35 | -0.83 | 0.64 | 0.51 | 0.14 |
| | Isu1p | 0.65 | -1.19 | -0.65 | 0.18 | 0.05 | 0.38 |
| | Isu2p | 4.31 | 1.99 | 1.40 | 0.39 | 0.48 | 0.61 |
| | Ssq1p | 0.06 | 0.23 | 0.10 | 0.74 | 0.19 | 0.58 |
| | Jac1p | -0.06 | -0.12 | -0.51 | 0.61 | 0.25 | 0.36 |
| | Mge1p | -0.31 | -0.24 | -0.27 | 0.33 | 0.12 | 0.09 |
| | Grx5p | -0.24 | -0.24 | -0.22 | 0.59 | 0.40 | 0.11 |
| | Ssc1p | 0.07 | -0.18 | -0.31 | 0.42 | 0.11 | 0.17 |
| ISC targeting | Isa2p | 0.28 | -0.23 | -0.16 | 0.51 | 0.30 | 0.40 |
| | Iba57p | 0.32 | 0.05 | -0.05 | 0.32 | 0.74 | 0.80 |
| | Nfu1p | -0.21 | -0.03 | -0.20 | 0.38 | 0.83 | 0.16 |
| Core CIA | Cfd1p | 0.20 | 0.25 | 0.14 | 0.48 | 0.25 | 0.41 |
| | Nbp35p | -0.03 | -0.15 | -0.37 | 0.89 | 0.32 | 0.38 |
| | Nar1p | 0.53 | 2.72 | 2.88 | 0.58 | 0.08 | 0.07 |
| | Cia1p | 0.24 | 0.56 | 0.67 | 0.49 | 0.04 | 0.07 |
| | Dre2p | 0.00 | -0.34 | -0.84 | 1.00 | 0.41 | 0.29 |
| | Met18p | 0.14 | 0.45 | 0.48 | 0.66 | 0.03 | 0.03 |
| | Tah18p | 0.50 | 0.59 | 0.57 | 0.43 | 0.21 | 0.21 |
| Iron trafficking | Grx3p | -0.01 | -0.07 | -0.13 | 0.95 | 0.48 | 0.35 |
| | Grx4p | -0.15 | 0.15 | -0.03 | 0.71 | 0.50 | 0.77 |
| ISC X-S export | Atm1p | -0.14 | 1.06 | 1.17 | 0.46 | 0.00 | 0.04 |
| | Erv1p | 0.01 | -0.18 | -0.24 | 0.95 | 0.15 | 0.07 |

# Chapter 4

# Improving isobutanol production in *S. cerevisiae* by identification of a high flux isobutanol pathway cassette

**Authors and Contributors:**

- **Francesca V. Gambacorta** designed and performed experiments, analyzed data, writing-methods, editing and reviewing manuscript.
- **Josh J. Dietrich** performed experiments, analyzed data, and provided guidance.
- **Justin J. Baerwald** designed and performed experiments.
- **Stephanie J. Brown** performed experiments and analyzed data.
- **Yun Su** aided in experimental design and assisted in experiments.
- **Dr. Brian F. Pfleger** Provided guidance, edited, and reviewed the manuscript.

## 4.1 Introduction

Isobutanol is a branched chain four-carbon alcohol targeted by many as a biofuel. Isobutanol can be produced biologically from pyruvate through five enzymatic reactions: acetolactate synthase (ALS), ketol-acid reductoisomerase (KARI), dihydroxyacid dehydratase (DHAD), $\alpha$-ketoacid decarboxylase (KDC), and alcohol dehydrogenase (ADH) (Fig.4.1a). Although there have been numerous efforts in engineering *Saccharomyces cerevisiae* for isobutanol production, the titers, rates, and yields achieved by academic researchers have remained below the threshold for industrial feasibility. This is due to the fact that isobutanol production is overpowered by *S. cereiviase*'s native pyruvate-to-ethanol flux. Efforts to eliminate ethanol production by deleting either the complete set of three pyruvate decarboxylase enzymes (*PDC1*, *PDC5*, and *PDC6*) or the set of six alcohol dehydrogenases (ADH1, *ADH2*, *ADH3*, *ADH4*, *ADH5*, and *SFA1*) has proven challenging since strains lacking these enzymes experience severe physiological defects. These defects are due to the fact that ethanol production, under aerobic and anaerobic conditions, plays an essential role in replenishing the $NAD^+$ cofactor which is required for glycolysis and cell growth.

Metabolic modeling suggests that isobutanol can theoretically replace ethanol as a product since it is redox balanced with glycolysis (i.e. requires 2 reducing equivalents) [57]. However, while isobutanol production is redox balanced with glycolysis, its cofactor specificity may not be. Naturally, most KARI's have a higher specificity towards NADPH which would result in a NADPH shortage and NADH excess [92]. This can be overcome by supplying a means for converting glycolytic NADH into NADPH, changing the KARI-cofactor specificity through protein engineering, or using a naturally NADH-dependent KARI enzyme.

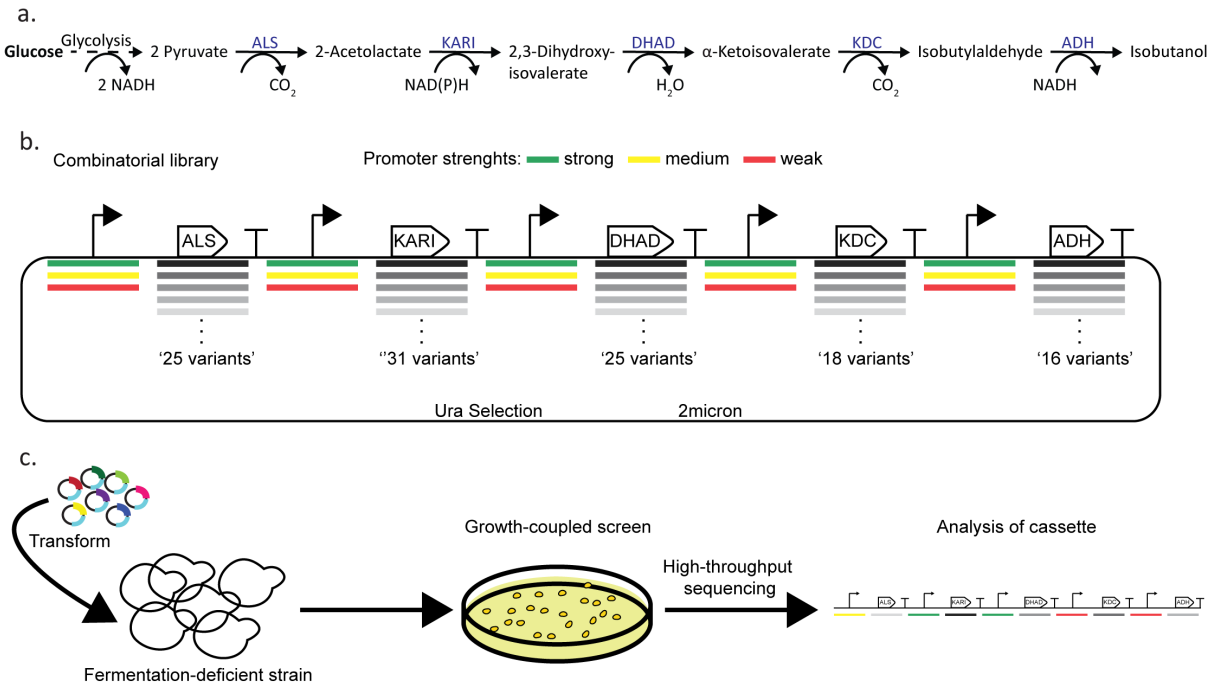


Figure 4.1: **Strategy for identifying a highly active isobutanol pathway cassettes. a)** Shows the 5-key enzymes responsible for isobutanol production from pyruvate: acetolactate synthase (ALS), ketol-acid reductoisomerase (KARI), dihydroxyacid dehydratase (DHAD), $\alpha$-ketoacid decarboxylase (KDC), and alcohol dehydrogenase (ADH). **b)** Combinatorial isobutanol pathway library design. There are 25 ALS homologs, 31 KARI homologs, 25 DHAD homologs, 18 KDC homologs, and 17 ADH homologs; each homolog is expressed with either a strong (green), medium (yellow), or weak (red) strength promoter in a high-copy ($2\mu$) plasmid containing uracil as a selectable marker. **c)** High throughput growth-coupled screening strategy for identifying highly active isobutanol pathway cassettes. The expression library is transformed into a fermentation-deficient strain (PDC-null). Cells that contain a functional isobutanol pathway cassette can grow due to the regeneration of $NAD^+$ via ADH and/or KARI. High producers can then be sequenced to identify the cassette.

In order for us to establish isobutanol as the predominant product in yeast, we must supply a balanced isobutanol pathway that can support the high carbon flux typically seen by ethanol production. To date, the optimal isobutanol pathway enzymes and their expression level to achieve this remains to be elucidated. In this study, we used bioinformatic methods to identify a diverse set of isobutanol enzyme homologs. We then built a combinatorial pathway library that had diversity in CDSs and expression levels by combining the bioprospected enzymes with varying strength promoters. By screening the combinatorial pathway library with a high-throughput growth-coupled strategy, we

identified a high-flux isobutanol cassette, designated as #3. We achieved an isobutanol titer of 364 mg/L and a yield of 36 mg isobutanol / g glucose under aerobic conditions in our Pdc$^-$ strain harboring the #3 cassette, sJD107.

In attempt to see if this #3 cassette could support anaerobic growth, we uncovered a limitation with this cassettes's capacity to replenish $NAD^+$ from a redox-cofactor imbalance between the engineered pathway and glycolysis. To overcome this limitation, we changed the cofactor preference of the KARI enzyme in the #3 cassette from NADPH to NADH-dependent, but the resulting pathway neither enabled anaerobic growth nor improved titers aerobically. We suspect this is due to the reduced specific activity of the engineered enzyme resulting in a bottleneck at the KARI node. In summary, while we were able to identify a high-flux pathway, additional engineering is needed to further enhance pathway flux to allow for the rapid regeneration of $NAD^+$ equivalents to achieve anaerobic growth. Our findings contribute towards improving the metabolic engineering designs for building further improved isobutanol producing Pdc$^-$ strains.

## 4.2 Materials and methods

### 4.2.1 Media

Defined synthetic complete media minus uracil contained 6.7 g/L yeast nitrogen base (YNB) without amino acids with ammonium sulfate, 1.52 g/L drop-out mix synthetic minus uracil and leucine, 380 mg/L leucine, and 20 g/L dextrose. Solid media also contained 2.5% agar.

### 4.2.2 Computational methods

Sequence similarity networks were created for each of the IBA enzymes (ALS, KARI, DHAD, KDC, and ADH) using Enzyme Function Initiative-Enzyme Similarity Tool (EFI-EST) [162] and visualized using Cytoscape [163]. The input for EFI-EST were either sequences or protein family: ALS from *Lactobacillus plantarum* (Uniprot ID: A0A0G9FA99), KARI from pfam PF01450 and PF07991, DHAD from *S. cerevisiae* (Uniprot ID: P39522), KDC from *S. cerevisiae* (Uniprot ID: Q06408), and ADH from *S. cerevisiae* (Uniprot ID: P38113). A diverse set of variants was chosen from the resulting network by a) gathering homologs from clusters known to contain active enzyme variants and b) bioprospecting the network to identify diverse sequences from a variety of kingdom/phylum (fungi, ascomycota, firmicutes, proteobacteria, and actinobacteria). A simple Hamming distance calculation was used to maximize diversity. To ensure we had a fully cytosolic compartmentalized isobutanol pathway, the sequences were run through Mitoprot [164] and any predicted mitochondrial localization sequences were removed. Pairwise amino acid identity between the proteins in each grouping was found using ClustalOmega [165]. See File S6 for sequences and File S7 for percent identity matrix.

### 4.2.3 Library construction

Library construction was performed by the DOE Joint Genome Institute (JGI). In brief, codon-optimized enzyme coding sequences (CDS), promoters, and terminators were first cloned into a pENTR vector to generate the parts vectors. Transcription units (promoter-gene-terminator sets) were generated by Golden Gate assembly of the parts vectors. The combinatorial library (5 gene isobutanol cassettes) was then assembled in a pooled fashion (one-pot) using Gibson into a high copy vector, pCC1FOS, which had URA3-selection.

Specifically the one-pot mixture consisted of 116 ORFs (25 ALS homologs, 31 KARI homologs, 25 DHAD homologs, 18 KDC homologs, and 17 ADH homologs), 15 promoters (3 ALS promoters, 3 KARI promoters, 3 DHAD promoters, 3 KDC promoters, and 3 ADH promoters), and 1 terminator (1 ALS terminator, 1 KARI terminator, 1 DHAD terminator, 1 KDC terminator, and 1 ADH terminator) . This yielded 1.44 billion unique 13 kb isobutanol pathway cassettes (35*25*31*25*18*17). The pooled library underwent Pacbio sequencing to determine library diversity and fidelity.

### 4.2.4 Library screening

Screening strain was generated by deleting *URA3* in GG570 [28] by CRISPR/Cas9. In brief, a sgRNA sequence targeting the CDS was identified by CRISpy-pop (sgRNA = gcacacggtgtggtgggccc) and cloned into the pXIPHOS (NatMx) plasmid as described previously [133]. The CRISPR/Cas9 plasmid was transformed along with a PCR repair template of the homology flanking the targeted gene and plated on NatMx. Gene deletion was confirmed by PCR of gDNA and Sanger-sequencing (Table.4.3).

The JGI library was then electroporated into FVG454, GG570*ura3*△, as previously described [166] and plated on SCD-ura + 0.71 mM sodium acetate. Plates were incubated at 30°C for ∼1 month. 28 randomly selected colonies from the initial screen were selected for fermentation experiments. Fermentation was performed under aerobic conditions in 24-well plates in synthetic complete media containing 2% glucose and 2% ethanol for 4 days.

### 4.2.5 Protein expression and purification

The wild-type LbKARI gene and its variants were cloned into pET-28a (from EMD Biosciences) with a C-terminal 6xHis tag. The pET28-LbKARI, pET28-LbKARI$^{DD}$, and pET28-LbKARI$^{DDV}$ plasmids were transformed into *E. coli* BL21(DE3) (from New England Biosciences or NEB). Cultures were grown at 37°C with shaking in LB supplemented with 50 mg/L kanamycin until the $OD_{600}$ reached 0.8. Flasks were cooled in a 16°C bath, induced with 100 $\mu$M isopropyl-$\beta$-d-thiogalactopyranoside (IPTG), and incubated overnight at 21°C. Cells were harvested by centrifugation (8000 rpm at 4°C for 15 minutes) and flash frozen as pellets in liquid nitrogen. The frozen cell pellets were broken by sonication (Fisher 550 Sonic Dismembrator, amplitude = 30%, time = 10 min with 1 sec on/ 1 sec off) while on ice in Buffer A (20 mM Tris pH 7.4, 30 mM imidazole, 100 mM NaCl, 10 mM $MgCl_2$). The lysate was cleared by centrifugation (12000 rpm at 4°C for 30 minutes) and filtered with a 0.4 $\mu$M filter. The proteins were purified by immobilized metal affinity chromatography (IMAC) over 5 mL Histrap High Performance (HP) columns (Cytiva, Sweden), using an AKTA Start system( d). All purification steps were performed at 4°C. The proteins were eluted with a linear gradient from buffer A to 100% buffer B (20 mM Tris pH 7.4, 500 mM imidazole, 100 mM NaCl, 10 mM $MgCl_2$ , and 1 mM DTT (added before use). Fractions containing the protein were pooled, buffer exchanged, and concentrated into Buffer C (8 mM Tris pH 7.4, 20 mM NaCl, 1 mM $MgCl_2$ , and 5 wt% glycerol) using Amicon Ultra centrifugal filters. Aliquots were stored at -80°C and used within 1 month.

### 4.2.6 Kinetic assay

Lb-IlvC activities were assayed by monitoring NAD(P)H consumption at 340 nm on a Nanodrop. The assay buffer contained 250 mM potassium phosphate pH 7, 1 mM DTT, 200 uM NADPH or NADH, 10 mM 2-acetolactate, 10 mM $MgCl_2$, and 1500 nM purified enzyme. The concentrations of the purified enzymes were determined using the Nanodrop.

## 4.3 Results and discussion

### 4.3.1 Combinatorial isobutanol pathway library design

In order to identify an isobutanol pathway capable of supporting high flux we constructed a combinatorial isobutanol pathway library. Variability was introduced on 2 levels: coding sequences (e.g. gene variants via homologs) and gene dosage (e.g. translational control via promoters). We identified homologs of each enzyme within the isobutanol pathway by the use of bioprospecting. A diverse set of variants were chosen from the EFI-EST [162] sequence similarity map by a) gathering homologs from clusters known to contain active enzyme variants and b) bioprospecting the network to identify diverse sequences from a variety of kingdom/phylum (fungi, ascomycota, firmicutes, proteobacteria, and actinobacteria) (see section 4.2.2). Specifically, 25 ALS homologs, 31 KARI homologs, 25 DHAD homologs, 18 KDC homologs, and 17 ADH homologs were chosen (Fig.4.1b). To ensure we had an entirely cytosolic localized isobutanol pathway, any predicted mitochondrial localization sequences were removed and each homolog was expressed under a strong, medium, or weak promoter. The resulting transcriptional units were used to build the final pooled plasmid library which consisted of 1.44 billion unique combinations

(Fig.4.1b). Validation that the library was sufficiently diverse was performed by counting all the occurrences of promoters and CDSs after assembly using PacBio sequencing. All promoters and CDSs in the library were represented and their distribution is summarized in File S8. Overall, the sequencing results indicate that the library achieved maximum diversity.

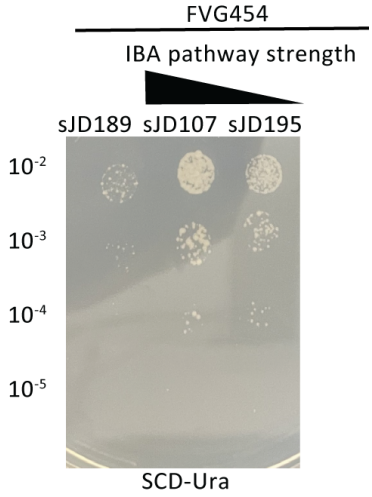


Figure 4.2: **Growth complementation assay to validate high-throughput screening approach.** An empty vector (e.v.) and two isobutanol pathway cassettes with varying strengths were transformed in FVG454 resulting in strains sJD189, sJD107, and sJD195, respectively. The strains were grown up and 10 $\mu$L cell suspensions with 10-fold serial dilutions were spot plated on synthetic complete media minus uracil with 2% glucose as the primary carbon source (SCD-Ura). After 14 days of growth under aerobic conditions, the plates were imaged, and the strains harboring the isobutanol pathways exhibited more growth than the empty vector control.

### 4.3.2 Using a growth-coupled strategy for high-throughput library screening

Due to the library size, a high-throughput screening strategy was used (Fig.4.1c). We opted for a growth-coupled approach since there is not currently a eukaryotic biosensor that senses isobutanol directly. For the growth-coupled method, we started with a strain designated GG570 [28] which had reactions corresponding to ethanol production deleted (*Pdc1*$\triangle$, *Pdc5*$\triangle$, and *Pdc6*$\triangle$) and deleted *URA3* resulting in strain FVG454 (Table.4.3). With the main fermentative pathway in FVG454 deleted, cell growth is dependent on

having a functional pathway for $NAD^+$ regeneration during glucose catabolism; in the isobutanol pathway, NADH can be recycled by the ADH enzyme and the KARI enzyme (if NADH-dependent). Growth coupling can be achieved under aerobic conditions since *S. cerevisiae* undergoes glucose repression caused by the Crabtree-effect when glucose concentrations are high thus preventing sufficient $NAD^+$ regeneration through oxidative phosphorylation (See Section 2.1.2). To validate this method, we performed a growth complementation assay by transforming an empty vector control and two isobutanol pathway cassettes with varying strengths into FVG454 resulting in strains sJD189, sJD107, and sJD195, respectively. The strains were grown up and spot plated on synthetic complete media minus uracil with 2% glucose as the primary carbon source (SCD-ura). After 14 days of growth under aerobic conditions, the plates were imaged and indeed the strains harboring the stronger isobutanol pathways exhibited more growth than the empty vector control thus validating the screening strategy (Fig.4.2).

The combinatorial isobutanol pathway library was transformed into FVG454 via electroporation, plated onto synthetic complete media minus uracil with 2% glucose and 70 mM acetate, and allowed to grow aerobically at 30°C for 1 month. Approximately, $5x10^4$ unique genotypes were screened (estimated library coverage of 0.0035%). A comprehensive screen was not possible due the limited transformation efficiency ($10^3$ cfu/$\mu$g) of the screening strain and the large plasmid size 25.3 kb. The isobutanol production of 28 randomly selected colonies was tested by performing a fermentation experiment in synthetic complete media minus uracil with 2% glucose and 2% ethanol for 4 days (Fig.4.3). 14/28 colonies produced isobutanol with the highest titer being 633 mg/L which validated our growth-coupled approach to isolate high isobutanol producers. The top 10 isobutanol pathway cassettes were isolated and sequenced by Sanger sequencing

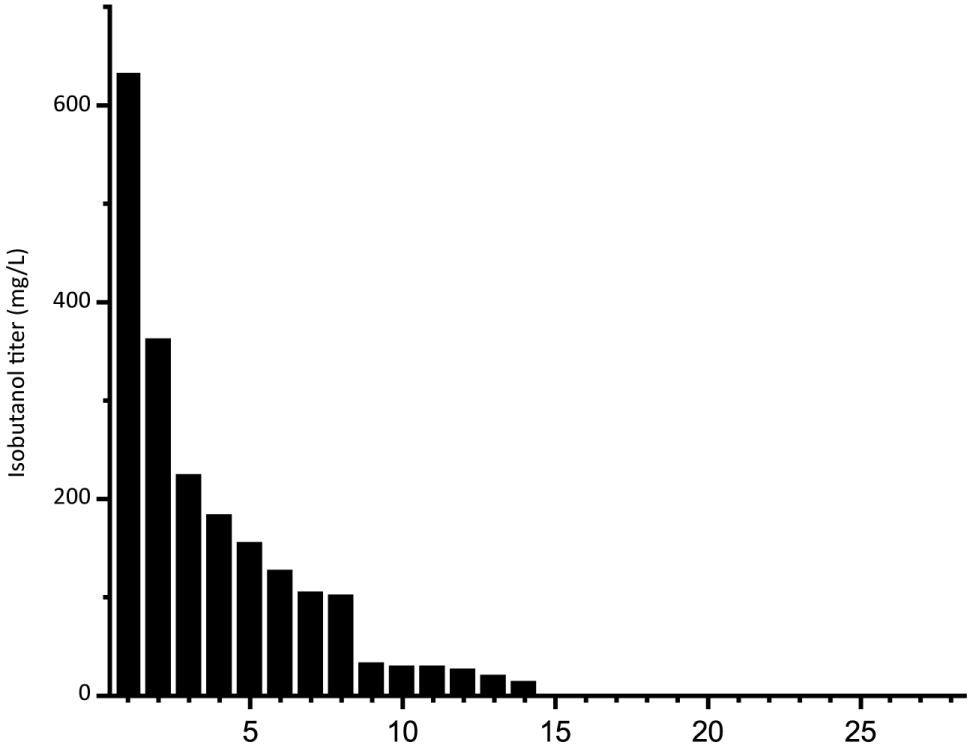


Figure 4.3: **High-throughput growth-coupled screening results.** Isobutanol titer from 28 randomly selected colonies from the initial screen. Fermentation was performed under aerobic conditions in 24-well plates in synthetic complete media with 2% glucose and 2% ethanol for 4 days.

to identify the homologs and expression level of each enzyme in the cassettes (Table.4.1).

While our initial screening strategy demonstrated the feasibility of the growth-coupled approach to isolate high isobutanol producers, high ethanol producers were also identified. A subset of the 28 initial colonies were subjected to a $2^{nd}$ round of fermentations in synthetic complete media lacking ethanol so we could accurately measure ethanol production (Fig.4.4). Interestingly, of the 6 cassettes tested, 4 produced significant amounts of ethanol; specifically, the highest producers were the F1 and F2 cassettes which produced 53 and 42-fold more ethanol than isobutanol, respectively. We hypothesize that the KDC homologs in the F1 and F2 cassettes had activity on pyruvate thus allowing the strain to regenerate $NAD^+$ via ethanol production. To test this hypothesis, we conducted a growth complementation assay by expressing the KDC homologs on a high copy vector and transforming them into the $Pdc^-$ strain, FVG454, to observe which ones could re-

Table 4.1: Homolog and expression level identification of the top 10 isobutanol producers from Fig.4.3 via Sanger sequencing. Green, yellow, and red box represents a strong, medium, or weak strength promoter, respectively (See File S6 for uniport IDs).

| **IBA enzyme** | **Cassette** | **P** | **Homolog** |
|---|---|---|---|
| ALS | 14 | $P_{SAC6}$ | *Trichoderma gamsii* |
| | 3 | $P_{SAC6}$ | *Trichoderma gamsii* |
| | 33 | $P_{SAC6}$ | *Talaromyces stipitatus* |
| | 40 | $P_{HTB2}$ | *Brevibacterium linens* |
| | F2 | $P_{SAC6}$ | *Oidiodendron maius Zn* |
| | F1 | $P_{SAC6}$ | *Streptomyces viridochromogenes* |
| | 12.17 | $P_{SAC6}$ | *Aspergillus nomius* |
| | 12.12 | $P_{SAC6}$ | *Bifidobacterium mongoliense* |
| | 12.13 | $P_{SAC6}$ | n.d. |
| | 12.5 | $P_{PGK1}$ | n.d. |
| KARI | 14 | $P_{HHF2}$ | *Olsenella scatoligenes* |
| | 3 | $P_{HHF2}$ | *Lachnospiracae bacterium* |
| | 33 | $P_{RNR2}$ | *Brevundimonas vesicularis* |
| | 40 | $P_{RNR2}$ | *Streptomyces griseorubiginosus* |
| | F2 | $P_{RNR2}$ | *Shewanella sp.* |
| | F1 | $P_{RNR2}$ | *Shewanella sp.* |
| | 12.17 | $P_{HHF1}$ | *Clostridium populeti* |
| | 12.12 | $P_{RNR2}$ | *Slackia exigua* |
| | 12.13 | $P_{HHF2}$ | n.d. |
| | 12.5 | $P_{RNR2}$ | *Alphaproteobacteria bacterium* |
| DHAD | 14 | $P_{RET2}$ | *Hypoxylon sp.* |
| | 3 | $P_{RET2}$ | *Jeotgalibaca sp.* |
| | 33 | $P_{RPL18B}$ | *Saccharomonospora marina* |
| | 40 | $P_{RPL18B}$ | *Acidimicrobiaceae bacterium* |
| | F2 | $P_{RPL18B}$ | *Lactococcus piscium MKFS47* |
| | F1 | $P_{RPL18B}$ | *Methanobrevibacter smithii* |
| | 12.17 | $P_{THD3}$ | *Methanosphaera stadtmanae* |
| | 12.12 | $P_{RPL18B}$ | *Arthrobacter alpinus* |
| | 12.13 | $P_{RPL18B}$ | n.d. |
| | 12.5 | $P_{THD3}$ | *Thiohalobacter thiocyanaticus* |

store growth on medium containing glucose. As expected, the KDC homologs in cassettes F1 (KDC07 from *Helicobacter ailurogastricus*) and F2 (KDC09 from *Enterococcus rotai*) exhibited robust growth confirming their activity on pyruvate (Fig.4.5).

To validate the isobutanol titers of our top 2 producers, designated #3 and #14, a fermentation experiment was performed. Specifically, we re-transformed the isolated plasmids, #3 and #14, back into the base screening strain, FVG454, resulting in strains sJD107 and sJD195, respectively. The stains were cultivated aerobically (test tube)

Table 4.1: Homolog and expression level identification of the top 10 isobutanol producers from Fig.4.3 via Sanger sequencing. Green, yellow, and red box represents a strong, medium, or weak strength promoter, respectively (See File S6 for uniport IDs) (CONTINUED).

| IBA enzyme | Cassette | P | Homolog |
|---|---|---|---|
| KDC | 14 | $P_{POP6}$ | *Dermatophilus congolenis* |
| | 3 | $P_{ALD6}$ | *Frondihabitans sp.* |
| | 33 | $P_{TEF1}$ | *Enterococcus rotai* |
| | 40 | $P_{TEF1}$ | *Helicobacter ailurogastricus* |
| | F2 | $P_{TEF1}$ | *Enterococcus rotai* |
| | F1 | $P_{TEF1}$ | *Helicobacter ailurogastricus* |
| | 12.17 | $P_{TEF1}$ | *Enterococcus rotai* |
| | 12.12 | $P_{TEF1}$ | *Enterococcus rotai* |
| | 12.13 | $P_{TEF1}$ | n.d. |
| | 12.5 | $P_{TEF1}$ | n.d. |
| ADH | 14 | $P_{PAB1}$ | *Lactococcus lactis* |
| | 3 | $P_{PAB1}$ | *Gluconacetobacter diazotrophicus* |
| | 33 | $P_{PAB1}$ | *Acetobacter indonesiensis* |
| | 40 | $P_{TEF2}$ | n.d. |
| | F2 | $P_{RNR1}$ | *Tanticharoenia sakaeratensis* |
| | F1 | $P_{PAB1}$ | *Chlamydia trachomatis* |
| | 12.17 | $P_{PAB1}$ | n.d. |
| | 12.12 | $P_{RNR1}$ | *Tanticharoenia sakaeratensis* |
| | 12.13 | $P_{PAB1}$ | n.d. |
| | 12.5 | $P_{PAB1}$ | n.d. |

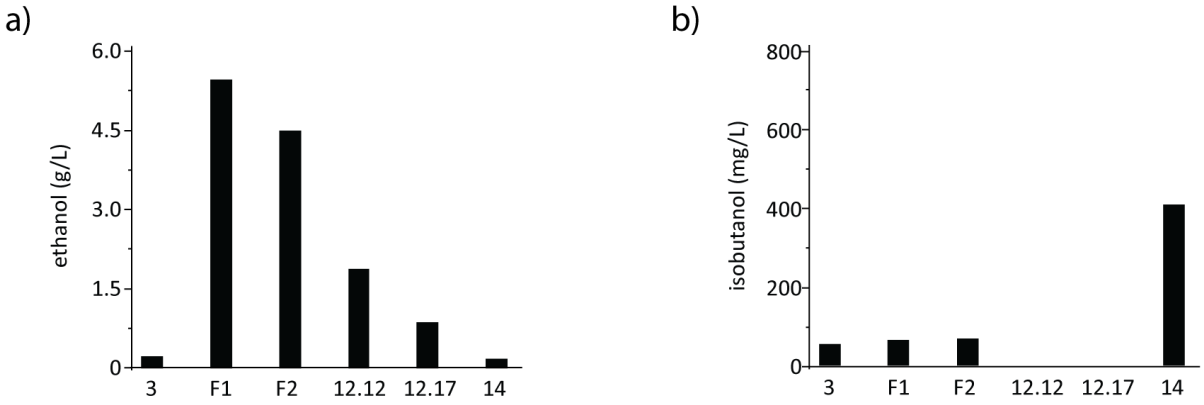


Figure 4.4: **Ethanol and isobutanol production from select colonies from Fig.4.3. a)** ethanol and **b)** isobutanol titers from select colonies from the initial screen in Fig.4.3, FVG454 + IBA cassettes (#3, F1, F2, 12.12, 12.17, or #14). Fermentation was performed under aerobic conditions in synthetic complete media with 2% glucose and 0.71 mM acetate for 4 days.

and semi-anaerobically (serum vial) at 30°C (Fig.4.6). sJD107 outperformed sJD195 under both semi-anaerobic and aerobic conditions. Specifically, the highest producer was sJD107 under aerobic conditions which produced 364 mg/L isobutanol and had a yield

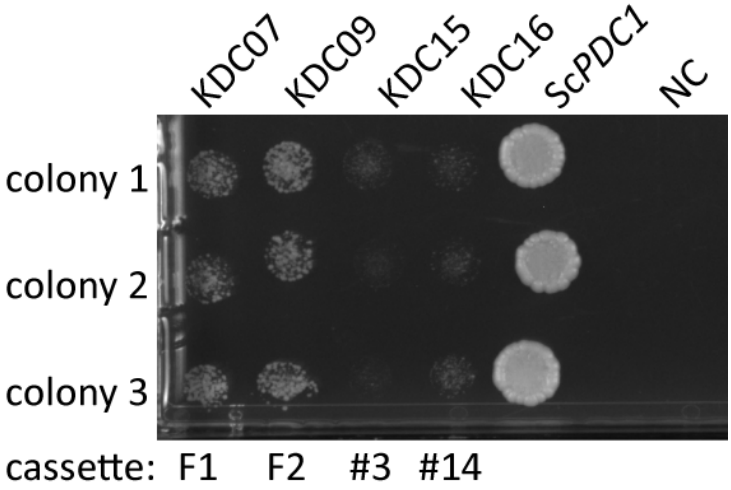


Figure 4.5: **Growth complementation assay to determine which KDC homologs have activity on pyruvate.** The KDC homologs from cassettes F1, F2, #3, #14 and *S. cerevisiae PDC1* (positive control) were cloned into a high copy ura-selectable vector with a strong promoter. All were transformed into the FVG454 strain along with an empty vector (negative control or NC). 10 $\mu$L cell suspensions of 1:100 diluted culture were spot plated on synthetic complete media minus uracil with 2% glucose (SCD-Ura). After 4 days of growth under aerobic conditions, the plates were imaged and the strains containing KDC homologs that have activity on pyruvate grew indicating that $NAD^+$ was regenerated via ethanol production. Spot plate was done in biological triplicate.

of 36 mg isobutanol / g glucose which corresponds to 8.8% of the theoretical maximum yield. sJD107 also performed well under semi-anaerobic conditions where it produced 50 mg/L isobutanol and had a yield of 27.3 mg isobutanol / g glucose which corresponds to 6.6% of the theoretical maximum yield.

To further explore why the #3 and #14 cassettes were so successful (i.e. high isobutanol producers) we took a closer look at the homologs and expression level of the isobutanol pathway enzymes in these cassettes. The KARI promoter and the KDC homolog stood out. The gene dosage for the KARI homolog in both the #3 and #14 cassettes was high (strong promoter), while the weaker isobutanol pathway cassettes (#33, #40, F1, F2, 12.17, 12.12, and 12.5) had a low gene dosage (weak/medium promoter) (Table.4.1). The strong strength promoter being required for KARI in our top 2 producers suggests that KARI is a limiting enzyme in the isobutanol pathway; this result is in agreement with

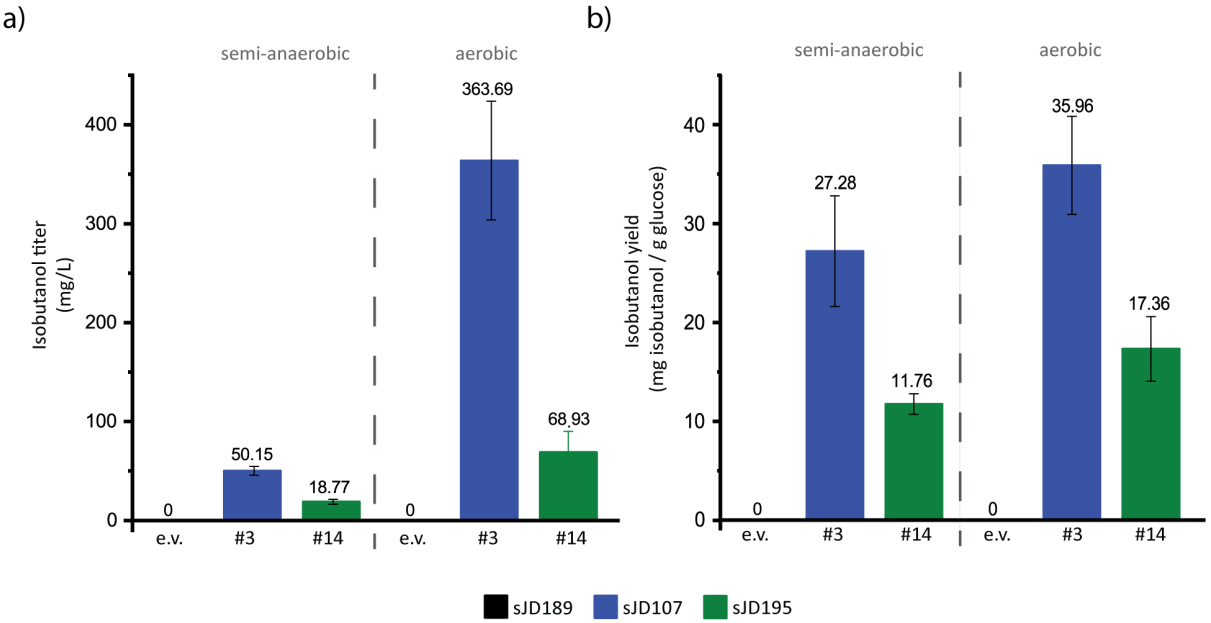


Figure 4.6: **Validation of high-throughput growth-coupled screening results.** Validation of isobutanol production **a)** titer **b)** yield from the top 2 producers in Fig.4.3. An empty vector, #3, and #14 plasmids were re-transformed into FVG454 resulting in strains sJD189, sJD107, and sJD195. Fermentations were performed under aerobic and semi-anaerobic conditions in synthetic complete media minus uracil with 2% glucose and 2% ethanol. Aerobic fermentations were conducted in test tubes for 3 days while semi-anaerobic fermentations were conducted in serum vials for 10 days. Under aerobic conditions, sJD107 produced the highest isobutanol titer of 364 mg/L and yield of 36 mg isobutanol/ g glucose which corresponds to 8.8% of the maximum theoretical yield. Error bars represent the standard deviation of the 3 biological replicates.

previous conducted studies in *E. coli* where KARI required the highest level of enzyme expression [135]. Additionally, the KDC homologs in the #3 (KDC15 from *Frondihabitans sp.*) and #14 (KDC16 from *Dermatophilus congolenis*) cassettes were characterized as having minimal activity on pyruvate (Fig.4.5); this is as expected since sJD107 and sJD195 produced no ethanol during fermentation in Fig.4.6 and instead consumed it from the media (ethanol was provided as a C2-compound) (data not shown). Taken together, both the isobutanol pathway homologs and promoter strength are important factors for production.

### 4.3.3 Anaerobic growth unachievable after balancing NADH/NAD$^+$ between glycolysis and isobutanol production

We next aimed to test our best isobutanol producer, sJD107, under industrially relevant anaerobic conditions. Under these conditions, cell growth is completely dependent on isobutanol production for NAD$^+$ regeneration as oxidative phosphorylation cannot occur anaerobically. We hypothesized that the capacity of the strain to replenish NAD$^+$ by the isobutanol pathway may be limited by a redox cofactor imbalance between the engineering pathway and glycolysis; this is a result of the KARI enzyme from our #3 cassette (*Lachnospiracae bacterium* orthlog) being an NADPH-dependent enzyme. We set out to switch the cofactor preference of the *Lachnospiracae bacterium* KARI enzyme from being NADPH-dependent to NADH-dependent. The specific residues required for this switch have been previously determined and this strategy was successful in increasing isobutanol production of a different engineered isobutanol pathway in *E. coli* [63, 92]. We generated 2 KARI variants, Lb-llvC$^{DD}$ and Lb-llvC$^{DDV}$, and confirmed our variants exhibited a changed cofactor preference (from NADPH to NADH) by purifying the proteins and measuring the specific activity with either NADH or NADPH. Specifically, the in vitro assay consisted of monitoring the consumption of NAD(P)H over time at 340 nm when the substrate, 2-acetolactate, was in excess. The Lb-llvC$^{DD}$ and Lb-llvC$^{DDV}$ variant exhibited a ratio of NADH/NADPH activity (in U/mg) of 4.7 and 5.1, which is 10.3 or 11.2-fold higher than that for Lb-llvC, respectively (Table.4.2, Fig.4.7a).

Table 4.2: Specific activity ratio of Lb-IlvC variants on NADH/NADPH with 2-Acetolactate as substrate in excess.

| **Enzyme** | **Mutations** | **U/mg Ratio (NADH/NADPH)** |
|---|---|---|
| Lb_IlvC | - | 0.46 |
| Lb_IlvCDD | Ser53Asp, Ser55Asp | 4.72 |
| Lb_IlvCDDV | Ser53Asp, Ser55Asp, Ile87Val | 5.09 |

Once we validated the Lb-llvC$^{DD}$ and Lb-llvC$^{DDV}$ variants cofactor preference was switched, we cloned them into the #3 cassette in place of the wild-type Lb-llvC and transformed them into the FVG454 strain resulting in strains sFVG612 and sFVG613, respectively. We then performed a fermentation experiment under anaerobic conditions and unfortunately, the strains could not support anaerobic growth indicating that the isobutanol pathway cassette does not support a high enough carbon flux to rapidly replenish the NAD$^+$ equivalents needed for glycolysis (i.e. isobutanol production is too low to meet the cellular maintenance energy requirement) (data not shown).

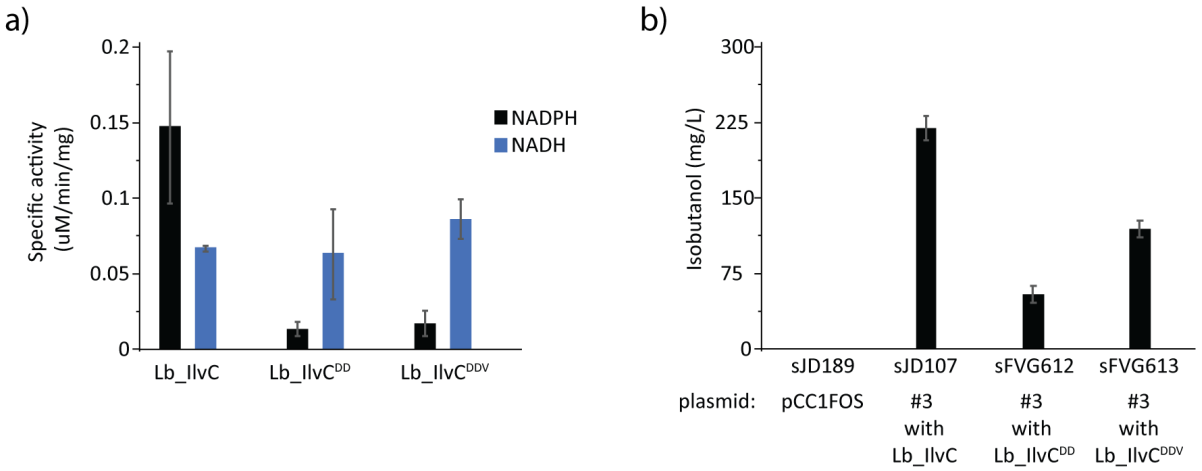


Figure 4.7: **Characterization and production of Lb-IlvC variants. a)** Specific activities of Lb-IlvC variants using NADPH or NADH, with 2-acetolactate as substrate in excess. All enzymes were purified prior to characterization. Each value represents the average of three independent measurements. The enzyme activities were determined in 250 mM potassium phosphate pH 7 with 1 mM DTT, 200 mM NADPH or NADH, 10 mM 2-acetolactate, and 10 mM $MgCl_2$. The concentrations of the purified enzymes were determined using the nanodrop. **b)** Aerobic isobutanol titer of strains sJD189, sJD107, sFVG612, and sFVG613. Fermentations were performed in synthetic complete media minus uracil containing 2% glucose and 0.41% ethanol. Isobutanol production was measured after 3 days. sJD107 produced the highest isobutanol titer of 280 mg/L and a yield of 14.2 mg isobutanol / g glucose which corresponds to 3.45% of the maximum theoretical yield. Error bars represent the standard deviation of the 3 biological replicates.

We next asked if the Lb-llvC$^{DD}$ and Lb-llvC$^{DDV}$ variants would perform better under aerobic conditions. We conducted a fermentation experiment with sJD189, sJD107,

sFVG612, and sFVG613 for 3 days in synthetic complete media minus uracil with 2% glucose and 0.41% ethanol aerobically. sFVG612 and sFVG613, containing either of the NADH-dependent variants, Lb-llvC$^{DD}$ and Lb-llvC$^{DDV}$, did not outperform sJD107 with the wild-type, NADPH-dependent Lb-llvC. sJD107 produced 280 mg/L isobutanol, which is 4.0 and 1.8-fold higher than the sFVG612 and sFVG613, respectively (Fig.4.7b). We suspect the lower isobutanol titer with the Lb-llvC$^{DD}$ and Lb-llvC$^{DDV}$ variants was due to a reduced specific activity of the KARI enzyme; the Lb-llvC$^{DD}$ and Lb-llvC$^{DDV}$ variants exhibited a 2-fold reduction in catalytic activity (catalytic efficiency of using NADH) relative to Lb-llvC when using NADPH (Fig.4.7a). While sJD107 produced the highest isobutanol titer, that strain, along with all the other engineered strains, excreted significant amounts of pyruvate (0.7-1.6 g/L) indicating overflow metabolism at the pyruvate node (Fig.4.8). Additional work is needed to enhance flux through the isobutanol pathway to prevent overflow metabolism and allow for the rapid regeneration of $NAD^+$ equivalents to develop a truly anaerobic isobutanol fermentative pathway for *S. cerevisiae*.

### 4.3.4 Comparisons to the literature

To date, an anaerobically growing isobutanol producing Pdc$^-$ strain has not been reported on in academic literature [57, 104]. While we were also unable to achieve anaerobic growth, our yields semi-aerobically exceeded previous similar approaches; our FVG454 strain harboring the #3 cassette, sJD107, achieved a yield of 27.3 mg isobutanol / g glucose which is ∼3.7-fold higher than Milne et. al [57] who achieved a yield of 7.4 mg isobutanol / g glucose with a Pdc$^-$ strain harboring a cytosolic localized pathway under micro-aerobic conditions (serum vial cultivation). Our yields under aerobic conditions also come close (1.7-fold lower) than the highest yield reported in literature by Wess

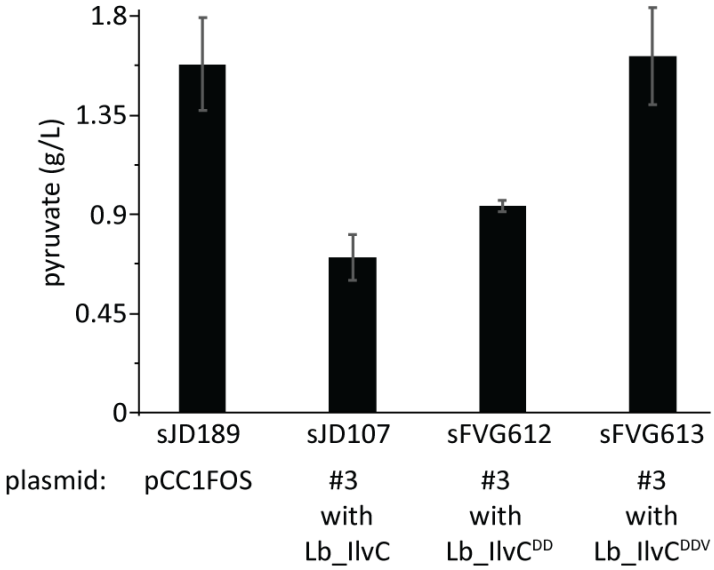


Figure 4.8: **Pyruvate titers from aerobic production of #3 cassettes with Lb-llvC and variants.** Fermentations were performed with strains sJD189, sJD107, sFVG612, and sFVG613 under aerobic conditions in synthetic complete media minus uracil containing 2% glucose and 0.41% ethanol. Pyruvate was measured after 3 days. All strains excreted pyruvate at an elevated level indicating that the cell is experiencing overflow metabolism at the pyruvate node due to the isobutanol pathway cassette not supporting the high carbon flux occurring through glycolysis. Error bars represent the standard deviation of the 3 biological replicates.

et. al. of 59.55 mg isobutanol / g glucose [90]; this was achieved in a strain with a cytosolic-localized isobutanol pathway and by blocking a number of non-essential isobutanol competing pathways, JWY23 (*ilv2*△; *bdh1*△; *bdh2*△; *leu4*△; *leu9*△; *ecm31*△; *ilv1*△; *adh1*△; *gpd1* △; *gpd2*△; *ald6*△). The strain in Wess et. al., JWY23, also produced 3-fold more ethanol (∼6 g/L) than isobutanol (∼2 g/L), while FVG454 strain harboring the #3 cassette, sJD107, strains produced no ethanol. Overall, high-yielding isobutanol producing strains have been reported in industry, however, the strategies remain elusive to academic researches as pathway intermediate buildup and by-product formation still remain a major challenge to developing a high flux pathway.

Table 4.3: *S. cerevisiae* strains used in this study

| **Strain Name** | **Description** |
|---|---|
| GG570 [28] | T2-3D, *Pdc1*△, *Pdc5*△, *Pdc6*△ |
| FVG454 | GG570, △*URA3* |
| sJD189 | FVG454 + e.v. (pCC1FOS) |
| sJD107 | FVG454 + #3 cassette |
| sJD195 | FVG454 + #14 cassette |
| FVG612 | FVG454 + #3 cassette with Lb-llvC$^{DD}$ |
| FVG613 | FVG454 + #3 cassette with Lb-llvC$^{DDV}$ |

## 4.4 Conclusions

Here, we used a combinatorial library design, high-throughput growth coupled screen, and protein engineering to generate an isobutanol producing Pdc$^-$ *S. cerevisiae* strain. First, a diverse set of isobutanol pathway enzyme homologs were identified by building a similarity network for each of the five enzymes in the pathway and sampling across the sequencing space. The library was then built by combining those bioprospected enzymes with varying strength promoters in a pooled fashion. By the use of a high-throughput growth-coupled screen that relied on having a functional isobutanol pathway for $NAD^+$ regeneration during glucose catabolism (NADH can be recycled by the ADH enzyme and the KARI enzyme (if NADH-dependent)), we isolated a high producer, #3. The #3 cassette however could not support anaerobic growth, due to a redox-cofactor imbalance between the engineered pathway and glycolysis. To overcome this limitation, we changed the cofactor preference of the KARI enzyme in the #3 cassette from NADPH to NADH-dependent but we did not observe a beneficial effect. We hypothesize that the capacity of the isobutanol pathway must be further enhanced to achieve anaerobic growth.

The work performed here leaves several opportunities for further improvement. First, it should be noted that our screening method can select for both high isobutanol and high ethanol producing strains so additional screening methods are required to eliminate

the false-positive hits or extra care must be taken when selecting KDC homologs. Additionally, work to develop a eukaryotic isobutanol biosensor will expand the number of library members that can be screened as it would eliminate the need to transform into a $Pdc^-$ strain which has low transformation efficiency. Furthermore, continued efforts in developing a stable multi-copy integration system will aid in the need for enhancing copy number to achieve anaerobic growth. Finally, process optimization in terms of balancing gene expression and media formulations may increase production.

## 4.5 Acknowledgements

We would like to thank Russell Wrobell and Chris Hittinger for the GG570 strain [28].

## 4.6 Funding

Part of this work (doi:10.46936/10.25585/6000129) was conducted by the U.S. Department of Energy Joint Genome Institute (https://ror.org/04xm1d337), a DOE Office of Science User Facility, is supported by the Office of Science of the U.S. Department of Energy operated under Contract No. DE-AC02-05CH11231.

## 4.7 Data availability

The supplemental files (File S6-S8) is available on GitHub (https://github.com/Pfleger-Lab/Theses/tree/main/Francesca%20Gambacorta/Chapter4).

# Chapter 5

# Efforts in developing a cellulosic consuming isobutanol producing *S. cerevisiae* strain

**Authors and Contributors:**

- **Francesca V. Gambacorta** designed and performed experiments, analyzed data, writing-methods, editing and reviewing manuscript.
- **Justin J. Baerwald** aided in experimental design, performed experiments and analyzed data.
- **Josh J. Dietrich** performed experiments, analyzed data, and provided guidance for section 5.3.
- **Malia E. Dziedzic** implemented experiments for section 5.3.
- **Stephanie J. Brown** implemented experiments for section 5.3.
- **Dr. Trey Sato** designed and performed experiments, analyzed data and provided guidance for section 5.4.1.
- **Dr. Audrey Gasch** designed experiments, analyzed data and provided guidance for section 5.4.1.
- **Lisa Liu** aided in experiments for section 5.4.1.
- **Megan Young** aided in experiments for section 5.4.1.

- **Dr. Mike Place** analyzed BarSeq data for section 5.4.1.
- **Dr. Brian F. Pfleger** funding acquisition, conceptualization, design of experiments, editing and reviewing manuscript.

## 5.1 Introduction

In Chapters 3 and 4 we focused on enhancing isobutanol production from medium containing glucose. In this Chapter, we will move away from glucose only medium and focus on the engineering required to generate a *S. cerevisiae* strain capable of growth on lignocellulosic hydrolysates. The main challenges with working with lignocellulosic hydrolysates are the fact that it contains unusable fermentable sugars and inhibitory compounds from the biomass pretreatment and chemical hydrolysis steps (see section 2.3). The Great Lakes Bioenergy Research Center (GLBRC) is interested in GVL processed switchgrass hydrolysates. In GVL hydrolysate, xylose accounts for 30-50% of the total fermentable sugars [81] and inhibitory compounds (GVL, LA, and HMF) account for ∼10% of the total carbon recovered. Improving *S. cerevisiae*'s utilization of xylose and enhancing tolerance to inhibitory compounds is necessary to increase the yield and economic viability of fermentations using lignocellulosic feedstocks.

## 5.2 Materials and methods

### 5.2.1 Media

Defined synthetic complete medium minus uracil contained 1.7 g/L yeast nitrogen base (YNB) without amino acids without ammonium sulfate, 5 g/L ammonium sulfate or 1 g/L MSG, 1.52 g/L drop-out mix synthetic minus uracil and leucine, 380 mg/L leucine, and 20 g/L dextrose. SC* additionally contained 19.5 g/L MES, 4 mL/L 250X tween/ergosterol stock (62.5 mL Tween80 + 625 mg Ergosterol in 187 mL 95% ethanol) and was pH adjusted to 5.5. Solid media also contained 2.5% agar. 200 µg/mL Geneticin (US Biological, Swampscott, MA), 200 µg/mL Hygromycin B (US Biological, Swampscott, MA), 100

µg/mL Nourseothricin (Jena Bioscience, Jena, Germany), or 200 µg/mL Zeocin (Thermo Fisher Scientific, Waltham, MA) were added for maintenance of expression constructs where needed. 1 g/L 5'FOA was added to solid media plates where needed.

### 5.2.2 LoxP and CRISPR/Cas9 mediated genome editing

Deletions of *TMA29*, *ALD6*, *ECM31*, *PDC6*, *BAT2*, and *PDC5* were obtained by integration of PCR products generated from *LoxP-KanMX-LoxP* (pUG6) [132], *LoxP-HphMX-LoxP* (pUG75) [167], *LoxP-bleMX-LoxP* (pUG66) [167], or *LoxLE-HphMX-LoxRE* (pZC3) [168] plasmid templates and primers containing 60-80 bp of homology flanking the targeted genes. PCR products were purified, transformed into the appropriate strains, and selected for growth on the appropriate antibiotic selection marker. Deletion of *URA3*, *BDH1/2*, and *PDC1* were achieved via CRISPR/Cas9-mediated genome editing. In brief, an sgRNA sequence targeting the gene of interest was designed via CRISpy-pop (*URA3*, gcacacggtgtggtgggccc; *BDH1/2*, ggtgcgggtgtgcagagcgg; *PDC1*, caaaatgtctgaaattactt) and cloned into the pXIPHOS ($NAT^R$) or pFVG531 (URA-selection) plasmid as described previously [133]. pFVG531 was generated by replacing the Nat CDS in pXIPHOS with the *URA3* CDS from [153]. For *pdc1*, a *LoxLE-HphMX-LoxRE* antibiotic marker with 500 bp of flanking homology was commercially synthesized and used to replace the *PDC1* ORF. For *bdh1/2* and *ura3*, a PCR product containing 40-250 bp of flanking homology was used to replace the respective ORF. PCR products were purified, transformed into the appropriate strains along with the CRISPR/Cas9 plasmid (pXIPHOS or pFVG531), and selected for growth on the appropriate selection marker (antibiotic, auxotroph, or both). All gene deletions were confirmed by PCR of gDNA and Sanger-sequencing. Antibiotic markers were rescued by cre-recombinase-mediated

excision as described elsewhere [132] using pSH65 ($ZEO^R$) [132], pSH66 ($NAT^R$) [167], or pFVG533 (URA-selection). pFVG533 was generated by inserting the CRE-recombinase from pSH65 into pJD25 (high copy, uracil selection plasmid) generated from MoClo toolkit parts [153]. pXIPHOS CRISPR/Cas9 plasmid was cured out via passaging the cells in YPD or YPGE (non-selection media) and pFVG531 CRISPR/Cas9 plasmid was cured out via plating on SC-5'FOA.

### 5.2.3 Yeast fermentations with GVL

Yeast cells were grown aerobically in YPD until stationary phase ∼12 h. The cultures were then diluting to $OD_{600}$ 0.2 in YPD and allowed to reach exponential phase ∼8.5 h. The cells were washed once with sterile water and then used to inoculate a 24-well plate at $OD_{600}$ 0.2 with SynBase medium (refered to as SynH without inhibitors in [169]) with 0, 1, 2.5 and 5% GVL that was degased for >12 h prior to use. Anaerobic growth was then performed in a 30°C Coy anaerobic chamber (10% $H_2$, 10% $CO_2$, and 80% $N_2$) for 66 hours in a Tecan Spark-stacker.

### 5.2.4 Cloning pFVG153

The pFVG153 plasmid was made by first amplifying the CDS of *lvaA*, *lvaB*, *lvaC*, *lvaD*, and *lvaE* from the *P. putida* gDNA with multiple primer sets. The CDS were then cloned in frame with promoters (P) and terminators (T) from the MoClo toolkit [153] resulting in the following pairs: $P_{RAD27}$-*lvaA*-$T_{ENO1}$; $P_{SAC6}$-*lvaE*-$T_{SSA1}$; $P_{RNR2}$-*lvaD*-$T_{ENO2}$; $P_{PAB1}$-*lvaB*-$T_{ENO2}$; $P_{RET2}$-*lvaC*-$T_{TDH1}$. The transcriptional units (promoters-gene-terminator pairs) were then assembled in a high copy ($2\mu$) vector with Kan-resistance via golden gate cloning also made from parts in the MoClo toolkit [153]. Sanger sequencing was

used to confirm the construct.

### 5.2.5 Yeast fermentations with LA

Yeast cells were grown aerobically in YPD until stationary phase ∼12 h. The cultures were then diluting to $OD_{600}$ 0.2 in YPD and allowed to reach exponential phase ∼8.5 h. The cells were then used to inoculate a 24-well plate at $OD_{600}$ 0.2 with YPD or YP with varying concentrations of LA (0, 0.5, 1, 1.5, 2, 2.5, 3 g/L) and G418 for selection as needed. Fermentation was performed under aerobic conditions in a 24-well plate in a Tecan Spark.

## 5.3 Engineering a base *S. cereivisae* strain for isobutanol production from glucose and xylose

### 5.3.1 Selecting a highly active isobutanol pathway cassette to drive the carbon-to-isobutanol flux

In order to build an isobutanol pathway cassette capable of supporting high flux, we first screened existing patent and literature articles for highly active isobutanol pathway enzyme homologs. We identified an acetolactate synthase (*alsS*, from *Lactobacillus plantarum* [41]), a ketol-acid reductoisomerase ($ilvC^{P2D1\text{-}A1}$, from *Escherichia coli* [92]), a dihydroxyacid dehydratase ($ilvD^{L385V}$, from *Streptococcus mutans* [93] or *ilvD*, from *Streptococcus macacae* [93]), an ketoacid decarboxylase (*kdcA*, from *Lactococcus lactis* [94]), and an alcohol dehydrogenase ($adhA^{29C8}$, from *Lactococcus lactis* [95]). Each open reading frame was codon-optimized, synthesized commercially, and cloned in frame with promot-

ers (P) and terminators (T) resulting in the following pairs: $P_{PGK1}$-*alsS*-$T_{PGK1}$; $P_{HHF2}$-$ilvC^{P2D1\text{-}A1}$-$T_{ENO2}$; $P_{TDH3}$-$ilvD^{L385V}$-$T_{TDH1}$; $P_{TDH3}$-*ilvD*-$T_{TDH1}$; $P_{TEF1}$-*kdcA*-$T_{ADH1}$; $P_{TEF2}$-$adhA^{29C8}$-$T_{SSA1}$.

Table 5.1: Homologs and promoters used for isobutanol pathway cassettes.

| **IBA enzyme** | **Promoter** | **2.3 Homolog** | **2.4 Homolog** |
|---|---|---|---|
| ALS | $P_{PGK1}$ | *Lactobacillus plantarum* | *Lactobacillus plantarum* |
| KARI | $P_{HHF2}$ | *Escheveria coli P2D1-A1* | *Escheveria coli P2D1-A1* |
| DHAD | $P_{THD3}$ | *Streptococcus macacae* | *Streptococcus mutans L385V* |
| KDC | $P_{TEF1}$ | *Lactococcus lactis* | *Lactococcus lactis* |
| ADH | $P_{TEF2}$ | *Lactococcus lactis 29C8* | *Lactococcus lactis 29C8* |

A DNA cassette containing four out of the five isobutanol genes was assembled:$P_{PGK1}$-*alsS*-$T_{PGK1}$; $P_{HHF2}$-$ilvC^{P2D1\text{-}A1}$-$T_{ENO2}$; $P_{TEF1}$-*kdcA*-$T_{ADH1}$; $P_{TEF2}$-$adhA^{29C8}$-$T_{SSA1}$. From this cassette, we constructed 2 complete IBA pathway cassettes designated as 2.4 and 2.3 which added the last IBA pathway enzyme $ilvD^{L385V}$ from *Streptococcus mutans* [93] and *ilvD* from *Streptococcus macacae* [93], respectively (Table.5.1). We then performed a fermentation experiment to test isobutanol production by transforming the cassettes, 2.3 and 2.4, into the fermentation-deficient strain FVG454 (T2-3D:*pdc1*△, *pdc5*△, *pdc6*△, *ura3*△) resulting in strains sFVG600 and sFVG601, respectively. For an isobutanol production reference, we included sJD107 and sJD195 which are strains with previously characterized IBA pathway cassettes #3 and #14, respectively from Section 4.3.2. The fermentation was performed under aerobic conditions in SC-ura + 0.71 mM acetate and isobutanol production was measured after 3 days. sFVG601 outperformed all the other engineered strains and produced 350 mg/L isobutanol which corresponds to a yield of 37 mg isobutanol / g glucose or 9% of the theoretical maximum yield (Fig.5.1). sFVG601 also performed ∼2-fold better than sFVG600 indicating that $ilvD^{L385V}$ from *Streptococcus mutans* has a higher activity than *ilvD* from *Streptococcus macacae*. Overall, the 2.4 cassette performed the best and was used in future studies.

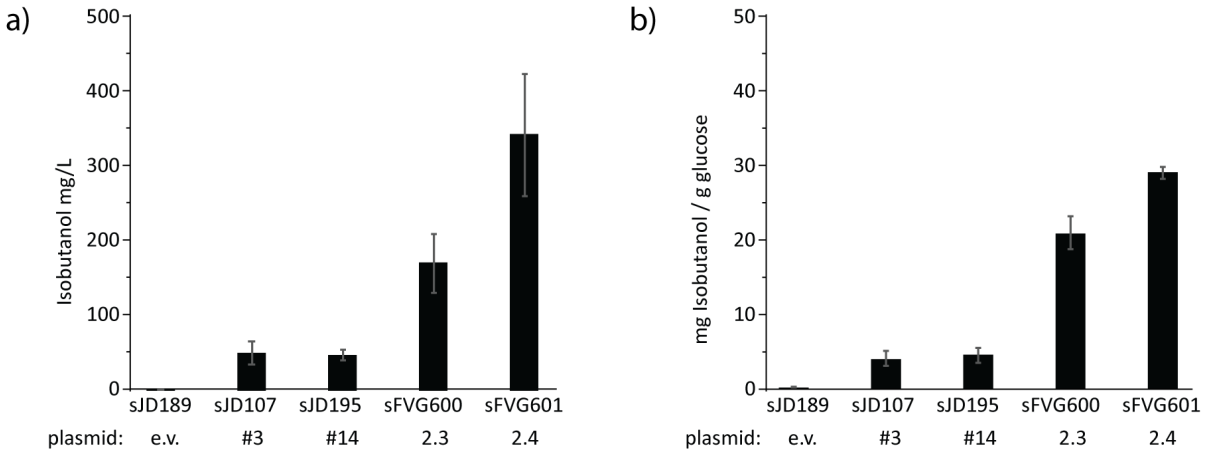


Figure 5.1: **Isobutanol production of varying isobutanol pathway cassettes.** An empty vector (e.v.) and four isobutanol pathway cassettes (#3, #14, 2.3 and 2.4) were transformed in FVG454 resulting in strains sJD189, sJD107, sJD195, sFVG600, and sFVG601, respectively. A fermentation experiment was performed under aerobic conditions in synthetic complete medium minus uracil containing 2% glucose and 0.71 mM acetate. Isobutanol **a)** titer and **b)** yield were measured after 3 days. Error bars represent the standard deviation of the biological replicates.

### 5.3.2 Improving isobutanol production by deleting non-essential competing pathways in an industrially relevant strain

Next, to further streamline the flux to isobutanol, we build a base *S. cerevisiae* strain that was deficient in pathways that compete with isobutanol production. We started with an industrial relevant strain with the capability to consume both glucose and xylose (GLBRCY1625, provided by Trey Sato). We then iteratively deleted key enzymes in competing pathways responsible for ethanol, acetoin/2,3-butanediol, 2,3-dihydroxy-2-methyl butanoate, valine, pantothenate, and isobuytric acid production: *PDC1/5/6*, *BDH1/2*, *TMA29*, *BAT2*, *ECM31*, and *ALD6* respectively (Table.5.2, Figure.5.2).

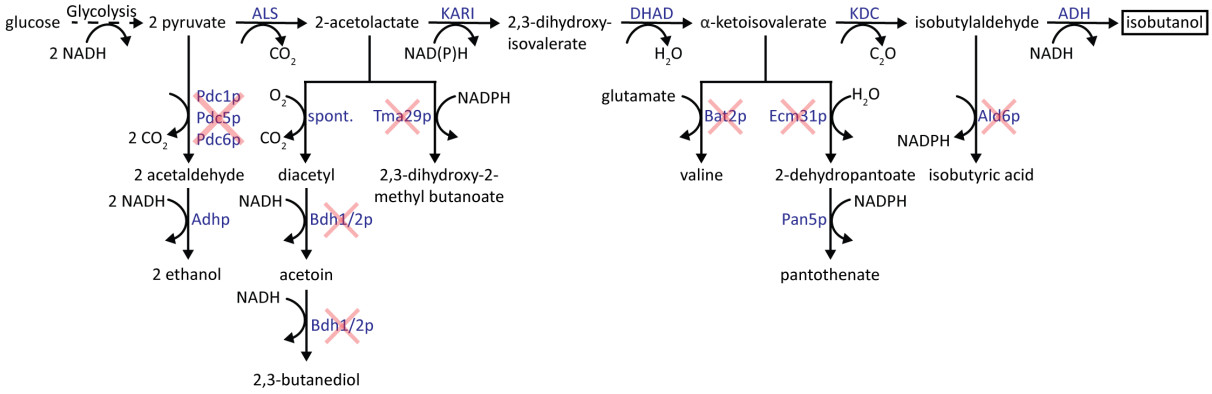


Figure 5.2: **Isobutanol competing pathways in *S. cerevisiae*.** Pathways can be eliminated by deleting key enzymes: *PDC1/5/6* for ethanol, *BDH1/2* for acetoin/2,3-butanediol, *TMA29* for 2,3-dihydroxy-2-methyl butanoate, *BAT2* for valine, *ECM31* for pantothenate, and *ALD6* for isobuytric acid production.

Table 5.2: *S. cerevisiae* strains used in this study.

| **Strain Name** | **Relevant genotype** |
|---|---|
| GLBRCY1625 | YB210 *ho*△::*ScTAL1/CpXI/PsXYL3*, *gre3*△::xylose cassette, *ChrI::TKL1*, *ira2*△::*MR*, *hog*1△::*MR*, *fra2*△::*MR* |
| FVG537 | GLBRCY1625 *ura3*△ |
| FVG539 | yFVG537 *bdh1/2*△ |
| FVG541 | yFVG537 *bdh1/2*△, *tma29*△::*LoxP-hphMX-LoxP* |
| FVG518 | yFVG537 *bdh1/2*△, *tma29*△::*MR*, *ald6*△::*MR* |
| FVG520 | yFVG537 *bdh1/2*△, *tma29*△::*MR*, *ald6*△::*MR*, *ecm31*△::*LoxLE-hphMX-LoxRE* |
| FVG522 | yFVG537 *bdh1/2*△, *tma29*△::*MR*, *ald6*△::*MR*, *ecm31*△::*LoxLE-hphMX-LoxRE*, *pdc6*△::*LoxP-kanMX-LoxP* |
| FVG525 | yFVG537 *bdh1/2*△, *tma29*△::*MR*, *ald6*△::*MR*, *ecm31*△::*MR*, *pdc6*△::*MR*, *bat2*△::*MR* |
| FVG527 | yFVG537 *bdh1/2*△, *tma29*△::*MR*, *ald6*△::*MR*, *ecm31*△::*MR*, *pdc6*△::*MR*, *bat2*△::*MR*, *pdc5*△::*LoxP-bleMX-LoxP* |
| FVG624 | yFVG537 *bdh1/2*△, *tma29*△::*MR*, *ald6*△::*MR*, *ecm31*△::*MR*, *pdc6*△::*MR*, *bat2*△::*MR*, *pdc5*△::*MR*, pdc1△::*MR* |

To investigate the effect of the deletions on isobutanol production, a fermentation experiment was performed. Each strain was transformed with the 2.4 cassette and cultivated at 30°C in SC* (synthetic complete medium minus uracil with tween/ergosterol) anaerobically. End products were analyzed after 120 h (Table.5.3). Strain FVG624 was not included as it could not grow anaerobically; additionally, FVG525, FVG522, and FVG520 were not included due to inconsistent growth. Of the strains cultivated, ethanol yield was not altered; this is as expected since all of the engineered strains had an intact *PDC1* gene (Table.5.3). Of the gene deletions tested, the *BDH1/2* and *TMA29* deletions had no effect on isobutanol production, while the *ALD6* deletion boosted isobutanol titers by ∼1.4-fold; the isobutanol enhancement from the *ALD6* deletion is in agreement with [90]. Further characterization of the deletion strains is needed to determine if the results hold true with xylose as a carbon source (see section 6.2.3).

Table 5.3: Isobutanol and ethanol yield from fermentation experiment. Plasmid 2.4 harboring an isobutanol cassette or empty vector (e.v.) were transformed into the KO strains in Table.5.2. Fermentation was performed under anaerobic conditions in SC* medium for 120h. Error represent the standard deviation of three biological replicates. Strains FVG624, FVG525, FVG522, and FVG520 were not included.

| **Strain** | **mg isobutanol / g glucose** | **g ethanol / g glucose** |
|---|---|---|
| FVG537+e.v. | 0.57±0.07 | 0.56±0.02 |
| FVG537+2.4 | 0.78±0.23 | 0.56±0.02 |
| FVG539+2.4 | 0.67±0.02 | 0.58±0.03 |
| FVG541+2.4 | 0.64±0.09 | 0.57±0.01 |
| FVG518+2.4 | 1.09±0.26 | 0.58±0.04 |
| FVG527+2.4 | 0.27±0.03 | 0.58±0.03 |

## 5.4 Attempts to confer *S. cerevisiae* with the ability to attenuate lignocellulosic inhibitor toxicity

### 5.4.1 Improve *S. cerevisiae*'s Tolerance to GVL

$\gamma$-valerolactone (GVL) is a green solvent effective at solubilizing biomass, however, residual amounts in hydrolysate can be toxic to fermenting microbes (compromises membrane integrity). Chemical genomics or chemogenomic profiling is a pooled fitness experiment that uses a barcoded yeast library and their response to different chemical inhibitors to identify genes important for tolerance. In the assay, the strain abundance of each mutant is compared before and after growth on inhibitors by deep sequencing of DNA barcodes (BarSeq). The relative abundance of each mutant strain is dependent on the impact of the underlying gene to tolerance. If a gene deletion library is used, negative gene fitness values indicate the gene is important for growth while a positive value indicates the gene is detrimental to growth. There has been one GVL chemogenomic profiling experiment conducted with a gene deletion library [170] aerobically at the half-maximum inhibitory concentration of 270 mM or 2.3% GVL in YP galactose medium. Tolerance genes identified were related to ergosterol accumulation (*pad1*$\triangle$ and *fdc1*$\triangle$) [107], however, the deletion's tolerance benefit was not transferable to different fermentation conditions; under industrially relevant anaerobic conditions, the final ethanol production and $OD_{600}$ were fairly unchanged in the $\triangle$*pad1*$\triangle$*fdc1* strain compared to the wild-type (control) (see supplemental information 3 from [107]). We sought out to repeat the GVL chemogenomic profiling experiment under anaerobic conditions and then compare the results to the Bottoms et. al. [107] paper.

A GVL chemogenomic profiling experiment under anaerobic conditions in 1.5 % GVL

SynBase medium (refered to as SynH without inhibitors in [169]) was performed as described previously [107]. 1094 genes showed a statistically significant (FDR $< 0.05$) altered fitness score when deleted: 506 had a negative fitness score and 588 had a positive fitness score. Enrichment analysis using Funspec [2] was performed on hits to identify any enriched patterns. Genes that led to a negative gene fitness value were enriched in amino acid biosynthesis, phosphatidylcholine biosynthesis, microtubules, regulation of Rho signaling, and cellular response to hypoxia. Genes that led to a positive gene fitness value were enriched for cation homeostasis, ribosomal subunits, and trehalose/glycerol/citrate/arsentite biosynthesis/transport.

Table 5.4: Select chemical genomics profiling results with GVL. 3 genes associated with enhanced fitness and 3 genes associated with reduced fitness were selected for further verification.

| **Gene** | **Putative Function** | **$Log_2FC$** |
|---|---|---|
| *GCN20* | regulation of translational elongation | 1.97 |
| *SEY1* | endoplasmic reticulum organization | 1.74 |
| *SLX8* | protein sumoylation | 2.24 |
| *LAS21* | integral plasma membrane protein | -5.94 |
| *SEC28* | late endosome to vacuole transport | -11.44 |
| *DID2* | late endosome to vacuole transport | -1.65 |

Three genes associated with enhanced fitness (*gnc20*△, *sey1*△, and *slx8*△) and three genes associated with reduced fitness (*las21*△, *sec28*△, and *did2*△) were selected for verification (Table.5.4) along with the hits identified from [107], *pad1*△ and *fdc1*△. Growth inhibition was monitored by performing a fermentation experiment under anaerobic conditions in SynBase media with 1, 2.5 and 5% GVL for 66 hr in 24-well plates and comparing the final $OD_{600}$ to the 0% GVL control (Table.5.5). As expected, the *pad1*△ and *fdc1*△ did not consistently improve GVL tolerance as seen in Bottoms et. al. [107]. Additionally, the *gnc20*△, *sey1*△, and *slx8*△ strains and showed an increased tolerance to GVL with *gnc20*△ and *sey1*△ performing the best and exhibiting robust growth in both duplicates in 2.5% GVL.

Table 5.5: **Growth inhibition of GVL on single mutants and the control strain.** Growth inhibition was monitored by performing a fermentation experiment with the selected strains in Table.5.4 under anaerobic conditions in SynBase media with 1, 2.5 or 5% GVL for 66 hr in 24-well plates and comparing the final $OD_{600}$ to the 0% GVL control. ++ indicates robust growth (75-100% of control or 0% GVL), + indicates medium growth (50-75% of control or 0% GVL), and - indicates minimal growth (0-50% of control or 0% GVL). The experiment was conducted in duplicate.

| % GVL | control | | *gcn20*△ | | *sey1*△ | | *slx8*△ | | *las21*△ | | *sec28*△ | | *did2*△ | | *pad1*△ | | *fdc1*△ | |
|---|---|---|---|---|---|---|---|---|---|---|---|---|---|---|---|---|---|---|
| 0 | ++ | ++ | ++ | ++ | ++ | ++ | ++ | ++ | ++ | ++ | ++ | ++ | ++ | ++ | ++ | ++ | ++ | ++ |
| 1 | ++ | ++ | ++ | ++ | ++ | ++ | ++ | ++ | ++ | ++ | ++ | ++ | ++ | ++ | + | ++ | ++ | ++ |
| 2.5 | + | - | + | + | + | + | + | - | - | - | - | - | - | - | - | + | - | - |
| 5 | - | - | - | - | - | - | - | - | - | - | - | - | - | - | - | - | - | - |

While the *gnc20*△ and *sey1*△ led to the highest tolerance improvement, additional work is needed to confirm if the tolerance enhancement is transferable to a industrially-relevant background strain. Additionally, the deletion's affect on fermentation conditions (biomass accumulation, glucose/xylose consumption, and ethanol production) should be tested (see section 6.2.2). While Bottoms et. al saw that ergosterol accumulation improved GVL tolerance aerobically, ergosterol biosynthesis is an oxygen-dependent process and thus under anaerobic conditions the cells likely use a different mechanism to overcome toxicity. Additional work is needed to uncover the exact mechanism for detoxifying GVL under anaerobic conditions (i.e. uncover the effect of the *gnc20*△ and *sey1*△).

### 5.4.2 Levulinic acid bioconversion to central carbon metabolites

LA is a 5-carbon $\gamma$-keto acid produced from the degradation of cellulose and hemicellulose during biomass conversion to lignocellulosic hydrolysate [106]. The amount of LA present in hydrolysate can vary depending on the pretreatment process and biomass used; for example, in GVL processed switchgrass hydrolysate, LA consists of 2.5% of the total carbon recovered [108], while in weak acid processed spruce hydrolysate, LA is present at 2.6 g/L [106]. *S. cerevisiae*'s growth is severely inhibited by concentrations of LA higher than 1.5% (Fig.5.3) so inhibitor toxicity must be overcome for successful fermentations. Biodetoxification is an environmentally attractive and cost-effective approach to mitigate the effect of hydrolysate inhibitors; this strategy has been successful in detoxifying furan derivatives (HMF and furfural) from corn stover hydrolysates [171, 172].

To test if biodetoxification was a valid strategy for levulinic acid, we engineered a *S. cerevisiae* strain with the LA catabolic pathway from *P. putida* [173]. A DNA cassette for expressing the five genes was created by cloning the CDSs in frame with promoters (P)

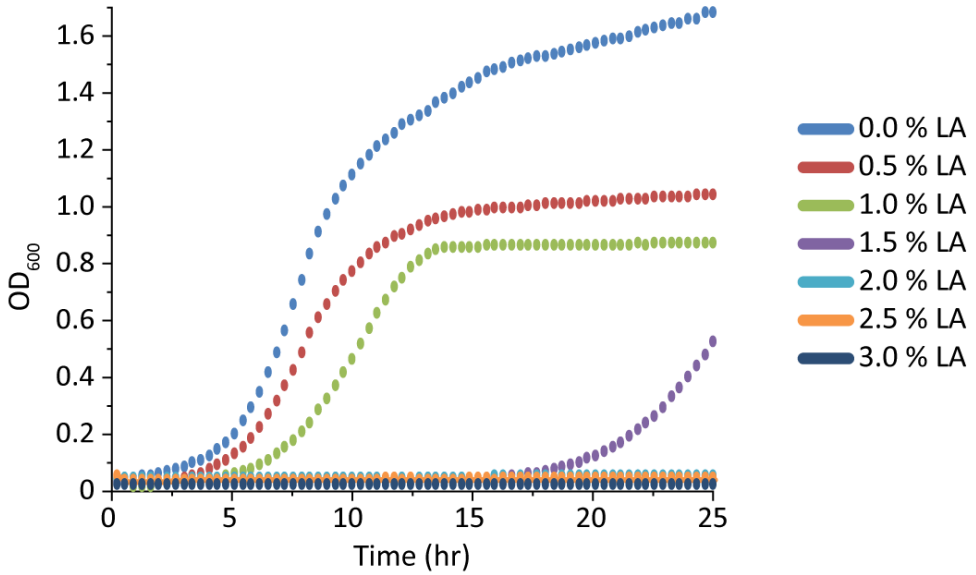


Figure 5.3: **1.5% LA inhibits *S. cerevisiae*'s growth.** Growth curve of *S. cerevisiae* on YPD with increasing concentrations of LA (0, 0.5, 1, 1.5, 2, 2.5, 3%). Fermentation was performed under aerobic conditions in a 24-well plate for 24 hrs.

and terminators (T) resulting in the following pairs: $P_{RAD27}$-*lvaA*-$T_{ENO1}$; $P_{SAC6}$-*lvaE*-$T_{SSA1}$; $P_{RNR2}$-*lvaD*-$T_{ENO2}$; $P_{PAB1}$-*lvaB*-$T_{ENO2}$; $P_{RET2}$-*lvaC*-$T_{TDH1}$. The DNA cassette was assembled in a high copy ($2\mu$) vector resulting in pFVG153 and transformed in *S. cerevisiae* CEN.PK113-5D. A growth experiment was then performed to evaluate and compare the engineered strain and wild-type's growth in the presence of LA. The strains were cultured aerobically in YP with 0 or 1.5% LA at 30°C and by the end of the fermentation, the growth of the CEN.PK strain harboring pFVG153 was reduced compared to the control (CEN.PK + empty vector) (Fig.5.4). Additionally, the LA concentration at the end of the fermentation was measured and it remained unchanged for the CEN.PK strain harboring pFVG153 indicating that the catabolism pathway was non-functional. We hypothesize that the enzymes are either not being expressed or that LA is not actively transported into the cell. Additional experiments such as shotgun proteomics and crude cell lysate assays are therefore needed to uncover the mechanism of inactivity.

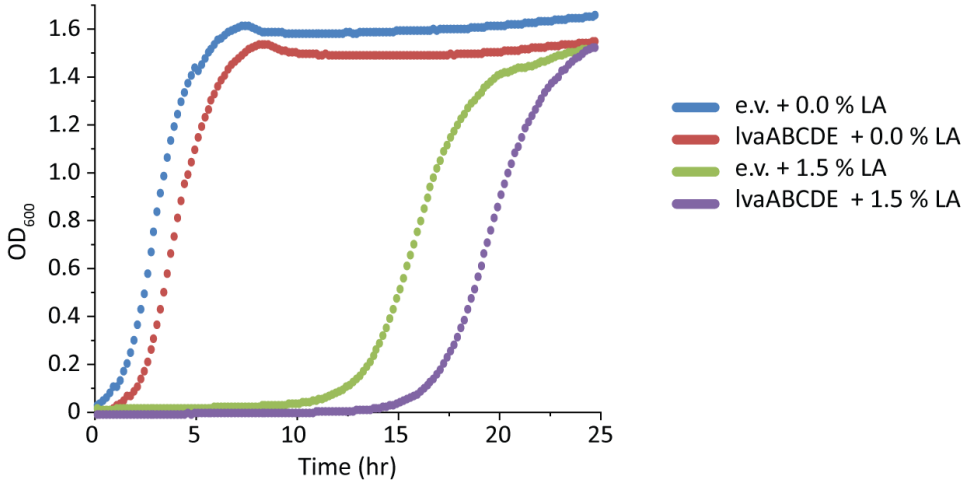


Figure 5.4: **LA catabolism pathway non-functional in *S. cerevisiae*.** Growth curve of CEN.PK113-5D with pFVG95 (e.v.) or pFVG513 (lvaABCDE) on YP + G418 + 0 or 1.5 % LA. Fermentation was performed under aerobic conditions in a 24-well plate for 24 hrs.

## 5.5 Acknowledgements

We thank Sae-buyk Lee and Trey Sato for the GLBRCY1625 strain, pSH65, and pUG6.

We thank Russell Wrobell and Chris Hittinger for the Moclo kit parts and pXIPHOS.

We thank Taylor Scott and Megan McClean for pZC3.

# Chapter 6

# Conclusions and Future directions

**Authors and Contributors:**

- **Francesca V. Gambacorta** researched, designed and performed experiments, analyzed data, writing-methods, editing and reviewing manuscript.
- **Hugh Purdy** provided guidance for section 6.2.6.
- **Stephanie J. Brown** implemented experiments for section 6.2.5.
- **Dr. Brian F. Pfleger** funding acquisition, conceptualization, design of experiments, editing and reviewing manuscript.

## 6.1 Summary of thesis research

The yeast *S. cerevisiae* has long been an important species to humans, from its use in brewing and baking to its role as a model organism for studying eukaryotic biology. The work presented here aims to expand our knowledge of the organism and gain an understanding on how its metabolism could be rewired for isobutanol production. This is a difficult challenge due to *S. cerevisiae*'s dominate native flux to ethanol.

In **Chapter 1**, we introduced the tools and strategies that were used in this thesis to enhance isobutanol flux. Specifically, we touched on establishing the desired pathway using characterized parts (manipulating DNA, RNA, and protein) and then we focus on enhancing isobutanol production using metabolic flux optimization approaches such as the push-pull-block strategy and systems-level multi-omics.

In **Chapter 2**, we learned that isobutanol can replace ethanol as a fermentation product if flux through the pathway is sufficiently high for $NAD^+$ regeneration. Unfortunately though, the strategies to create high-yielding isobutanol producing strains remain elusive to academic researchers.

In **Chapter 3** and **Chapter 4**, we focus on on 2 different metabolic engineering approaches to enhance the carbon-to-isobutanol flux. Specifically, in **Chapter 3**, we investigated how pathway localization and redox cofactor-balancing affect the performance and physiology of isobutanol producing strains. We equipped yeast with isobutanol cassettes which had either a mitochondrial or cytosolic localized isobutanol pathway and used either a redox-imbalanced (NADPH-dependent) or redox-balanced (NADH-dependent) ketol-acid reductoisomerase enzyme. Then through a multi-omic analysis, we uncovered that the cytosolic-localized isobutanol pathway had low performance due to a limitation in the supply of Fe-S clusters, which are required cofactors for the dihydroxyacid

dehydratase enzyme. We then demonstrated that this cofactor limitation may be partially recovered by disrupting iron homeostasis with a *fra2* mutation, thereby increasing cellular iron levels. This was an important finding as a cytosolic-localized isobutanol pathway is preferable when growing under industrially relevant conditions such as high glucose concentrations or anaerobic growth. This is in part because the mitochondria are known to enter a minimal energy-requirement mode under those conditions and thus we want to avoid localizing our pathway to that compartment [98, 99]. Additionally, a cytosolic localization would eliminate any bottleneck associated with the need to transport intermediates in/out of the mitochondria.

In **Chapter 4**, we investigate if flux through the isobutanol pathway can be enhanced by identification of highly active isobutanol enzyme homologs and balancing their expression. Taking our findings from Chapter 3, we constructed a fully cytosolic combinatorial isobutanol pathway library that had variability introduced on 2 levels: coding sequences (homologs) and gene dosage (promoters). Then through a high-throughput growth-coupled screen, that relied on having an active isobutanol pathway for $NAD^+$ regeneration, we identified and characterized a high-flux isobutanol cassette. We then aimed to balance the high-flux cassette's cofactor specificity with glycolysis via protein engineering, but the resulting pathway's flux was too low to achieve anaerobic growth. This study motivates future research on enhancing the copy number of the isobutanol pathway enzymes within the cell to boost production.

In **Chapter 5**, we begin to look at the variables associated with using biomass as a carbon source. Specifically, we focus on generating a xylose-to-isobutanol platform strain and improving the tolerance to 2 inhibitors, $\gamma$-valerolactone and levulinic acid. While we were unable to engineer *S. cerevisiae* with a biodetoxificaiton strategy to overcome

levulinic acid toxicity, we did identify 2 gene deletions, $\triangle$*gnc20* and $\triangle$*sey1*, associated with improved $\gamma$-valerolactone tolerance using a chemical genomic study. Future work is still needed to combine the findings here with the isobutanol pathway cassettes developed in Chapter 3 and 4 and to validate the benefit of these deletions when growing on real hydrolysate.

Overall, future work is still required to rewire *S. cerevisiae*'s metabolism for isobutanol production. Pathway intermediate buildup and by-product formation still remain a major challenge and flux through the pathway must be further enhanced to achieve anaerobic growth.

## 6.2 Future directions

There are several aspects of the work in this document that can be extended. The following section will describe these opportunities and highlight the challenges.

### 6.2.1 Multi-copy genomic integration

In Chapter 4, we attempted to create an anaerobically growing, isobutanol producing *S. cereivisae* strain. However, anaerobic growth could not be achieved since the isobutanol pathway cassette did not support a high enough carbon flux to rapidly replenish the $NAD^+$ equivalents needed for glycolysis (i.e. isobutanol production is too low to meet the cellular maintenance energy requirement). The capacity of the pathway can be enhanced by integrating multiple copies of the cassette in the genome in addition to expressing the cassette on a high-copy episomal plasmid ($2\mu$ origin). The most common existing approach for achieving multi-copy integrations is integrating into the transposable elements, long terminal repeats (LTR), however, this approach is unstable without a selection pres-

sure. I propose implementing the newly developed method, HapAmp, which relies on coupling the dosage of a haploinsufficient gene to cell fitness; this is accomplished by replacing the native promoter with a weaker one and coupling it to expression of your gene of interest along with a autonomous replication sequence (ARS). The ARS will facilitate amplification of the cassette as the yeast evolve towards faster growth and this results in a genetically stable integration (up to 47-copies using construct 4) [174]. To implement this, the isobutanol pathway cassette, #3 with Lb-llvC$^{DDV}$ needs to be cloned in place of the gene of interest in construct 4 (pILGFP3AA5) from [174]. Then the cassettes can be transformed into the strain of interest, FVG454 (T2-3D:*pdc1*△, *pdc5*△, *pdc6*△, and *ura3*△) and tested for anaerobic growth.

### 6.2.2 GVL tolerance study in an industrial relevant strain

In Chapter 5, we identified two gene deletions, △*gnc20* and △*sey1*, that improved *S. cerevisiae*'s tolerance to 2.5% GVL under anaerobic conditions. The original study was conducted using a hypersensitive lab strain background, and future work is needed to test if the tolerance enhancement can also be seen in an industrially relevant strain background, Y22-3. I propose using the engineered Y22-3 background strain that has the capacity to consume both glucose and xylose (GLBRC Y1327, provided by Trey Sato [175]) and deleting *GCN20* and *SEY1*. The resulting strains along with the parent (control) should be subjected to a fermentation experiment under anaerobic conditions in synthetic hydrolysate without inhibitors (SynH) [169] spiked with 3% GVL. Growth, xylose consumption, glucose consumption, and ethanol production should be monitored and compared.

### 6.2.3 Hydrolysate-to-isobutanol

In Chapter 5, we constructed a platform production strain that had the capacity to consume both glucose and xylose. In brief, we started with GLBRCY1625 and deleted key enzymes in pathways that compete with isobutanol production. Preliminary experiments involving the knock out strains with a redox-balanced, high-flux isobutanol pathway cassette reveled a low glucose-to-isobutanol flux. Further characterization is needed to determine the xylose-to-isobutanol flux. I propose the characterization be performed with the engineered strains along with the parent (control). The fermentation experiments should be performed under anaerobic conditions in SC* (see section 6.2.5.1) with 25 g/L xylose. Growth, xylose consumption, and ethanol production should be monitored and compared.

### 6.2.4 Overcoming the C2-auxotroph in PDC$^-$ *S. cerevisiae* strains

Pdc$^-$ strains are auxotrophic for C2-compounds due to their inability to produce cytosolic acetyl-CoA with the native pyruvate dehydrogenase (Pdh) bypass consisting of pyruvate decarboxylase (Pdc), acetaldehyde dehydrogenase (Ald), and acetyl-CoA synthetase (Acs) (Fig.2.1). In the work presented in this thesis, C2-compounds (ethanol and acetate) were supplemented into the media to overcome this auxotroph. Alternatively, the C2-auxotrophy can be circumvented by providing a heterologous synthesis pathway such as the phosphoketolase (PK)/phosphotransacetylase (PTA) pathway [33, 34].

In efforts to implement this pathway in *S. cerevisiae* the open reading frame of PK from *Leuconostoc mesenteroides* and PTA from *Bacillus subtilis* were codon-optimized, synthesized commercially, and cloned in frame with promoters (P) and terminators (T) resulting in the following pairs: $P_{TEF1}$-$PK$-$T_{ADH1}$; $P_{TEF1}$-$PTA$-$T_{ADH1}$ [176]. The tran-

scriptional units (promoters-gene-terminator pairs) were then assembled in a low copy (cen/ars) vector with Kan resistance made from parts in the MoClo toolkit resulting in pFVG199 [153]. Next steps include testing the construct to ensure enzyme expression (shotgun proteomics). Additionally, characterization of the cassette in a PDC$^-$ background strain is needed. I propose transforming pFVG199 and the empty vector control, pFVG95, into FVG624 (see section 5.3.2) and performing a fermentation experiment. The experiment should be performed under aerobic conditions in SC 2% glycerol medium + G418 with and without C2-supplement (2% ethanol); if the PK/PTA pathway is active, the strain should grow faster in medium without C2-supplementation. Strain GG570 (T2-3D:*pdc1*△, *pdc5*△, *pdc6*△) cannot be used as it is Kan/G418 resistant [28].

### 6.2.5 Gene deletions required for adaptive laboratory evolution experiments

ALE is a powerful tool that relies on natural selection for achieving a desired phenotype in the presence of a selection pressure. Cell growth can be coupled to isobutanol production under anaerobic conditions if other fermentative pathways in *S. cerevisiae* are deleted (i.e isobutanol production reoxidizes the NADH produced from glycolysis). Ethanol is the main fermentative pathway in *S. cerevisiae* however its deletion alone is not sufficient to achieve growth-coupling. We performed an anaerobic ALE experiment by transforming a redox-balanced isobutanol pathway cassette designated as 2.4 (see section 5.3.1) into FVG454, a Pdc$^-$ strain. Over the course of 6-passages, the strain lost its ability to produce isobutanol and instead reverted to a lactate producer; at the end of the 6$^{th}$ passage, the evolved strain was producing lactate at 40% of the theoretical maximum yield (Table.6.1). Future work can involve sequencing the resulting evolved strain using

next-generation sequencing (NGS) to uncovering the genotypic changes related to the increased lactate production. Furthermore, to prevent this result from occurring in future ALE experiments, additional gene deletions are required to eliminate lactate (*did1*△), malate (*mls1*△), glycerol (*gpd1/2*△), and succinate production (*icl1*△) production to achieve strict growth coupling.

Table 6.1: Lactate and isobutanol production from ALE strain. Lactate and isobutanol data reported as % theoretical yield.

| **Passage** | **Isobutanol** | **Lactate** |
|---|---|---|
| 1 | 3 | 29 |
| 2 | N/A | N/A |
| 3 | 0 | 23 |
| 4 | 0 | 37 |
| 5 | 0 | 18 |
| 6 | 0 | 39 |

#### 6.2.5.1 Methods- ALE

Yeast cells were grown aerobically in SCGE-Ura for ∼26 h. The cultures were then diluted to $OD_{600}$ 0.2 in SC* and allowed to reach exponential phase ∼24 h. The cells were diluted for anaerobic growth to $OD_{600}$ 0.2 in SC* medium that was degassed for >12h prior to use. Anaerobic growth was then performed in a Coy anaerobic chamber (5% $H_2$, 5% $CO_2$, and 90% $N_2$) with stir bars on a magnetic stir plate to prevent flocculation. Cells were continually diluted into fresh SC* media after reaching exponential phase ∼ 3 days. 7 passages were completed. Samples were pulled periodically for HPLC analysis.

Defined SC* medium contained 1.72 g/L yeast nitrogen base (YNB) without amino acids or ammonium sulfate, 1.54 g/L drop out mix complete minus leucine and uracil, 19.5 g/L MES, 20 g/L dextrose, 5 g/L ammonium sulfate, 380 mg/L leucine, 4 mL/L 250X tween/ergosterol stock (62.5mL Tween80 + 625mg Ergosterol in 187 mL 95% EtOH), 4.1 mL/L 200 proof ethanol and pH adjusted to 5.5 with HCl.

### 6.2.6 Challenges with utilizing a pathway that contains a Fe-S cluster requiring protein

There are several biotechnologically relevant pathways that contain Fe-S cluster dependent enzymes and working with these enzymes can be challenging as there are many factors that can influence activity. Pathways that utilize Fe-S cluster requiring enzymes include xylose catabolism (XylD or D-xylonate dehydratase) [158], isoprenoid synthesis (IspG or 2-C-methyl-D-erythritol-2, 4-cyclodiphosphate reductase and IspH 4-hydroxyl-3-methylbut-2-enyl diphosphate reductase [177], Entner-Doudoroff pathway (PGDH or 6-phosphogluconate dehydratase) [160], adipic acid synthesis (ER or enoate reductase) [178], nitrogen fixation (NifH or dinitrogenase reductase) [179], and isobutanol synthesis (DHAD or dihydroxy-acid dehydratase). In Chapter 3, we saw that the availability of the Fe-S cluster itself was a limiting factor and thus reduced the activity of our Fe-S cluster requiring protein, Ilv3p. While we could relieve the bottleneck in our pathway by increasing Fe-S biogenesis, this solution cannot be generalized to any Fe-S cluster requiring protein in a pathway; for example, increasing the availability of iron in the cell had no effect on another Fe-S cluster requiring protein, 6-phosphogluconate dehydratase [160]. Thus, increasing Fe-S cluster biogenesis via increasing the availability of iron in the cell is only a valid strategy if cytosolic Fe-S cluster availability is a limitation. Other factors that can influence the activity of an Fe-S cluster requiring enzyme is the environment where the enzyme is localized (pH, reducing potential, oxygen level etc.) and whether the enzyme is recognized for cluster incorporation; these challenges are thoroughly reviewed here [180].

The obvious choice to avoid the challenges associated with expressing an Fe-S cluster requiring protein is to find an alternative enzyme that catalyzes the desired reaction but

utilizes a different cofactor such as $Mg^{2+}$. There have been attempts to identify an enzyme that catalyzes the DHIV to KIV reaction in the isobutanol pathway without success; Oki et. al. attempted to modify the binding pocket of a sugar acid dehydratase via protein engineering but the resulting variants had no activity with the desired substrate, DHIV [181]. It is worth looking into if there is an alternative starting base other than the sugar acid dehydratase. This can be done by first identifying metabolic reactions that "look similar" to the DHAD reaction, then checking if any of the identified enzymes are characterized as not Fe-S containing. The BridgIT, a BNICE-related tool, and the Rhea reaction database are good places to start.

# References


[1] Kyeong Rok Choi, Woo Dae Jang, Dongsoo Yang, Jae Sung Cho, Dahyeon Park, and Sang Yup Lee. Systems Metabolic Engineering Strategies: Integrating Systems and Synthetic Biology with Metabolic Engineering. *Trends in Biotechnology*, 37(8):817–837, 2019.

[2] Mark D. Robinson, Jörg Grigull, Naveed Mohammad, and Timothy R. Hughes. FunSpec: A web-based cluster interpreter for yeast. *BMC Bioinformatics*, 3(1):1–5, nov 2002.

[3] Daniel R Hyduke, Nathan E Lewis, and Bernhard Ø Palsson. Analysis of Omics Data with GEMs. *Mol. BioSyst.*, 9(2):167–174, 2013.

[4] Joao G.R. Cardoso, Kristian Jensen, Christian Lieven, Anne Sofie Lærke Hansen, Svetlana Galkina, Moritz Beber, Emre Özdemir, Markus J. Herrgård, Henning Redestig, and Nikolaus Sonnenschein. Cameo: A Python Library for Computer Aided Metabolic Engineering and Optimization of Cell Factories. *ACS Synthetic Biology*, 7(4):1163–1166, apr 2018.

[5] Ali Ebrahim, Joshua A. Lerman, Bernhard O. Palsson, and Daniel R. Hyduke. COBRApy: COnstraints-Based Reconstruction and Analysis for Python. *BMC Systems Biology*, 7, 2013.

[6] Cameron Cotten and Jennifer L. Reed. Constraint-based strain design using continuous modifications (CosMos) of flux bounds finds new strategies for metabolic engineering. *Biotechnology Journal*, 8(5):595–604, 2013.

[7] Jocelyn F. Krey, Phillip A. Wilmarth, Jung Bum Shin, John Klimek, Nicholas E. Sherman, Erin D. Jeffery, Dongseok Choi, Larry L. David, and Peter G. Barr-Gillespie. Accurate label-free protein quantitation with high- and low-resolution mass spectrometers. *Journal of Proteome Research*, 13(2):1034–1044, feb 2014.

[8] Fast Facts: U.S. Transportation Sector Greenhouse Gas Emissions 1990-2020. Technical Report May, 2022.

[9] Jacob Peyton Crigler. *Improving biological detoxification of furfural and acetate in lignocellulosic hydrolysates using metabolic engineering.* PhD thesis, 2018.

[10] Nicolaas A. Buijs, Verena Siewers, and Jens Nielsen. Advanced biofuel production by the yeast saccharomyces cerevisiae. *Current Opinion in Chemical Biology*, 17(3):480–488, 2013.

[11] Chuhan Fu, Zhuoxi Li, Chuhua Jia, Wanli Zhang, Yulei Zhang, Conghua Yi, and Shaoqu Xie. Recent advances on bio-based isobutanol separation. *Energy Conversion and Management: X*, 10:100059, dec 2021.

[12] Kuk-Ki Hong and Jens Nielsen. Metabolic engineering of Saccharomyces cerevisiae: A key cell factory platform for future biorefineries. *Cellular and Molecular Life Sciences*, 69(16):2671–2690, 2012.

[13] E Ofuonye, K Kutin, and D T Stuart. Engineering Saccharomyces cerevisiae fermentative pathways for the production of isobutanol. *Biofuels*, 4(2):185–201, 2013.

[14] Avraam Roussos, Nikiforos Misailidis, Alexandros Koulouris, Francesco Zimbardi, and Demetri Petrides. A feasibility study of cellulosic isobutanol production-process simulation and economic analysis. *Processes*, 7(10), 2019.

[15] Francesca V. Gambacorta, Joshua J. Dietrich, Qiang Yan, and Brian F. Pfleger. Rewiring yeast metabolism to synthesize products beyond ethanol, dec 2020.

[16] Binbin Chen, Hui Ling Lee, Yu Chyuan Heng, Niying Chua, Wei Suong Teo, Won Jae Choi, Susanna Su Jan Leong, Jee Loon Foo, and Matthew Wook Chang. Synthetic biology toolkits and applications in Saccharomyces cerevisiae. *Biotechnology Advances*, 36(7):1870–1881, nov 2018.

[17] Jiazhang Lian, Shekar Mishra, and Huimin Zhao. Recent advances in metabolic engineering of Saccharomyces cerevisiae: new tools and their applications. *Metabolic Engineering*, 50:85–108, 2018.

[18] Roshanak Salari and Rosita Salari. Investigation of the Best Saccharomyces cerevisiae Growth Condition. *Electronic physician*, 9(1):3592–3597, jan 2017.

[19] Sean J. McIlwain, David Peris, Maria Sardi, Oleg V. Moskvin, Fujie Zhan, Kevin S. Myers, Nicholas M. Riley, Alyssa Buzzell, Lucas S. Parreiras, Irene M. Ong, Robert Landick, Joshua J. Coon, Audrey P. Gasch, Trey K. Sato, and Chris Todd Hittinger. Genome sequence and analysis of a stress-tolerant, wild-derived strain of Saccharomyces cerevisiae used in biofuels research. *G3: Genes, Genomes, Genetics*, 6(6):1757–1766, 2016.

[20] David Jullesson, Florian David, Brian Pfleger, and Jens Nielsen. Impact of synthetic biology and metabolic engineering on industrial production of fine chemicals. *Biotechnology Advances*, 33(7):1395–1402, 2015.

[21] Christopher R. Mehrer, Matthew R. Incha, Mark C. Politz, and Brian F. Pfleger. Anaerobic production of medium-chain fatty alcohols via a $\beta$-reduction pathway. *Metabolic Engineering*, 48(May):63–71, 2018.

[22] N. G. Vemuri, A. M. Eiteman, E. J McEwen, L Olsson, and J Nielse. Increasing NADH oxidation reduces overflow metabolism in Saccharomyces cerevisiae. *Pnas*, 104(7):2402–2407, 2007.

[23] Ömur Kayikci and Jens Nielsen. Glucose repression in Saccharomyces cerevisiae. *FEMS Yeast Research*, 15(6), 2015.

[24] Elisabetta de Alteriis, Fabrizio Cartenì, Palma Parascandola, Jacinta Serpa, and Stefano Mazzoleni. Revisiting the Crabtree/Warburg effect in a dynamic perspective: a fitness advantage against sugar-induced cell death. *Cell Cycle*, 17(6):688–701, mar 2018.

[25] Thomas Pfeiffer and Annabel Morley. An evolutionary perspective on the Crabtree effect. *Frontiers in Molecular Biosciences*, 1(17):1–6, 2014.

[26] Avlant Nilsson and Jens Nielsen. Metabolic Trade-offs in Yeast are Caused by F1F0-ATP synthase. *Scientific Reports*, 6(22264), mar 2016.

[27] Benjamín J Sánchez, Cheng Zhang, Avlant Nilsson, Petri-Jaan Lahtvee, Eduard J Kerkhoven, and Jens Nielsen. Improving the phenotype predictions of a yeast genome-scale metabolic model by incorporating enzymatic constraints. *Molecular Systems Biology*, 13(935):1–16, 2017.

[28] Marcel Flikweert, Linda Van der Zanden, Wouter M. TH. M Janssen, H. YDE STEENSMA, Johannes P. Van Dijken, and Jack T. Pronk. Pyruvate Decarboxylase: An Indispensable Enzyme for Growth of Saccharomyces cerevisiae on Glucose. *Yeast*, 12:247–257, 1996.

[29] Yoshihiro Ida, Chikara Furusawa, Takashi Hirasawa, and Hiroshi Shimizu. Stable disruption of ethanol production by deletion of the genes encoding alcohol dehydrogenase isozymes in Saccharomyces cerevisiae. *Journal of Bioscience and Bioengineering*, 113(2):192–195, 2012.

[30] Bart Oud, Carmen-lisset Flores, Carlos Gancedo, Xiuying Zhang, Joshua Trueheart, Jean-marc Daran, Jack T Pronk, and Antonius J A Van Maris. An internal deletion in MTH1 enables growth on glucose of pyruvate-decarboxylase negative , non-fermentative Saccharomyces cerevisiae. 11(131):1–10, 2012.

[31] Harmen M. van Rossum, Barbara U. Kozak, Matthijs S. Niemeijer, Hendrik J. Duine, Marijke A.H. Luttik, Viktor M. Boer, Peter Kötter, Jean Marc G. Daran, Antonius J.A. van Maris, and Jack T. Pronk. Alternative reactions at the interface of glycolysis and citric acid cycle in Saccharomyces cerevisiae. *FEMS Yeast Research*, 16(3):1–13, 2016.

[32] Yiming Zhang, Guodong Liu, Martin K.M. Engqvist, Anastasia Krivoruchko, Björn M. Hallström, Yun Chen, Verena Siewers, and Jens Nielsen. Adaptive mutations in sugar metabolism restore growth on glucose in a pyruvate decarboxylase negative yeast strain. *Microbial Cell Factories*, 14(116):1–11, 2015.

[33] Hu Liu, Jingjing Fan, Chen Wang, Chun Li, and Xiaohong Zhou. Enhanced $\beta$-Amyrin Synthesis in Saccharomyces cerevisiae by Coupling An Optimal Acetyl-CoA Supply Pathway. *Journal of Agricultural and Food Chemistry*, 67(13):3723–3732, apr 2019.

[34] Harmen M. van Rossum, Barbara U. Kozak, Jack T. Pronk, and Antonius J.A. van Maris. Engineering cytosolic acetyl-coenzyme A supply in Saccharomyces cerevisiae: Pathway stoichiometry, free-energy conservation and redox-cofactor balancing. *Metabolic Engineering*, 36:99–115, 2016.

[35] Juana M. Gancedo. The early steps of glucose signalling in yeast. *FEMS Microbiology Reviews*, 32(4):673–704, 2008.

[36] Jeong-Ho Kim, Adhiraj Roy, David Jouandot II, and Kyu Hong Cho. The glucose signaling network in yeast. *Biochimica et Biophysica Acta (BBA) - General Subjects*, 1830(11):5204–5210, 2013.

[37] Christopher J. L. Klein, Lisbeth Olsson, and Jens Nielsen. Glucose control in Saccharomyces cerevisiae : the role of Mig1 in metabolic functions. *Microbiology*, 144:13–24, 1998.

[38] Loïc Habegger, Kelly Rodrigues Crespo, and Michal Dabros. Preventing Overflow Metabolism in Crabtree-Positive Microorganisms through On-Line Monitoring and Control of Fed-Batch Fermentations. *Fermentation*, 4(3):79, 2018.

[39] Soo Jung Kim, Seung Oh Seo, Yong Su Jin, and Jin Ho Seo. Production of 2,3-butanediol by engineered saccharomyces cerevisiae. *Bioresource Technology*, 146:274–281, 2013.

[40] Antonius J A van Maris, Jan-maarten A Geertman, Alexander Vermeulen, Matthijs K Groothuizen, Aaron A Winkler, Matthew D W Piper, Johannes P van Dijken, and Jack T Pronk. Directed evolution of pyruvate decarboxylase-negative Saccharomyces cerevisiae, yielding a C2-independent, glucose-tolerant, and pyruvate-hyperproducing yeast. *Applied and environmental microbiology*, 70(1):159–166, 2004.

[41] Jun Ishii, Keisuke Morita, Kengo Ida, Hiroko Kato, Shohei Kinoshita, Shoko Hataya, Hiroshi Shimizu, Akihiko Kondo, and Fumio Matsuda. A pyruvate carbon flux tugging strategy for increasing 2,3-butanediol production and reducing ethanol subgeneration in the yeast Saccharomyces cerevisiae. *Biotechnology for Biofuels*, 11(180):1–21, dec 2018.

[42] Tao Yu, Yongjin J. Zhou, Mingtao Huang, Quanli Liu, Rui Pereira, Florian David, and Jens Nielsen. Reprogramming yeast metabolism from alcoholic fermentation to lipogenesis. *Cell*, 174(6):1549–1558, 2018.

[43] Cecilia Martinez-Ortiz, Andres Carrillo-Garmendia, Blanca Flor Correa-Romero, Melina Canizal-García, Juan Carlos González-Hernández, Carlos Regalado-Gonzalez, Ivanna Karina Olivares-Marin, and Luis Alberto Madrigal-Perez. SNF1 controls the glycolytic flux and mitochondrial respiration. *Yeast*, 36(8):487–494, 2019.

[44] Mónica Rosas Lemus, Elodie Roussarie, Noureddine Hammad, Alexis Mougeolle, Stéphane Ransac, Razanne Issa, Jean Pierre Mazat, Salvador Uribe-Carvajal, Michel Rigoulet, and Anne Devin. The role of glycolysis-derived hexose phosphates in the induction of the Crabtree effect. *Journal of Biological Chemistry*, 293(33):12843–12854, aug 2018.

[45] Seung-Ho Baek, Eunice Y. Kwon, Seon-Young Kim, and Ji-Sook Hahn. GSF2 deletion increases lactic acid production by alleviating glucose repression in Saccharomyces cerevisiae. *Scientific Reports*, 34812(October):1–12, oct 2016.

[46] Rebeca L. Vicente, Lucie Spina, Jose P.L. Gómez, Sebastien Dejean, Jean Luc Parrou, and Jean Marie François. Trehalose-6-phosphate promotes fermentation and glucose repression in Saccharomyces cerevisiae. *Microbial Cell*, 5(10):444–459, 2018.

[47] Sujin Kim and Ji-Sook Hahn. Efficient production of 2,3-butanediol in Saccharomyces cerevisiae by eliminating ethanol and glycerol production and redox rebalancing. *Metabolic Engineering*, 31:94–101, 2015.

[48] Jin-Woo Kim, Seung-Oh Seo, Guo-Chang Zhang, Yong-Su Jin, and Jin-Ho Seo. Expression of Lactococcus lactis NADH oxidase increases 2,3-butanediol production in Pdc-deficient Saccharomyces cerevisiae. *Bioresource Technology*, 191:512–519, 2015.

[49] Jin-Woo Kim, Jungyeon Kim, Seung-Oh Seo, Kyoung Heon Kim, Yong-Su Jin, and Jin-Ho Seo. Enhanced production of 2,3-Butanediol by engineered Saccharomyces cerevisiae through fine-tuning of Pyruvate decarboxylase and NADH oxidase activities. *Biotechnology for Biofuels*, 9(265):1–12, dec 2016.

[50] Jin-Woo Kim, Ye-Gi Lee, Soo-Jung Kim, Yong-Su Jin, and Jin-Ho Seo. Deletion of glycerol-3-phosphate dehydrogenase genes improved 2,3-butanediol production by reducing glycerol production in pyruvate decarboxylase-deficient Saccharomyces cerevisiae. *Journal of Biotechnology*, 304:31–37, oct 2019.

[51] Yoshihiro Ida, Takashi Hirasawa, Chikara Furusawa, and Hiroshi Shimizu. Utilization of Saccharomyces cerevisiae recombinant strain incapable of both ethanol and glycerol biosynthesis for anaerobic bioproduction. *Applied Microbiology and Biotechnology*, 97(11):4811–4819, 2013.

[52] Takashi Hirasawa, Yoshihiro Ida, Chikara Furusawa, and Hiroshi Shimizu. Potential of a Saccharomyces cerevisiae recombinant strain lacking ethanol and glycerol biosynthesis pathways in efficient anaerobic bioproduction. *Bioengineered*, 5(2):123–128, 2013.

[53] Antonius J.A. Van Maris, Aaron A. Winkler, Danilo Porro, Johannes P. Van Dijken, and Jack T. Pronk. Homofermentative lactate production cannot sustain anaerobic growth of engineered Saccharomyces cerevisiae: Possible consequence of energy-dependent lactate export. *Applied and Environmental Microbiology*, 70(5):2898–2905, 2004.

[54] Seung-Ho Baek, Eunice Y. Kwon, Yong Hwan Kim, and Ji-Sook Hahn. Metabolic engineering and adaptive evolution for efficient production of D-lactic acid in Saccharomyces cerevisiae. *Applied Microbiology and Biotechnology*, 100(6):2737–2748, mar 2016.

[55] Wei Zhong, Maohua Yang, Tingzhen Mu, Fan Wu, Xuemi Hao, Ruonan Chen, Moustafa Mohamed Sharshar, Anders Thygesen, Qinhong Wang, and Jianmin

Xing. Systematically redesigning and optimizing the expression of D -lactate dehydrogenase efficiently produces high-optical-purity D -lactic acid in Saccharomyces cerevisiae. *Biochemical Engineering Journal*, 144:217–226, apr 2019.

[56] Rintze M. Zelle, Erik De Hulster, Wouter A. Van Winden, Pieter De Waard, Cor Dijkema, Aaron A. Winkler, Jan-Maarten A. Geertman, Johannes P. Van Dijken, Jack T. Pronk, and Antonius J.A. Van Maris. Malic acid production by Saccharomyces cerevisiae: Engineering of pyruvate carboxylation, oxaloacetate reduction, and malate export. *Applied and Environmental Microbiology*, 74(9):2766–2777, may 2008.

[57] N. Milne, S.A. Wahl, A.J.A. van Maris, J.T. Pronk, and J.M. Daran. Excessive by-product formation: A key contributor to low isobutanol yields of engineered Saccharomyces cerevisiae strains. *Metabolic Engineering Communications*, 3:39–51, 2016.

[58] Aiqin Shi, Xinna Zhu, Jiao Lu, Xueli Zhang, and Yanhe Ma. Activating transhydrogenase and NAD kinase in combination for improving isobutanol production. *Metabolic Engineering*, 16(1):1–10, 2013.

[59] Kengo Ida, Jun Ishii, Fumio Matsuda, Takashi Kondo, and Akihiko Kondo. Eliminating the isoleucine biosynthetic pathway to reduce competitive carbon outflow during isobutanol production by Saccharomyces cerevisiae. *Microbial Cell Factories*, 14(62):1–9, 2015.

[60] Zhikun Wang, Cuijuan Gao, Qian Wang, Quanfeng Liang, and Qingsheng Qi. Production of pyruvate in Saccharomyces cerevisiae through adaptive evolution and rational cofactor metabolic engineering. *Biochemical Engineering Journal*, 67:126–131, aug 2012.

[61] Fumio Matsuda, Jun Ishii, Takashi Kondo, Kengo Ida, Hironori Tezuka, and Akihiko Kondo. Increased isobutanol production in Saccharomyces cerevisiae by eliminating competing pathways and resolving cofactor imbalance. *Microbial Cell Factories*, 12(119):1–11, 2013.

[62] Ruiqi Feng, Jingzhi Li, and Aili Zhang. Improving isobutanol titers in Saccharomyces cerevisiae with over-expressing NADPH-specific glucose-6-phosphate dehydrogenase (Zwf1). *Annals of Microbiology*, 67(12):785–791, 2017.

[63] Sabine Bastian, Xiang Liu, Joseph T. Meyerowitz, Christopher D. Snow, Mike M.Y. Chen, and Frances H. Arnold. Engineered ketol-acid reductoisomerase and alcohol dehydrogenase enable anaerobic 2-methylpropan-1-ol production at theoretical yield in Escherichia coli. *Metabolic Engineering*, 13(3):345–352, 2011.

[64] Derek A. Abbott, Rintze M. Zelle, Jack T. Pronk, and Antonius J.A. Van Maris. Metabolic engineering of Saccharomyces cerevisiae for production of carboxylic acids: Current status and challenges. *FEMS Yeast Research*, 9(8):1123–1136, dec 2009.

[65] Mohammad Pooya Naghshbandi, Meisam Tabatabaei, Mortaza Aghbashlo, Vijai Kumar Gupta, Alawi Sulaiman, Keikhosro Karimi, Hamid Moghimi, and Mina

Maleki. Progress toward improving ethanol production through decreased glycerol generation in Saccharomyces cerevisiae by metabolic and genetic engineering approaches. *Renewable and Sustainable Energy Reviews*, 115:109353, nov 2019.

[66] Paula Jouhten, Eija Rintala, Anne Huuskonen, Anu Tamminen, Mervi Toivari, Marilyn Wiebe, Laura Ruohonen, Merja Penttilä, and Hannu Maaheimo. Oxygen dependence of metabolic fluxes and energy generation of Saccharomyces cerevisiae CEN.PK113-1A. *BMC Systems Biology*, 2(60):1–19, jul 2008.

[67] Elke Nevoigt and Ulf Stahl. Osmoregulation and glycerol metabolism in the yeast Saccharomyces cerevisiae. *FEMS Microbiology Reviews*, 21(3):231–241, nov 1997.

[68] Daojiang Yan, Caixia Wang, Jiemin Zhou, Yilan Liu, Maohua Yang, and Jianmin Xing. Construction of reductive pathway in Saccharomyces cerevisiae for effective succinic acid fermentation at low pH value. *Bioresource Technology*, 156:232–239, mar 2014.

[69] Ahmed Zahoor, Felix T. F. Küttner, Lars M. Blank, and Birgitta E. Ebert. Evaluation of pyruvate decarboxylase-negative Saccharomyces cerevisiae strains for the production of succinic acid. *Engineering in Life Sciences*, 19(10):711–720, oct 2019.

[70] Ioannis Papapetridis, Maaike Goudriaan, María Vázquez Vitali, Nikita A. De Keijzer, Marcel Van Den Broek, Antonius J.A. Van Maris, and Jack T. Pronk. Optimizing anaerobic growth rate and fermentation kinetics in Saccharomyces cerevisiae strains expressing Calvin-cycle enzymes for improved ethanol yield. *Biotechnology for Biofuels*, 11(1):1–17, 2018.

[71] Víctor Guadalupe Medina, Marinka J.H. Almering, Antonius J.A. Van Maris, and Jack T. Pronk. Elimination of glycerol production in anaerobic cultures of a saccharomyces cerevisiae strain engineered to use acetic acid as an electron acceptor. *Applied and Environmental Microbiology*, 76(1):190–195, 2010.

[72] Naveen Venayak, Axel Von Kamp, Steffen Klamt, and Radhakrishnan Mahadevan. MoVE identifies metabolic valves to switch between phenotypic states. *Nature Communications*, 9(5332):1–9, 2018.

[73] Yoshihiro Toya and Hiroshi Shimizu. Flux controlling technology for central carbon metabolism for efficient microbial bio-production. *Current Opinion in Biotechnology*, 64:169–174, aug 2020.

[74] Makoto A. Lalwani, Evan M. Zhao, and José L. Avalos. Current and future modalities of dynamic control in metabolic engineering. *Current Opinion in Biotechnology*, 52:56–65, aug 2018.

[75] Sue Zanne Tan, Shawn Manchester, and Kristala L. J. Prather. Controlling Central Carbon Metabolism for Improved Pathway Yields in Saccharomyces cerevisiae. *ACS Synthetic Biology*, 5(2):116–124, 2016.

[76] Evan M. Zhao, Yanfei Zhang, Justin Mehl, Helen Park, Makoto A. Lalwani, Jared E. Toettcher, and José L. Avalos. Optogenetic regulation of engineered cellular metabolism for microbial chemical production. *Nature*, 555(7698):683–687, 2018.

[77] Yanfei Zhang, Stephan Lane, Jhong-Min Chen, Sarah K. Hammer, Jake Luttinger, Lifeng Yang, Yong-Su Jin, and José L. Avalos. Xylose utilization stimulates mitochondrial production of isobutanol and 2-methyl-1-butanol in Saccharomyces cerevisiae. *Biotechnology for Biofuels*, 12(1):1–15, 2019.

[78] Stephan Lane, Yanfei Zhang, Eun Ju Yun, Leah Ziolkowski, Guochang Zhang, Yong-Su Jin, and José L. Avalos. Xylose Assimilation Enhances Production of Isobutanol in Engineered Saccharomyces cerevisiae. *Biotechnology and Bioengineering*, 117(2):1–10, 2019.

[79] Yong-Su Jin, Jose M. Laplaza, and Thomas W. Jeffries. Saccharomyces cerevisiae engineered for xylose metabolism exhibits a respiratory response. *Applied and Environmental Microbiology*, 70(11):6816–6825, 2004.

[80] Suryang Kwak, Jung Hyun Jo, Eun Ju Yun, Yong-Su Jin, and Jin-Ho Seo. Production of biofuels and chemicals from xylose using native and engineered yeast strains. *Biotechnology Advances*, 37(2):271–283, 2018.

[81] Trey K. Sato, Mary Tremaine, Lucas S. Parreiras, Alexander S. Hebert, Kevin S. Myers, Alan J. Higbee, Maria Sardi, Sean J. McIlwain, Irene M. Ong, Rebecca J. Breuer, Ragothaman Avanasi Narasimhan, Mick A. McGee, Quinn Dickinson, Alex La Reau, Dan Xie, Mingyuan Tian, Jennifer L. Reed, Yaoping Zhang, Joshua J. Coon, Chris Todd Hittinger, Audrey P. Gasch, and Robert Landick. Directed evolution reveals unexpected epistatic interactions that alter metabolic regulation and enable anaerobic xylose use by Saccharomyces cerevisiae. *PLoS Genetics*, 12(10):1–31, 2016.

[82] Zia-ul Islam, Mathias Klein, Maximilian R. Aßkamp, Anders S.R. Ødum, and Elke Nevoigt. A modular metabolic engineering approach for the production of 1,2-propanediol from glycerol by Saccharomyces cerevisiae. *Metabolic Engineering*, 44:223–235, nov 2017.

[83] Soo-Jung Kim, Hee-Jin Sim, Jin-Woo Kim, Ye-Gi Lee, Yong-Cheol Park, and Jin-Ho Seo. Enhanced production of 2,3-butanediol from xylose by combinatorial engineering of xylose metabolic pathway and cofactor regeneration in pyruvate decarboxylase-deficient Saccharomyces cerevisiae. *Bioresource Technology*, 245:1551–1557, dec 2017.

[84] Vera Novy, Bernd Brunner, and Bernd Nidetzky. l-Lactic acid production from glucose and xylose with engineered strains of Saccharomyces cerevisiae: aeration and carbon source influence yields and productivities. *Microbial Cell Factories*, 17(59):1, dec 2018.

[85] Timothy L. Turner, Guo Chang Zhang, Soo Rin Kim, Vijay Subramaniam, David Steffen, Christopher D. Skory, Ji Yeon Jang, Byung Jo Yu, and Yong Su Jin. Lactic acid production from xylose by engineered Saccharomyces cerevisiae without PDC or ADH deletion. *Applied Microbiology and Biotechnology*, 99(19):8023–8033, oct 2015.

[86] Zongjie Dai, Mingtao Huang, Yun Chen, Verena Siewers, and Jens Nielsen. Global rewiring of cellular metabolism renders Saccharomyces cerevisiae Crabtree negative. *Nature Communications*, 9(1):3059, 2018.

[87] Virginia Schadeweg and Eckhard Boles. n-Butanol production in Saccharomyces cerevisiae is limited by the availability of coenzyme A and cytosolic acetyl-CoA. *Biotechnology for Biofuels*, 9(44):2–12, jul 2016.

[88] Soo-Jung Kim, Seung-Oh Seo, Yong-Cheol Park, Yong-Su Jin, and Jin-Ho Seo. Production of 2,3-butanediol from xylose by engineered Saccharomyces cerevisiae. *Journal of Biotechnology*, 192:376–382, 2014.

[89] Lucie A. Hazelwood, Jean Marc Daran, Antonius J A Van Maris, Jack T. Pronk, and J. Richard Dickinson. The Ehrlich pathway for fusel alcohol production: A century of research on Saccharomyces cerevisiae metabolism. *Applied and Environmental Microbiology*, 74(12):3920, 2008.

[90] Johannes Wess, Martin Brinek, and Eckhard Boles. Improving isobutanol production with the yeast Saccharomyces cerevisiae by successively blocking competing metabolic pathways as well as ethanol and glycerol formation. *Biotechnology for Biofuels*, 12(1):1–15, 2019.

[91] Wesley Cardoso Generoso, Virginia Schadeweg, Mislav Oreb, and Eckhard Boles. Metabolic engineering of Saccharomyces cerevisiae for production of butanol isomers. *Current Opinion in Biotechnology*, 33(Figure 1):1–7, 2015.

[92] Sabine Brinkmann-Chen, Tilman Flock, Jackson K.B. B. Cahn, Christopher D. Snow, Eric M. Brustad, John A. McIntosh, Peter Meinhold, Liang Zhang, and Frances H. Arnold. General approach to reversing ketol-acid reductoisomerase cofactor dependence from NADPH to NADH. *Proceedings of the National Academy of Sciences*, 110(27):10946–10951, 2013.

[93] Lori Ann Maggio-Hall, Brian James Paul, Steven Cary Rothman, and Rick W. YE. DHAD VARANTS FOR BUTANOL PRODUCTION, 2017.

[94] N. Milne, A. J A Van Maris, J. T. Pronk, and J. M. Daran. Comparative assessment of native and heterologous 2-oxo acid decarboxylases for application in isobutanol production by Saccharomyces cerevisiae. *Biotechnology for Biofuels*, 8(1):1–15, 2015.

[95] Xiang Liu, Sabine Bastian, Christopher D. Snow, Eric M. Brustad, Tatyana E. Saleski, Jian-He Xu, Peter Meinhold, and Frances H. Arnold. Structure-guided engineering of Lactococcus lactis alcohol dehydrogenase LlAdhA for improved conversion of isobutyraldehyde to isobutanol. *Journal of Biotechnology*, 164(2):188–195, dec 2012.

[96] José L Avalos, Gerald R Fink, and Gregory Stephanopoulos. Compartmentalization of metabolic pathways in yeast mitochondria improves the production of branched-chain alcohols. *Nature Biotechnology*, 31(4):335–341, 2013.

[97] Dawid Brat, Christian Weber, Wolfram Lorenzen, Helge B Bode, and Eckhard Boles. Cytosolic re-localization and optimization of valine synthesis and catabolism enables increased isobutanol production with the yeast Saccharomyces cerevisiae. *Biotechnology for Biofuels*, 5:1–16, 2012.

[98] Daisuke Shiiba, Isamu Miyakawa, and Nobundo Sando. Dynamic Changes in Mitochondrial Nucleoids during the Transition from Anaerobic to Aerobic Culture in the Yeast Saccharomyces cerevisiae. *Cytologia*, 70(3):287–293, 2005.

[99] Isamu Miyakawa. Organization and dynamics of yeast mitochondrial nucleoids. *Proceedings of the Japan Academy, Series B*, 93(5):339–359, 2017.

[100] Sarah K. Hammer and José L. Avalos. Uncovering the role of branched-chain amino acid transaminases in Saccharomyces cerevisiae isobutanol biosynthesis. *Metabolic Engineering*, 44:302–312, 2017.

[101] Seong-Hee Park, Sujin Kim, and Ji-Sook Hahn. Improvement of isobutanol production in Saccharomyces cerevisiae by increasing mitochondrial import of pyruvate through mitochondrial pyruvate carrier. *Applied Microbiology and Biotechnology*, 100(17):7591–7598, 2016.

[102] Seong-Hee Park and Ji-Sook Hahn. Development of an efficient cytosolic isobutanol production pathway in Saccharomyces cerevisiae by optimizing copy numbers and expression of the pathway genes based on the toxic effect of $\alpha$-acetolactate. *Scientific Reports*, 9(1):1–11, 2019.

[103] Xiao Chen, Kristian F Nielsen, Irina Borodina, Morten C Kielland-Brandt, and Kaisa Karhumaa. Increased isobutanol production in Saccharomyces cerevisiae by overexpression of genes in valine metabolism. *Biotechnology for Biofuels*, 4(1):1–12, 2011.

[104] Takashi Kondo, Hironori Tezuka, Jun Ishii, Fumio Matsuda, Chiaki Ogino, and Akihiko Kondo. Genetic engineering to enhance the Ehrlich pathway and alter carbon flux for increased isobutanol production from glucose by Saccharomyces cerevisiae. *Journal of Biotechnology*, 159(1-2):32–37, 2012.

[105] J Jönsson Leif, Nils-Olof Nilvebrant, and Björn Alriksson. Bioconversion of lignocellulose: Inhibitors and detoxification. *Biotechnology for Biofuels*, 6(1):1–10, 2013.

[106] Joao RM Almeida, Tobias Modig, Anneli Petersson, Barbel Hahn-Hagerdal, Gunnar Liden, and Marie F Gorwa-Grauslund. Increased tolerance and conversion of inhibitors in lignocellulosic hydrolysates by Saccharomyces cerevisiae. *Journal of Chemical Technology & Biotechnology*, 82:340–349, 2007.

[107] Scott Bottoms, Quinn Dickinson, Mick McGee, Li Hinchman, Alan Higbee, Alex Hebert, Jose Serate, Dan Xie, Yaoping Zhang, Joshua J. Coon, Chad L. Myers, Robert Landick, and Jeff S. Piotrowski. Chemical genomic guided engineering of gamma-valerolactone tolerant yeast. *Microbial Cell Factories*, 17(1):1–12, 2018.

[108] Jeremy S Luterbacher, Jacqueline M. Rand, David Martin Alonso, Jeehoon Han, J. Tyler Youngquist, Christos T. Maravelias, Brian F. Pfleger, and James A. Dumesic. Nonenzymatic sugar production from biomass using biomass-derived $\gamma$ -valerolactone. 343:277–281, 2014.

[109] Akinori Matsushika, Hiroyuki Inoue, Tsutomu Kodaki, and Shigeki Sawayama. Ethanol production from xylose in engineered Saccharomyces cerevisiae strains: Current state and perspectives. *Applied Microbiology and Biotechnology*, 84(1):37–53, 2009.

[110] Guo Chang Zhang, Jing Jing Liu, In Iok Kong, Suryang Kwak, and Yong Su Jin. Combining C6 and C5 sugar metabolism for enhancing microbial bioconversion. *Current Opinion in Chemical Biology*, 29:49–57, 2015.

[111] Liang Sun and Yong-Su Jin. Xylose Assimilation for the Efficient Production of Biofuels and Chemicals by Engineered Saccharomyces cerevisiae. *Biotechnology Journal*, 16(4):2000142, apr 2021.

[112] Xiaowei Li, Yun Chen, and Jens Nielsen. Harnessing xylose pathways for biofuels production. *Current Opinion in Biotechnology*, 57(Xi):56–65, 2019.

[113] Jae Won Lee, Sangdo Yook, Hyungi Koh, Christopher V. Rao, and Yong-Su Jin. Engineering xylose metabolism in yeasts to produce biofuels and chemicals. *Current Opinion in Biotechnology*, 67:15–25, feb 2021.

[114] Dawid Brat and Eckhard Boles. Isobutanol production from d-xylose by recombinant Saccharomyces cerevisiae. *FEMS Yeast Research*, 13(2):241–244, 2013.

[115] Peerada Promdonkoy, Wuttichai Mhuantong, Verawat Champreda, Sutipa Tanapongpipat, and Weerawat Runguphan. Improvement in D-xylose utilization and isobutanol production in S. cerevisiae by adaptive laboratory evolution and rational engineering. *Journal of Industrial Microbiology and Biotechnology*, 47(6-7):497–510, jul 2020.

[116] Wesley Cardoso Generoso, Martin Brinek, Heiko Dietz, Mislav Oreb, and Eckhard Boles. Secretion of 2,3-dihydroxyisovalerate as a limiting factor for isobutanol production in Saccharomyces cerevisiae. *FEMS Yeast Research*, (March):1–10, 2017.

[117] Jeff S. Piotrowski, Yaoping Zhang, Donna M. Bates, David H. Keating, Trey K. Sato, Irene M. Ong, and Robert Landick. Death by a thousand cuts: The challenges and diverse landscape of lignocellulosic hydrolysate inhibitors. *Frontiers in Microbiology*, 5(MAR):1–8, 2014.

[118] Daehwan Kim. Physico-chemical conversion of lignocellulose: Inhibitor effects and detoxification strategies: A mini review. *Molecules*, 23(2), 2018.

[119] Jeffrey M. Skerker, Dacia Leon, Morgan N. Price, Jordan S. Mar, Daniel R. Tarjan, Kelly M. Wetmore, Adam M. Deutschbauer, Jason K. Baumohl, Stefan Bauer, Ana B. Ibáñez, Valerie D. Mitchell, Cindy H. Wu, Ping Hu, Terry Hazen, and Adam P. Arkin. Dissecting a complex chemical stress: Chemogenomic profiling of plant hydrolysates. *Molecular Systems Biology*, 9(674), 2013.

[120] Yingying Chen, Jiayuan Sheng, Tao Jiang, Joseph Stevens, Xueyang Feng, and Na Wei. Transcriptional profiling reveals molecular basis and novel genetic targets for improved resistance to multiple fermentation inhibitors in Saccharomyces cerevisiae. *Biotechnology for Biofuels*, 9(1):1–18, 2016.

[121] Olivia A. Thompson, Gary M. Hawkins, Steven W. Gorsich, and Joy Doran-Peterson. Phenotypic characterization and comparative transcriptomics of evolved Saccharomyces cerevisiae strains with improved tolerance to lignocellulosic derived inhibitors. *Biotechnology for Biofuels*, 9(1):1–16, 2016.

[122] Weihua Guo, Yingying Chen, Na Wei, and Xueyang Feng. Investigate the metabolic reprogramming of Saccharomyces cerevisiae for enhanced resistance to mixed fermentation inhibitors via13C metabolic flux analysis. *PLoS ONE*, 11(8):1–15, 2016.

[123] Bianca A. Brandt, Maria D. P. García-Aparicio, Johann F. Görgens, and Willem H. van Zyl. Rational engineering of Saccharomyces cerevisiae towards improved tolerance to multiple inhibitors in lignocellulose fermentations. *Biotechnology for Biofuels*, 14(1):1–18, aug 2021.

[124] Yun-Cheng Li, Zi-Xi Gou, Ze-Shen Liu, Yue-Qin Tang, Takashi Akamatsu, and Kenji Kida. Synergistic effects of TAL1 over-expression and PHO13 deletion on the weak acid inhibition of xylose fermentation by industrial Saccharomyces cerevisiae strain. *Biotechnology Letters*, 36(10):2011–2021, jun 2014.

[125] Victor E. Balderas-Hernández, Kevin Correia, and Radhakrishnan Mahadevan. Inactivation of the transcription factor mig1 (YGL035C) in Saccharomyces cerevisiae improves tolerance towards monocarboxylic weak acids: acetic, formic and levulinic acid. *Journal of Industrial Microbiology and Biotechnology*, 45(8):735–751, 2018.

[126] Francesca V. Gambacort, Ellen R. Wagner, Tyler B. Jacobson, Mary Tremaine, Laura K. Muehlbauer, Mick A. McGee, Justin J. Baerwald, Russell L. Wrobel, John F. Wolters, Mike Place, Joshua J. Dietrich, Dan Xie, Jose Serate, Shabda Gajbhiye, Lisa Liu, Maikayeng Vang-Smith, Joshua J. Coon, Yaoping Zhang, Audrey P. Gasch, Daniel Amador-Noguez, Chris Todd Hittinger, Trey K. Sato, and Brian F. Pfleger. Comparative functional genomics identifies an iron-limited bottleneck in a Saccharomyces cerevisiae strain with a cytosolic-localized isobutanol pathway. *Synthetic and Systems Biotechnology*, 7(2):738–749, jun 2022.

[127] Scott Geleynse, Kristin Brandt, Manuel Garcia-Perez, Michael Wolcott, and Xiao Zhang. The Alcohol-to-Jet Conversion Pathway for Drop-In Biofuels: Techno-Economic Evaluation. *ChemSusChem*, 11(21):3728–3741, 2018.

[128] Enrico Bardone, Marco Bravi, Taj Keshavarz, Lucia Paciello, Palma Parascandola, and Carmine Landi. Auxotrophic Saccharomyces Cerevisiae CEN.PK Strains as New Performers in Ethanol Production. *Chemical Engineering Transactions*, 38:463–468, 2014.

[129] Robert H. Schiestl and R. Daniel Gietz. High efficiency transformation of intact yeast cells using single stranded nucleic acids as a carrier. *Current Genetics*, 16(5):339–346, dec 1989.

[130] Thomas W. Christianson, Robert S. Sikorski, Michael Dante, James H. Shero, and Philip Hieter. Multifunctional yeast high-copy-number shuttle vectors. *Gene*, 110(1):119–122, jan 1992.

[131] Warren P. Voth, James D. Richards, Janet M. Shaw, and David J. Stillman. Yeast vectors for integration at the HO locus. *Nucleic Acids Research*, 29(12):e59, 2001.

[132] U. Gueldener, J. Heinisch, G. J. Koehler, D. Voss, and J. H. Hegemann. A second set of loxP marker cassettes for Cre-mediated multiple gene knockouts in budding yeast. *Nucleic acids research*, 30(6):e23, 2002.

[133] Hayley R. Stoneman, Russell L. Wrobel, Michael Place, Michael Graham, David J. Krause, Matteo De Chiara, Gianni Liti, Joseph Schacherer, Robert Landick, Audrey P. Gasch, Trey K. Sato, and Chris Todd Hittinger. CRISpy-Pop: A Web Tool for Designing CRISPR/Cas9-Driven Genetic Modifications in Diverse Populations. *G3: Genes, Genomes, Genetics*, 10(11):4287–4294, nov 2020.

[134] Douglas A. Higgins, Megan K. M. Young, Mary Tremaine, Maria Sardi, Jenna M. Fletcher, Margaret Agnew, Lisa Liu, Quinn Dickinson, David Peris, Russell L. Wrobel, Chris Todd Hittinger, Audrey P. Gasch, Steven W. Singer, Blake A. Simmons, Robert Landick, Michael P. Thelen, and Trey K. Sato. Natural variation in the multidrug efflux pump SGE1 underlies ionic liquid tolerance in yeast. *Genetics*, 210(1):219–234, 2018.

[135] Indro N. Ghosh, Julia Martien, Alexander S. Hebert, Yaoping Zhang, Joshua J. Coon, Daniel Amador-Noguez, and Robert Landick. OptSSeq explores enzyme expression and function landscapes to maximize isobutanol production rate. *Metabolic Engineering*, 52:324–340, 2018.

[136] Ulrich Güldener, Susanne Heck, Thomas Fielder, Jens Beinhauer, and Jigabbes H. Hegemann. A new efficient gene disruption cassette for repeated use in budding yeast. *Nucleic Acids Research*, 24(13):2519–2524, 1996.

[137] Tyler B. Jacobson, Travis K. Korosh, David M. Stevenson, Charles Foster, Costas Maranas, Daniel G. Olson, Lee R. Lynd, and Daniel Amador-Noguez. In Vivo Thermodynamic Analysis of Glycolysis in Clostridium thermocellum and Thermoanaerobacterium saccharolyticum Using 13 C and 2 H Tracers. *mSystems*, 5(2):e00736–19, 2020.

[138] Tyler B. Jacobson, Paul A. Adamczyk, David M. Stevenson, Matthew Regner, John Ralph, Jennifer L. Reed, and Daniel Amador-Noguez. 2 H and 13 C metabolic flux analysis elucidates in vivo thermodynamics of the ED pathway in Zymomonas mobilis. *Metabolic Engineering*, 54(March):301–316, 2019.

[139] Eugene Melamud, Livia Vastag, and Joshua D. Rabinowitz. Metabolomic Analysis and Visualization Engine for LCMS Data. *Analytical Chemistry*, 82(23):9818–9826, dec 2010.

[140] Michelle F. Clasquin, Eugene Melamud, and Joshua D. Rabinowitz. LC-MS Data Processing with MAVEN: A Metabolomic Analysis and Visualization Engine. *Current Protocols in Bioinformatics*, 37(1):14–11, mar 2012.

[141] Audrey P. Gasch. *Yeast genomic expression studies using DNA microarrays*, volume 350. Academic Press, jan 2002.

[142] Anthony M. Bolger, Marc Lohse, and Bjoern Usadel. Trimmomatic: a flexible trimmer for Illumina sequence data. *Bioinformatics*, 30(15):2114–2120, aug 2014.

[143] Ben Langmead. *Aligning short sequencing reads with Bowtie*, volume 11. 2010.

[144] Mark D. Robinson, Davis J. McCarthy, and Gordon K. Smyth. edgeR: A Bioconductor package for differential expression analysis of digital gene expression data. *Bioinformatics*, 26(1):139–140, 2010.

[145] Yoav Benjamini and Yosef Hochberg. Controlling the False Discovery Rate: A Practical and Powerful Approach to Multiple Testing. *Journal of the Royal Statistical Society*, 57(1):289–300, 1995.

[146] M.J.L. de Hoon, S. Imoto, J. Nolan, and S. Miyano. Open source clustering software. *Bioinformatics*, 20(9):1453–1454, jun 2004.

[147] Alok J. Saldanha. Java Treeview—extensible visualization of microarray data. *Bioinformatics*, 20(17):3246–3248, nov 2004.

[148] Cedric Simillion, Robin Liechti, Heidi E.L. Lischer, Vassilios Ioannidis, and Rémy Bruggmann. Avoiding the pitfalls of gene set enrichment analysis with SetRank. *BMC Bioinformatics*, 18:1–14, mar 2017.

[149] Evgenia Shishkova, Alexander S. Hebert, Michael S. Westphall, and Joshua J. Coon. Ultra-High Pressure (>30,000 psi) Packing of Capillary Columns Enhancing Depth of Shotgun Proteomic Analyses. *Analytical Chemistry*, 90(19):11503–11508, oct 2018.

[150] Jürgen Cox and Matthias Mann. MaxQuant enables high peptide identification rates, individualized p.p.b.-range mass accuracies and proteome-wide protein quantification. *Nature Biotechnology*, 26(12):1367–1372, nov 2008.

[151] Dimitrov N. Lazar, Rachel B. Brem, Leonid Kruglyak, and Daniel E. Gottschling. Polymorphisms in multiple genes contribute to the spontaneous mitochondrial genome instability of Saccharomyces cerevisiae S288C strains. *Genetics*, 183(1):365–383, sep 2009.

[152] Sherman Fred. *Getting started with yeast*, volume 350. 2002.

[153] Michael E. Lee, William C. DeLoache, Bernardo Cervantes, and John E. Dueber. A Highly Characterized Yeast Toolkit for Modular, Multipart Assembly. *ACS Synthetic Biology*, 4(9):975–986, 2015.

[154] Jie Sun, Zengyi Shao, Hua Zhao, Nikhil Nair, Fei Wen, Jian-He Xu, and Huimin Zhao. Cloning and characterization of a panel of constitutive promoters for applications in pathway engineering in Saccharomyces cerevisiae. *Biotechnology and Bioengineering*, 109(8):2082–2092, 2012.

[155] María Teresa Martínez-Pastor, Ana Perea-García, and Sergi Puig. Mechanisms of iron sensing and regulation in the yeast Saccharomyces cerevisiae. *World Journal of Microbiology and Biotechnology*, 33(4):1–9, 2017.

[156] Per O. Ljungdahl and Bertrand Daignan-Fornier. *Regulation of Amino Acid, Nucleotide, and Phosphate Metabolism in Saccharomyces cerevisiae*, volume 190. Oxford Academic, mar 2012.

[157] Takahiro Bamba, Takahiro Yukawa, Gregory Guirimand, Kentaro Inokuma, Kengo Sasaki, Tomohisa Hasunuma, and Akihiko Kondo. Production of 1,2,4-butanetriol from xylose by Saccharomyces cerevisiae through Fe metabolic engineering. *Metabolic Engineering*, 56:17–27, 2019.

[158] Laura Salusjärvi, Mervi Toivari, Maija-Leena Vehkomäki, Outi Koivistoinen, Dominik Mojzita, Klaus Niemelä, Merja Penttilä, and Laura Ruohonen. Production of ethylene glycol or glycolic acid from D-xylose in Saccharomyces cerevisiae. *Applied Microbiology and Biotechnology*, 101(22):8151–8163, oct 2017.

[159] Yuko Yamaguchi-Iwai, Andrew Dancis, and Richard D. Klausner. AFT1: A mediator of iron regulated transcriptional control in Saccharomyces cerevisiae. *EMBO Journal*, 14(6):1231–1239, 1995.

[160] Feline Benisch and Eckhard Boles. The bacterial Entner-Doudoroff pathway does not replace glycolysis in Saccharomyces cerevisiae due to the lack of activity of iron-sulfur cluster enzyme 6-phosphogluconate dehydratase. *Journal of Biotechnology*, 171(1):45–55, feb 2014.

[161] Ron Edgar, Michael Domrachev, and Alex E. Lash. Gene Expression Omnibus: NCBI gene expression and hybridization array data repository. *Nucleic Acids Research*, 30(1):207–210, jan 2002.

[162] Rémi Zallot, Nils Oberg, and John A. Gerlt. The EFI Web Resource for Genomic Enzymology Tools: Leveraging Protein, Genome, and Metagenome Databases to Discover Novel Enzymes and Metabolic Pathways. *Biochemistry*, 58(41):4169–4182, oct 2019.

[163] Paul Shannon, Andrew Markiel, Owen Ozier, Nitin S. Baliga, Jonathan T. Wang, Daniel Ramage, Nada Amin, Beno Schwikowski, and Trey Ideker. Cytoscape: a software environment for integrated models of biomolecular interaction networks. *Genome research*, 13(11):2498–2504, nov 2003.

[164] Manuel G. Claros and Pierre Vincens. Computational Method to Predict Mitochondrially Imported Proteins and their Targeting Sequences. *European Journal of Biochemistry*, 241(3):779–786, nov 1996.

[165] Fábio Madeira, Matt Pearce, Adrian R N Tivey, Prasad Basutkar, Joon Lee, Ossama Edbali, Nandana Madhusoodanan, Anton Kolesnikov, and Rodrigo Lopez. Search and sequence analysis tools services from EMBL-EBI in 2022. *Nucleic Acids Research*, 50(April):276–279, 2022.

[166] Daniel M. Becker and Leonard Guarente. High-efficiency transformation of yeast by electroporation. *Methods in Enzymology*, 194:182–187, jan 1991.

[167] Johannes H. Hegemann and Sven Boris Heick. *Delete and Repeat: A Comprehensive Toolkit for Sequential Gene Knockout in the Budding Yeast Saccharomyces cerevisiae*, volume 765. Humana Press, 2011.

[168] Zorana Carter and Daniela Delneri. New generation of loxP-mutated deletion cassettes for the genetic manipulation of yeast natural isolates. *Yeast*, 27(9):765–775, sep 2010.

[169] Yaoping Zhang, Jessica M. Vera, Dan Xie, Jose Serate, Edward Pohlmann, Jason D. Russell, Alexander S. Hebert, Joshua J. Coon, Trey K. Sato, and Robert Landick. Multiomic Fermentation Using Chemically Defined Synthetic Hydrolyzates Revealed Multiple Effects of Lignocellulose-Derived Inhibitors on Cell Physiology and Xylose Utilization in Zymomonas mobilis. *Frontiers in Microbiology*, 10(November):1–18, 2019.

[170] Cheuk Hei Ho, Leslie Magtanong, Sarah L. Barker, David Gresham, Shinichi Nishimura, Paramasivam Natarajan, Judice L.Y. Koh, Justin Porter, Christopher A. Gray, Raymond J. Andersen, Guri Giaever, Corey Nislow, Brenda Andrews, David Botstein, Todd R. Graham, Minoru Yoshida, and Charles Boone. A molecular barcoded yeast ORF library enables mode-of-action analysis of bioactive compounds. *Nature Biotechnology*, 27(4):369–377, apr 2009.

[171] M. J. López, N. N. Nichols, B. S. Dien, J. Moreno, and R. J. Bothast. Isolation of microorganisms for biological detoxification of lignocellulosic hydrolysates. *Applied Microbiology and Biotechnology*, 64(1):125–131, 2004.

[172] Hong Ran, Jian Zhang, Qiuqiang Gao, Zhanglin Lin, and Jie Bao. Analysis of biodegradation performance of furfural and 5- hydroxymethylfurfural by Amorphotheca resinae ZN1. *Biotechnology for Biofuels*, 7(1):1–12, 2014.

[173] Jacqueline M. Rand, Tippapha Pisithkul, Ryan L. Clark, Joshua M. Thiede, Christopher R. Mehrer, Daniel E. Agnew, Candace E. Campbell, Andrew L. Markley, Morgan N. Price, Jayashree Ray, Kelly M. Wetmore, Yumi Suh, Adam P. Arkin, Adam M. Deutschbauer, Daniel Amador-Noguez, and Brian F. Pfleger. A metabolic pathway for catabolizing levulinic acid in bacteria. *Nature Microbiology*, 2(12):1624–1634, 2017.

[174] Bingyin Peng, Lygie Esquirol, Zeyu Lu, Qianyi Shen, Li Chen Cheah, Christopher B. Howard, Colin Scott, Matt Trau, Geoff Dumsday, and Claudia E. Vickers. An in vivo gene amplification system for high level expression in Saccharomyces cerevisiae. *Nature Communications*, 13(1):1–12, may 2022.

[175] Sae Byuk Lee, Mary Tremaine, Michael Place, Lisa Liu, Austin Pier, David J. Krause, Dan Xie, Yaoping Zhang, Robert Landick, Audrey P. Gasch, Chris Todd Hittinger, and Trey K. Sato. Crabtree/Warburg-like aerobic xylose fermentation by engineered Saccharomyces cerevisiae. *Metabolic Engineering*, 68:119–130, nov 2021.

[176] Alexandra Bergman, Verena Siewers, Jens Nielsen, and Yun Chen. Functional expression and evaluation of heterologous phosphoketolases in Saccharomyces cerevisiae. *AMB Express*, 6(1), 2016.

[177] James Kirby, Kevin L. Dietzel, Gale Wichmann, Rossana Chan, Eugene Antipov, Nathan Moss, Edward E.K. Baidoo, Peter Jackson, Sara P. Gaucher, Shayin Gottlieb, Jeremy LaBarge, Tina Mahatdejkul, Kristy M. Hawkins, Sheela Muley, Jack D. Newman, Pinghua Liu, Jay D. Keasling, and Lishan Zhao. Engineering a functional 1-deoxy-D-xylulose 5-phosphate (DXP) pathway in Saccharomyces cerevisiae. *Metabolic Engineering*, 38(July):494–503, 2016.

[178] Kaushik Raj, Siavash Partow, Kevin Correia, Anna N. Khusnutdinova, Alexander F. Yakunin, and Radhakrishnan Mahadevan. Biocatalytic production of adipic acid from glucose using engineered Saccharomyces cerevisiae. *Metabolic Engineering Communications*, 6:28–32, jun 2018.

[179] Gema López-Torrejón, Emilio Jiménez-Vicente, José María Buesa, Jose A. Hernandez, Hemant K. Verma, and Luis M. Rubio. Expression of a functional oxygen-labile nitrogenase component in the mitochondrial matrix of aerobically grown yeast. *Nature Communications*, 7(1):1–6, apr 2016.

[180] Alessandra Biz and Radhakrishnan Mahadevan. Overcoming Challenges in Expressing Iron–Sulfur Enzymes in Yeast. *Trends in Biotechnology*, 39(7):665–677, jul 2021.

[181] Kenji Oki, Frederick S Lee, and Stephen L Mayo. Attempts to develop an enzyme converting DHIV to KIV. *Protein Engineering, Design, and Selection*, pages 1–10, 2019.